UC San Diego

UC San Diego Electronic Theses and Dissertations

Title

The 20S proteasome as an antiparasitic drug target; activity-based probes, structure-activity relationship and in vivo efficacy

Permalink

https://escholarship.org/uc/item/0hs8b3jj

Author

Liu, Lawrence Jon

Publication Date

2024

Peer reviewed|Thesis/dissertation

eScholarship.org Powered by the California Digital Library
University of California

UNIVERSITY OF CALIFORNIA SAN DIEGO

The 20S proteasome as an antiparasitic drug target; activity-based probes, structure-activity relationship and *in vivo* efficacy

A Dissertation submitted in partial satisfaction of the requirements
for the degree Doctor of Philosophy

in

Chemistry

by

Lawrence Jon Liu

Committee in charge:

Professor Conor R. Caffrey, Chair
Professor Anthony J. O'Donoghue, Co-Chair
Professor Dionicio Siegel, Co-Chair
Professor Rommie Amaro
Professor Carlo Ballatore
Professor Lalit Deshmukh
Professor Robert Pomeroy

2024

Copyright

Lawrence Jon Liu, 2024

All rights reserved.

The Dissertation of Lawrence Jon Liu is approved, and it is acceptable in quality and form for publication on microfilm and electronically.

University of California San Diego

2024

DEDICATION

This dissertation is dedicated to my parents, Victor Liu and Hui Mei Chen, and grandparents, Bobby Joe Parker and Chin Yeh Parker, who always supported me through my PhD journey. Thank you for sacrificing many long hours, holidays and weekends so that I could see this through!

TABLE OF CONTENTS

DISSERTATION APPROVAL PAGE iii

DEDICATION iv

TABLE OF CONTENTS.....v

LIST OF FIGURES viii

LIST OF TABLES ix

LIST OF ABBREVIATIONS x

ACKNOWLEDGEMENTS xi

VITA xiv

ABSTRACT OF THE DISSERTATION xv

Chapter 1 The Proteasome as a Drug Target for the Treatment of Parasitic Diseases…….1

1.1. Introduction……..2

1.1.1. Proteasome structure and catalytic mechanism…….2

1.1.2. The ubiquitin proteasome system and the unfolded protein response……..3

1.1.3. History and application of the major proteasome inhibitor chemotypes…..…4

1.2. PIs as anti-parasitic agents…….……..7

1.2.1. Kinetoplastida…….……..9

1.2.1.1. *Trypanosoma brucei*…….…….....…....9

1.2.1.2. *Leishmani donovani* and *L. major*…….…13

1.2.2. Metamonada…….……..13

1.2.2.1. *Trichomonas vaginalis*…….……..14

1.3. Tools to characterize the proteasome……..……..16

1.4. Acknowledgements……..……17

1.5. References……...…..18

Chapter 2 Clickable Probes for Pathogenic Proteasomes: Synthesis and Applications 25

2.1. Introduction…….……26

2.2. Results…….……27

2.2.1. Synthesis of LJL-1 and LJL-2, and their differential engagement of c20S subunits…….....28

2.2.2. Parasite proteasome engagement and β subunit identification using LJL-1 and LJL-2……..……..33

2.3. Discussion…….……..36

2.4. Conclusion……..38

2.5. Methods……..39

2.5.1. Synthesis of LJL-1……...39

2.5.2. Synthesis of LJL-2……43

2.5.3. Cell culture……...……45

2.5.4. Preparation of cell lysates……...…….46

2.5.5. HEK293 cell viability assay……..……...46

2.5.6. Human c20S activity and inhibition assays……..47

2.5.7. Probe incubation, click chemistry and SDS-PAGE……..47

2.5.8. Affinity purification……..49

2.5.9. In gel trypsin digest……...…50

2.5.10. Proteomic sample preparation and analysis……..……50

2.6. Acknowledgements……..…...…51

2.7. References…….....…..52

2.8. Supplemental Information…….....…..57

2.8.1. Me_4BodipyFL-Ahx$_3$L$_3$VS reacts with cysteine proteases……...…..….57

2.8.2. HEK293 cell viability in the presence of proteasome inhibitors……....58

2.8.3. Inhibition of human c20S activity by CFZ and BTZ……..……..59

Chapter 3 Carmaphycin B-based proteasome inhibitors to treat human African trypanosomiasis; structure-activity relationship and *in vivo* efficacy.....……60

3.1. Introduction…….61

3.2. Results…….63

3.2.1. SAR for antitrypanosomal activity *in vitro* by CPB analogs……...63

3.2.2. CPB analogs engage the Tb20S β5 subunit……..69

3.2.3. J-80 is predicted to have greater selectivity towards the Tb20S β5 binding pocket……71

3.2.4. J-77 and J-80 decrease parasitemia in a mouse model of Stage I *T. brucei* infection……...73

3.2.5. J-80 extends the survival of mice infected with *T. brucei*……...…75

3.2.6. J-80 is equipotent against three sub-species of *T. brucei*…….76

3.3. Discussion……...76

3.4. Conclusion……..…78

3.5. Methods……..…79

3.5.1. CMP B analogs……..…..79

3.5.2. Maintenance of *T. brucei*……..…...79

3.5.3. *T. brucei* viability assay……..…….79

3.5.4. Docking studies…….……..80

3.5.5. CPB competition assay with the activity-based probe……..……..82

3.5.6. Mouse model efficacy study……83

3.6. Acknowledgements……84

3.7. References……...……...85

LIST OF FIGURES

Figure 1.1: The 20S, 26S and 30S proteasome structures. 3

Figure 1.2: Schematic of the UPS. 4

Figure 1.3: Schechter and Berger nomenclature for the interactions between proteolytic enzymes and their protein substrates……..8

Figure 1.4: Kinetoplast β4/β5 interface PIs……12

Figure 1.5: Carmaphycin B and its analog, CP-17, *vs*. *T. vaginalis in vitro*……..15

Figure 2.1: Synthetic schemes for LJL-1 and LJL-2……..29

Figure 2.2: Probe engagement with purified c20S and HepG2 cell lysate under various conditions……..….31

Figure 2.3: Inhibition of c20S catalytic β subunits by LJL-1 and LJL-2……...32

Figure 2.4: Probe engagement with, and enrichment and identification of, *L. donovani* promastigote 20S catalytic β subunits……34

Figure 2.5: Probe engagement with, and enrichment and identification of, *T. vaginalis* 20S catalytic β subunits…..……...36

Figure 3.1: CPB analogs decrease *T. brucei* growth and engage Tb20S β5 subunit……..71

Figure 3.2: Covalent and non-covalent docking simulations predict a greater selectivity of J-80 for Tb20S β5……...73

Figure 3.3: Effect of CPB analogs on blood parasitemia……...74

Figure 3.4: J-80 extends the survival of *T. brucei*-infected mice……..……75

LIST OF TABLES

Table 1.1: List of PIs, either in clinical trials or approved as drugs 6

Table 3.1: CPB and analogs……65

Table 3.2: ML9 based epoxyketone inhibitors……...69

Table 3.3: Susceptibility of the three *T. brucei* subspecies to J-80……..……...76

LIST OF ABBREVIATIONS

APB	Activity-based probe
BTZ	Bortezomib
c20S	Human constitutive 20S Proteasome
CFZ	Carfilzomib
CPB	Carmaphycin B
DND*i*	Drugs for Neglected Diseases *initiative*
DUBs	Deubiquitinating enzymes
IXZ	Ixazomib
Ld20S	*Leishmania donovani* 20S Proteasome
MSP-MS	Multiplex substrate profiling by mass spectrometry
MV151	Bodipy TMR-Ahx(3)Leu(3)VS
MZB	Marizomib
PI	Proteasome inhibitor
Sm20S	*Schistosoma mansoni* 20S Proteasome
Tb20S	*Trypanosoma brucei* 20S Proteasome
Tv20S	*Trichomonas vaginalis* 20S Proteasome
UPR	Unfolded protein response
UPS	Ubiquitin proteasome system

ACKNOWLEDGEMENTS

I would like to thank my primary supervisor Dr. Conor Caffrey for initially accepting me as a lab volunteer, and for then guiding me through my master's degree and, ultimately, my doctoral degree. When I first joined his team, I did not think that I would be where I am at today. Thank you for the many years of guidance and the many hours spent helping me to think and write in a scientific manner! I would also like to thank my co-supervisor Dr. Anthony O'Donoghue for allowing me to be a part of his team during my PhD and learn many valuable techniques, especially those pertaining to mass spectrometry and proteomics.

To all of my lab mates, past and present, thank you for always supporting me throughout the good and bad times. I hope that I was able to share some of my knowledge with you as you all have done with me.

Chapter 1 is an abridged version of a review of the proteasome literature that has been accepted by *Advances in Parasitology*. The authors in this review are Liu, Lawrence (corresponding); O'Donoghue, Anthony and Caffrey, Conor. The research of the authors regarding parasite proteasomes was supported in part by NIH awards R21AI133393 and R21AI171824 to AJO and CRC, and R01AI158612 and R21AI146387 to AJO. The content of the review is solely the responsibility of the authors and does not necessarily represent the official views of the National Institutes of Health.

Chapter 2, in full, is a reprint of a manuscript that is currently under review at *ACS Omega* as of May 2024. The authors are listed in the following order: Liu, Lawrence; Lucero, Bobby; Manriquez-Rodriguez, Cindy; Francisco, Karol; Teixeira, Thaiz; Yohannan, Darius; Ballatore; Carlo; Myers, Samuel; O'Donoghue, Anthony (corresponding) and Caffrey, Conor (corresponding). The dissertation author was the primary author of this manuscript. The research

described was supported by the NIH grants R21AI171824 to AJO and CRC, and R01AI158612 to AJO. The content of the manuscript is solely the responsibility of the author and does not necessarily represent the official views of the National Institutes of Health.

Chapter 3, in full, is a reprint of a manuscript that is currently under review in ACS *Infectious Diseases* as of May 2024. The authors are listed in the following order: Liu Lawrence; Francisco, Karol; Sun Yujie Uli; Serafim, Mateus; Amarasinghe, Dilini; Teixeira, Thaiz,; Lucero, Bobby; Kronenberger, Thales; Elsayed, Waad; Elwakil, Hala; Al-Hindy, Momen; Almaliti, Jehad; Gerwick, William; O'Donoghue, Anthony (corresponding) and Caffrey, Conor (corresponding). The dissertation author was the primary author of this paper. The research described was supported by the NIH grant R21AI171824 to AJO and CRC. The content of the manuscript is solely the responsibility of the authors and does not necessarily represent the official views of the National Institutes of Health.

VITA

2018 Bachelor of Science in Chemistry, University of California San Diego

2020 Master of Science in Chemistry, University of California San Diego

2024 Doctor of Philosophy in Chemistry, University of California San Diego

PUBLICATIONS

Bhaduri, S., Nejatfard, A., **Liu, L. J.**, Patrick, G., Strisovsky, K., O'Donoghue, A. & Neal, S. E. 2022. An *in vitro* platform enables catalytic characterization of an intramembrane rhomboid protease. *Biophysical Journal*, 121.

Fajtova, P., Hurysz, B. M., Miyamoto, Y., Serafim, M., Jiang, Z., Trujillo, D. F., **Liu, L. J.**, Somani, U., Almaliti, J., Myers, S. A., Caffrey, C. R., Gerwick, W. H., Kirk, C. J., Boura, E., Eckmann, L. & O'Donoghue, A. J. 2023. Development of subunit selective substrates for *Trichomonas vaginalis* proteasome. *bioRxiv*.

Francisco, K. R., Monti, L., Yang, W., Park, H., **Liu, L. J.**, Watkins, K., Amarasinghe, D. K., Nalli, M., Roberto Polaquini, C., Regasini, L. O., Eduardo Miller Crotti, A., Silvestri, R., Guidi Magalhães, L. & Caffrey, C. R. 2023. Structure-activity relationship of dibenzylideneacetone analogs against the neglected disease pathogen, *Trypanosoma brucei*. *Bioorg Med Chem Lett*, 81**,** 129123.

Hayat, O., Ullah, N., Sirajuddin, M., Giardini, M. A., Nguyen, J. V., Francisco, K. R., **Liu, L. J.**, Sun, Y. U., Maurya, S., Mcgrosso, D., Gonzalez, D. J., Caffrey, C. R., Debnath, A. & Siqueira-Neto, J. L. 2022. A broad spectrum antiparasitic activity of organotin (IV) derivatives and its untargeted proteomic profiling using *Leishmania donovani*. *Pathogens*, 11.

Jiang, Z., Silva, E. B., Liu, C., Fajtová, P., **Liu, L. J.**, El-Sakkary, N., Skinner, D. E., Syed, A., Wang, S. C., Caffrey, C. R., O'Donoghue, A. J. 2024. Development of subunit selective proteasome substrates for S*chistosoma species*. *biorxiv*.

Kanyanta, M., Lengwe, C., Mambwe, D., Francisco, K. R., **Liu, L. J.**, Sun, Y., Amarasinghe, D. K., Caffrey, C. R. & Mubanga Cheuka, P. 2023. Activity of N-phenylbenzamide analogs against the neglected disease pathogen, *Schistosoma mansoni*. *Bioorg Med Chem Lett*, 82**,** 129164.

Keller, L. J., Nguyen, T. H., **Liu, L. J.**, Hurysz, B. M., Lakemeyer, M., Guerra, M., Gelsinger, D. J., Chanin, R., Ngo, N., Lum, K. M., Faucher, F., Ipock, P., Niphakis, M. J., Bhatt, A. S., O'Donoghue, A. J., Huang, K. C. & Bogyo, M. 2023. Chemoproteomic identification of a DPP4 homolog in *Bacteroides thetaiotaomicron*. *Nat Chem Biol*, 19**,** 1469-1479.

Lucero, B., Francisco, K. R., **Liu, L. J.**, Caffrey, C. R. & Ballatore, C. 2023. Protein-protein interactions: developing small-molecule inhibitors/stabilizers through covalent strategies. *Trends Pharmacol Sci*, 44**,** 474-488.

Lucero, B., Francisco, K. R., Varricchio, C., **Liu, L. J.**, Yao, Y., Brancale, A., Brunden, K. R., Caffrey, C. R. & Ballatore, C. 2024. Design, Synthesis, and evaluation of an anti-trypanosomal [1,2,4]Triazolo[1,5-a]pyrimidine probe for photoaffinity labeling studies. *ChemMedChem***,** e202300656.

Monti, L., Cornec, A. S., Oukoloff, K., Kovalevich, J., Prijs, K., Alle, T., Brunden, K. R., Smith, A. B., El-Sakkary, N., **Liu, L. J.**, Syed, A., Skinner, D. E., Ballatore, C. & Caffrey, C. R. 2021. Congeners derived from microtubule-active phenylpyrimidines produce a potent and long-lasting paralysis of *Schistosoma mansoni in vitro*. *ACS Infect Dis,* 7**,** 1089-1103.

Monti, L., **Liu, L. J.**, Varricchio, C., Lucero, B., Alle, T., Yang, W., Bem-Shalom, I., Gilson, M., Brunden, K. R., Brancale, A., Caffrey, C. R. & Ballatore, C. 2023. Structure-activity relationships, tolerability and efficacy of microtubule-active 1,2,4-Triazolo[1,5-a]pyrimidines as potential candidates to treat Human African Trypanosomiasis. *ChemMedChem,* 18**,** e202300193.

Yeh, Y. T., Skinner, D. E., Criado-Hidalgo, E., Chen, N. S., Garcia-De Herreros, A., El-Sakkary, N., **Liu, L. J.**, Zhang, S., Kandasamy, A., Chien, S., Lasheras, J. C., Del Álamo, J. C. & Caffrey, C. R. 2022. Biomechanical interactions of *Schistosoma mansoni* eggs with vascular endothelial cells facilitate egg extravasation. *PLoS Pathog,* 18**,** e1010309.

Z, K. M., Sun, S., Mcconnon, C. L., Ma, K., Chen, E. K., Foil, D. H., Lane, T. R., **Liu, L. J.**, El-Sakkary, N., Skinner, D. E., Ekins, S. & Caffrey, C. R. 2021. A machine learning strategy for drug discovery identifies anti-schistosomal small molecules. *ACS Infect Dis,* 7**,** 406-420.

ABSTRACT OF THE DISSERTATION

The 20S proteasome as an antiparasitic drug target; activity-based probes, structure-activity relationship and *in vivo* efficacy

by

Lawrence Liu

Doctor of Philosophy in Chemistry

University of California San Diego, 2024

Professor Conor Caffrey, Chair
Professor Anthony O'Donoghue, Co-Chair
Professor Dionicio Siegel, Co-Chair

Worldwide, there are about 1,400 pathogens that infect humans. In particular, for the neglected diseases of poverty that are caused by eukaryotic pathogens, chemotherapy often relies on a small number of antiquated drugs that can be toxic, and for which resistance is either established or a concern.

Chapter 1 introduces the 20S proteasome, its biology and the use of small molecule inhibitors to treat various cancers, such as multiple myeloma. The chapter then describes the

current state-of-the-art regarding 20S proteasome inhibitor development for a range of parasitic diseases, not least, malaria and leishmaniasis, with the key point being that in spite of its conservation in life, inhibitor specificity to a particular 20S target can be achieved to deliver exciting new treatments.

Chapter 2 focuses on the synthesis and application of two novel activity-based probes, LJL-1 and LJL-2, each with a different specificity for the 20 proteasome of two parasitic organisms, *Leishmania donovani* and *Trichomonas vaginalis*. The probes were designed to enable the attachment of a bifunctional fluorescent-biotin handle via click chemistry to visualize and formally identify the component catalytic β subunits for each proteasome. Also, the probes are more specific to the 20S target and offer greater functionality compared to a well-described and commercially-available product.

Chapter 3 focuses on the whole-organism screening of *T. brucei* with and the development of a structure activity relationship (SAR) for a series of peptidyl, epoxyketone 20S inhibitors derived from the marine natural product, carmaphycin B (CPB). The compound collection stems from a campaign to develop *Plasmodium falciparum* 20S (Pf20S) inhibitors and the SAR arising is similar to that described for Pf20S. Not least is the strong toxicity differential between *T. brucei* and mammalian cells generated by the introduction of D stereochemistry at the P3 position of the CPB backbone. In a mouse model of *T. brucei* infection, one such inhibitor extended the survival of mice, thus, supporting the further development of this compound class as a potential treatment for African trypanosomiasis.

Chapter 1:

The Proteasome as a Drug Target for the Treatment of Parasitic Diseases

1.1. Introduction

The proteasome emerged as a validated drug target for cancer chemotherapy with the development and approval in 2003 of bortezomib (Velcade®) for treatment of multiple myeloma. Since then, progress has been rapid in the development of additional anti-cancer proteasome inhibitor (PI) drugs as well as the (pre)clinical progression of PIs that target the *Plasmodium* and trypanosomatid proteasomes, as discussed below. Here, we review the essential biology of the proteasome, PI development and the exciting prospect that this complex molecular machine is a useful drug target for treating a range of parasitic diseases.

1.1.1. Proteasome structure and catalytic mechanism

The proteasome comprises a 20S core complex of 28 proteins [1] that is often associated with a 19S cap that is bound at one or both ends of the core to yield a complex termed the 26S or 30S proteasome, respectively [2]. The cap recognizes proteins targeted for degradation and propels them into the catalytically active 20S core for degradation.[3-5] The 750 kDa 20S proteasome comprises two heptameric rings of β subunits (β1- β7) that are sandwiched between two rings of α subunits, α1- α7.[6] The catalytic (peptidolytic) activity resides in the β1, β2 and β5 subunits which generate caspase-like, trypsin-like and chymotrypsin-like activity, respectively (Fig. 1.1).[4, 5, 7-9]

Cleavage by each of the three catalytic subunits is characterized as endopeptidolytic, meaning that hydrolysis occurs within internal peptide bonds of the target protein rather than at the N- or C-termini (exopeptidolytic).[10] Each catalytic subunit utilizes an N-terminal threonine as the nucleophile for catalysis.[11] At the same time, the threonine's terminal amine acts as a general base by polarizing an ordered water molecule which then deprotonates the alcohol on the threonine to form an nucleophilic alkoxide.[11]

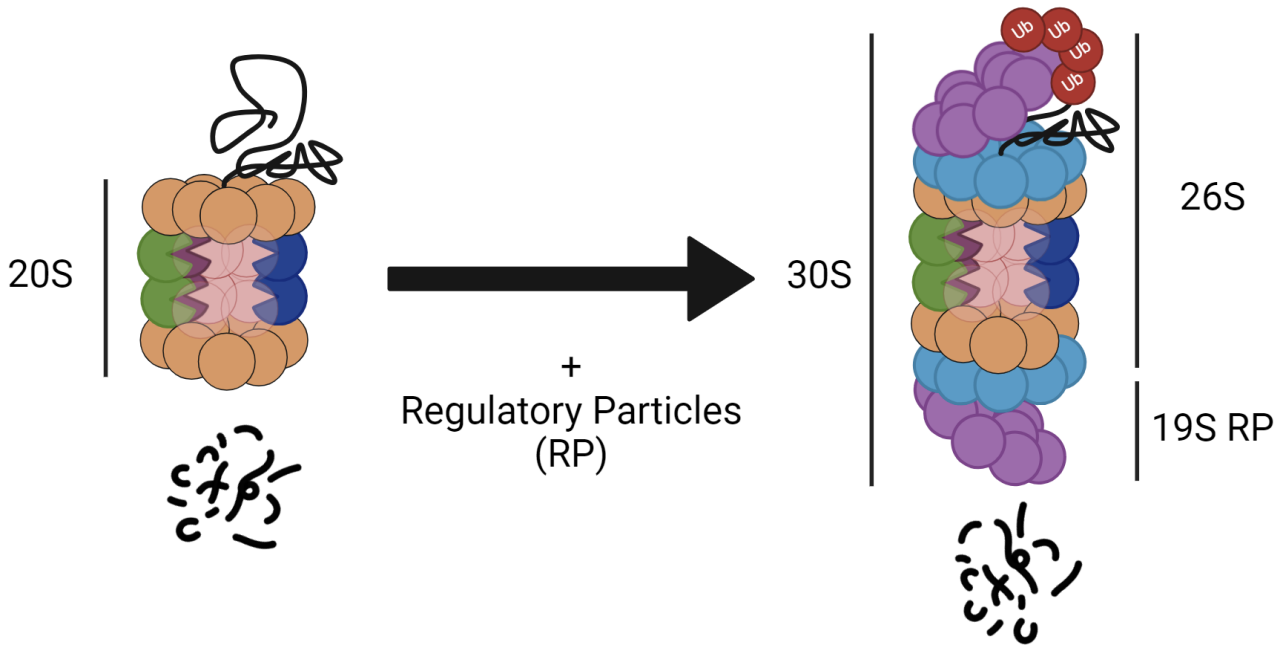


Figure 1.1. The 20S, 26S and 30S proteasome structures.

1.1.2. The ubiquitin proteasome system (UPS) and the unfolded protein response (UPR)

For the most part, proteins earmarked by the cell for degradation must be first ubiquitinated.[12] Ubiquitin is a conserved 76 amino acid protein that is found in all eukaryotic cells. Proteins that are targeted for degradation by the cell are tagged with one or more units of ubiquitin (Fig. 1.2), which requires the activity of three enzymes: E1 (ubiquitin-activating), E2 (ubiquitin-conjugating) and E3 (ubiquitin-ligating). The ubiquitinated protein then interacts with the 26S proteasome at which point the ubiquitin is released from the target protein via deubiquitinating enzymes (DUBs) and recycled [3], and the target protein is unfolded, directed into the 20S core and degraded into peptides.[13] This sequence of events makes up the ubiquitin proteasome system (UPS) and is ATP-dependent.[14]

The unfolded protein response (UPR) is a reactionary mechanism employed by the cell in response to an increase in misfolded proteins, especially in the endoplasmic reticulum.[15] The

response involves a cessation of protein translation, an increase in the production of molecular chaperones, and degradation of misfolded proteins by the proteasome, all in an attempt by the cell to return to normality.[16, 17] If the UPR is sustained, organelle dysfunction occurs along with the formation of reactive oxygen species, and, eventually, the cell enters into apoptosis.[18] The UPR relies on a functioning proteasome to degrade the misfolded proteins.[19] When the proteasome is inhibited, for example, by small molecule PIs, cell death via apoptosis can occur.[20]

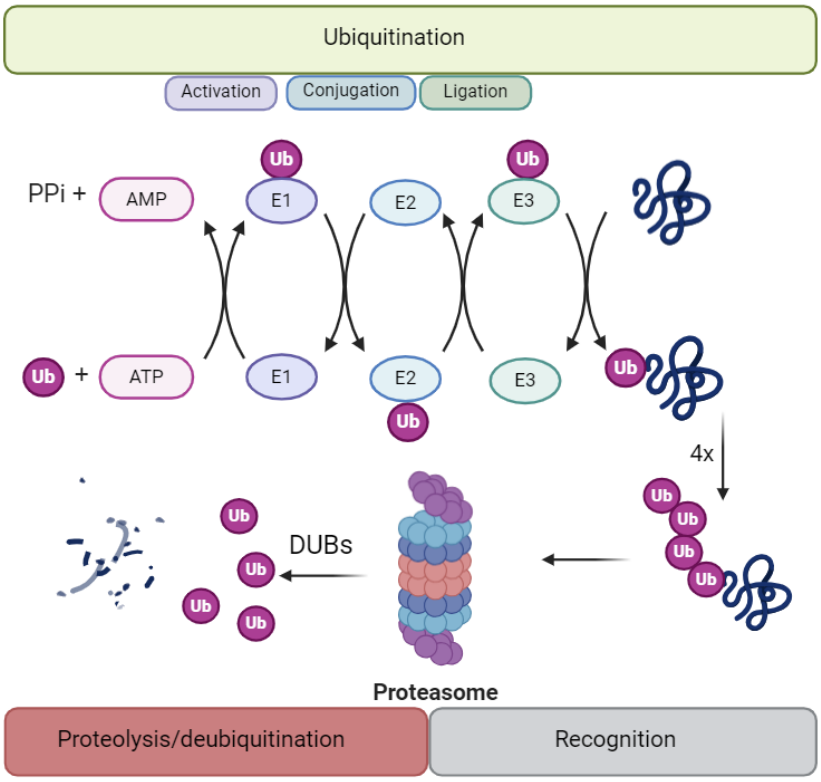


Figure 1.2. Schematic of the UPS. The UPS occurs once E1 uses ATP to activate ubiquitin (Ub). The activated Ub is transferred to E2 and finally to E3. E3 also recognizes and accepts the targeted protein on which polyubiquitination occurs. The polyubiquitinated protein is transferred to the 26S or 30S proteasome where proteolysis takes place. Ub is recycled by deubiquitinating enzymes (DUBs) to be used again.[18]

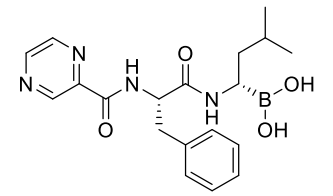
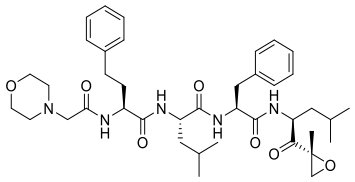
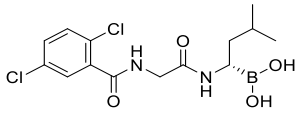
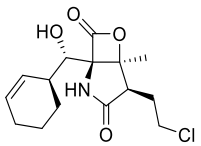
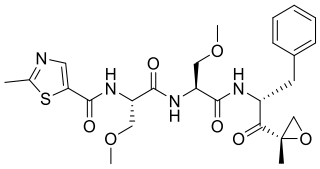
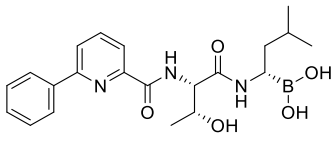
1.1.3. History and application of the major proteasome inhibitor (PI) chemotypes

There are currently three FDA approved PIs, bortezomib (BTZ), carfilzomib (CFZ) and ixazomib (IXZ) for treatment of multiple myeloma and mantle cell lymphoma, with several others

in stage II clinical trials [21] (Table 1). The peptidyl boronic acid, BTZ, was approved in 2003, leading the way for PIs as chemotherapeutics by demonstrating that inhibition of the proteasome was cidal and could eliminate tumors.[22] In 2012, CFZ was approved to treat multiple myeloma.[23] CFZ differs from BTZ in the composition of its peptidyl backbone and reactive group (also known as a warhead). The reversible covalent boronic acid group of BTZ is replaced by an irreversibly-binding epoxyketone group.[24] Studies have shown that CFZ is effective against several BTZ-resistant multiple myeloma cell lines.[25] Finally, IXZ was approved for use in humans in 2015, and has the advantage of being orally bioavailable, whereas BTZ and CFZ must be administered intravenously.[26] IXZ is a prodrug, ixazomib citrate, which contains a boronic citrate ester that is hydrolyzed under physiologic conditions into the active boronic acid form.[27]

Other PIs incorporating a BTZ- or CFZ-like scaffold include oprozomib and delanzomib (Table 1). These compounds are in clinical trials in which the goals are to improve oral bioavailability and demonstrate efficacy against BTZ-resistant multiple myeloma.[28, 29] Another PI in phase III clinical trials is salinosporamide A, also known as marizomib (MZB). This non-peptidic PI, isolated from the marine bacterium, *Salinispora tropica*, is unique in containing a β-lactone-γ-lactam structure.[30] Unlike BTZ, CFZ and IXZ, MZB inhibits all three catalytic β subunits (Table 1, see below), and its ability to cross the blood brain barrier has enabled its progress to phase III clinical trials for treatment of glioblastoma.[31, 32]

Table 1.1 List of PIs, either in clinical trials or approved as drugs.

Name	Bortezomib	Carfilzomib	Ixazomib	Marizomib	Oprozomib	Delanzomib
Structure						
Warhead	Boronate	Epoxyketone	Boronate	β-lactone	Epoxyketone	Boronate
Binding	Reversible	Irreversible	Reversible	Irreversible	Irreversible	Reversible
β subunit targeted	β5 > β1	β5 > β2	β5 > β1	β5 > β2 > β1	β5	β5 > β1
Clinical status	FDA approved	FDA approved	FDA approved	Stage III Clinical trials	Stage II Clinical trials	Stage II Clinical trials
Indication	First-line, refractory/relapsed multiple myeloma and mantle cell lymphoma	Refractory/ relapse multiple myeloma	Refractory/ relapsed multiple myeloma	Refractory/ relapsed multiple myeloma and glioblastoma	Refractory/ relapsed multiple myeloma	Refractory/ relapsed multiple myeloma

As summarized above, PIs are proven drugs in the treatment of various cancers.[33] Because the proteasome is evolutionarily conserved and essential to life, the possible application of PIs in

the treatment of parasitic diseases was considered as early as in the 1980s. From then and through the 1990s, research focused on identifying and characterizing the respective parasite proteasomes at the RNA or protein levels.[34] An antibody, MCP231, to the α subunits of the human constitutive proteasome (c20S), was also commonly used to identify the proteasome in parasite extracts (see below). Finally, the development of a fluorescent activity-based probe (ABP) called Bodipy tetramethylrhodamine (TMR)-Ahx(3)Leu(3)VS (aka MV151) in 2006 [35], and the subsequent commercialization of an analog containing Bodipy fluorescein (FL) instead of Bodipy TMR, made it possible to visualize functionally active proteasome subunits in cell extracts via SDS-PAGE.

At least initially, the possibility of generating inhibitor specificity was considered challenging due to the evolutionary conservation of the proteasome, and the fact that the small molecule PIs available at the time were non-discriminatory such that a selectivity index, *i.e.*, the differential between killing the parasite *versus* the host cell, was essentially zero. Over the past 15 years, however, this perception has changed dramatically. Inhibitors with improved specificity to the parasite 20S target have been developed, driven by the imperative to develop and/or maintain the drug development pipeline for infectious disease such as malaria and the trypanosomatid diseases, and aided by (i) access to industrial-scale small molecule libraries to perform high-throughput screens, and (ii) a better understanding of the cleavage specificities of the three catalytically active β subunits. For malaria and the trypanosomatid diseases, this research has had underwriting from international product development partnerships such as the Medicines for Malaria Venture (MMV) and the Drugs for Neglected Diseases *initiative* (DND*i*), which have generated a number of drug candidates that are preclinically or clinically advanced.[36, 37]

The interaction of any proteolytic enzyme, such as the 20S proteasome, with its peptidyl substrate can be viewed as a lock and key mechanism whereby specific subsites (S) in the catalytic

β subunits engage specific amino acid residue positions (P) along the backbone of the substrate (Fig. 1.3).[38] The amino acids are numbered in both directions from the scissile (cleavable) bond, with prime numbers being used for those residues to the right, or in the C-terminal direction, of the bond, and non-prime numbers in the N-terminal direction (Fig. 1.3). The efficiency of substrate cleavage by proteases is driven by the underlying preferences for particular amino acids at certain positions along the peptide backbone. Understanding these preferences in the 20S proteasome is critically important in the design of specific PIs, as illustrated throughout this thesis.

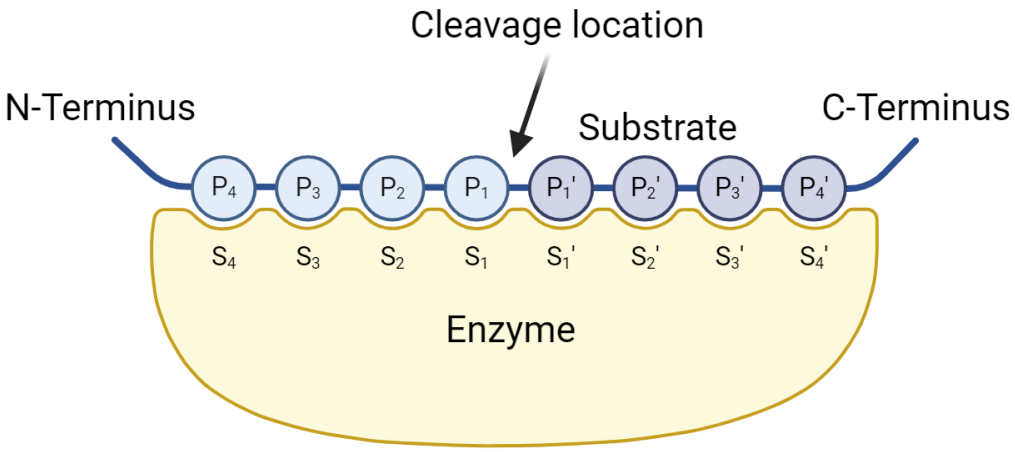


Figure 1.3. Schechter and Berger nomenclature for the interaction between proteolytic enzymes and their protein substrates. Amino acid residues in a protein substrate are numbered P1-P4 in the N-terminal direction, and P1'- P4' in the C-terminal direction from the cleavage point, which occurs between P1 and P1'. Subsites in the protease that accept the amino acid residues are correspondingly labelled S4 through S4'.[38]

Kinetoplastids comprise a diverse array of non-pathogenic and parasitic protozoa distinguished in their motility that employs a single flagellum and a specialized compartment of the mitochondrion, the kinetoplast, that contains concatenated DNA circles.[39] Kinetoplastids contain the important human pathogens, *Trypanosoma brucei*, *Trypanosoma cruzi* and *Leishmania*

spp., which are transmitted by various insect vectors and cause the diseases, African trypanosomiasis, Chagas' disease and leishmaniasis, respectively, which involve invasion of and proliferation within the skin, internal organs and/or central nervous system.[40]

1.2.1.1. *Trypanosoma brucei*

In 1996, Wang and colleagues first purified the *T. brucei* 20S proteasome (Tb20S) from parasite extracts and identified several differences between Tb20S and c20S, including mobility by SDS-PAGE, a lack of reactivity to anti-c20S antibodies and a greater β2 activity relative to the activity of β5.[41] Interestingly, β1 activity could not be identified by biochemical assays even though the genome indicates the presence of such, and that subsequent RNA interference (RNAi) to block the expression of β1 as well as the other subunits was lethal to the parasite.[41, 42] In a follow-up report, the same authors noted the presence of only the β2 and β5 subunits in *T. brucei* extracts by covalent affinity labeling with radiolabeled, tripeptidyl, vinyl sulfone PIs. Also, by using one position-fixed tetrapeptidyl substrate libraries, they identified differences in the cleavage specificities at the P1-P4 positions between Tb20S and c20S, particularly the preferential cleavage by Tb20S of P1-glutamine substrates.[43] Overall, the data indicated that there are likely functional differences between the trypanosome and human enzymes, encouraging from the point of view of developing specific anti-trypanosomal PIs.

Over a similar time period, Steverding and colleagues, using whole cell assays with *T. brucei*, demonstrated low nanomolar to low micromolar cidal activities of PIs containing aldehyde, boronate, vinyl sulfone and epoxyketone warheads.[44-46] Interestingly, the parasite was shown to be especially sensitive to inhibitors of the major trypsin-like (*i.e.*, β2) activity, which may provide a targeting differential given that the trypsin activity in the c20S anti-target is less pronounced.[45]

Although the foregoing studies indicated the possibility of targeting Tb20S as a therapy for African trypanosomiasis, it wasn't until 2013 when numerous PIs with the necessary specificity and low toxicity were discovered in overlapping programs. Whole organism (phenotypic) screens with *T. brucei* were crucial to the initial discovery of these inhibitors, however, their subsequent characterization and modification involved the use of both *T. cruzi* and *Leishmania donovani* to eventually develop a clinical drug candidate for treatment of visceral leishmaniasis, as discussed below.

The first breakthrough came with the report of Ferrins *et al.* [47] who performed a phenotypic screen of *T. brucei* using 87,000 small molecules to identify an azabenzoxazole compound that was identical to a molecule found a year later by Tatipacka *et al.* [48] who had used a similar screen employing 700,000 compounds. The compound emerged yet again as GNF5343 (Fig. 1.4A) in a third paper by Khare *et al.* who had phenotypically screened *T. brucei*, *T. cruzi* and *L. donovani* with 3 million small molecules.[49] Specifically, after triaging for compounds that had EC_{50} values <10 μM and selectivity index (SI) values >5 relative to mammalian cells, GNF5343 stood out with EC_{50} values of 150 and 75 nM for *T. brucei* and *T. cruzi,* respectively, and 7.3 μM for *L. donovani*. Extensive chemical modification to improve metabolic properties and potency yielded GNF6702 (Fig. 1.4A), which contained a triazolopyrimidine core instead of the previous azabenzoxazole. EC_{50} values of 70, 120 and 18 nM were measured for *T. brucei*, *T. cruzi* and *L. donovani,* respectively. Upon oral dosing, the molecule showed remarkable decreases of parasitemia or apparent cure in animal models of visceral and cutaneous leishmaniasis, Chagas disease and stage II (CNS-infiltrated) human African trypanosomiasis, competing with or outperforming the current standard of care drugs for these indications.[49]

In terms of the molecular target, by applying increasing drug pressure to *T. cruzi* epimastigotes over the course of one year with two azabenzoxazoles structurally related to GNF6702, a homozygous mutation, Ile29Met, in the gene encoding the β4 proteasome subunit, was identified, strongly implicating the proteasome as the molecular target for this class of inhibitor.[49] This was confirmed by assaying for *T. cruzi* 20S proteasome activity with catalytic β subunit-specific substrates which indicated that the target of GNF6702 was β5.[49] However, curious as to the non-competitive mode of inhibition measured and the genomic data from the resistance studies, the authors eventually discovered that the compound actually binds to a unique interface between the β4 and β5 subunits, which is not present in c20S, to sterically block access by substrate to the catalytic activity of β5.[49]

Separately, Wyllie *et al*. reported the discovery of a structurally similar compound, GSK-1 (Fig. 1.4B), after a phenotypic screen of *T. cruzi* axenic amastigotes with 15,659 diverse compounds.[50] GSK-1 and close analogs also had activity in a *L. donovani* intramacrophage assay. Focusing on the latter parasite, GSK-1 was optimized for solubility, genotoxicity and metabolic properties to yield GSK245 (aka GSK3494245, DDD01305143; Fig. 1.4B) that had EC_{50} values of ~1 μM against various clinical isolates of *L. donovani*, including a strain resistant to antimony – the active ingredient in pentavalent antimonial drugs.

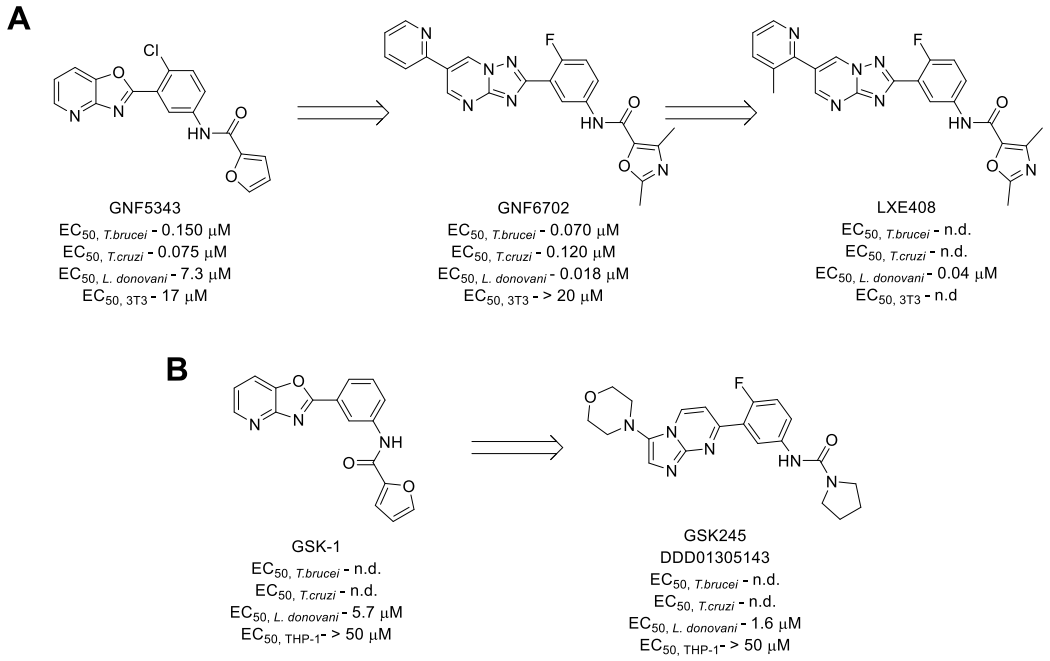


Figure 1.4 Kinetoplast β4/β5 interface PIs. A. Optimization of LXE408 [51] from GNF5343 [49] and then GNF6702.[49] **B.** Optimization of GSK245.[50] *T. brucei* bloodstream forms, *T. cruzi* amastigotes and *L. donovani* amastigotes, as well as the fibroblast and monocyte cell lines, 3T3 and THP-1, respectively, were used to generate the data shown. n.d., not determined.

When 25 mg/kg GSK245 was administered orally to mice infected with *L. donovani* twice a day for 10 days, a >95% reduction of parasitemia was measured, similar to that recorded with the current anti-leishmanial drug, miltefosine, given at 30 mg/kg once daily.[50] Mode of action investigations with RNAi suggested that the ubiquitin-proteasome system was being perturbed by GSK245, consistent with the data arising from the resistance studies performed by Khare *et al.* (2016).[49] Three independently-generated resistant clones were sequenced to reveal homozygous mutations within the genes encoding the β4 and β5 subunits. Cryo-electron microscopy (EM) structures of GSK245 bound to the *Leishmania tarentolae* 20S proteasome identified a new binding site that is situated between the β4 and β5 subunits and that differs from the site suggested by Khare *et al*. in *T. cruzi*.[49] As of December 2023, GSK245 is advancing toward clinical trials

under the stewardship of the DND*i*. The latest project update on the DND*i* website (as of March 2024) indicates that a planned Phase I single ascending dose trial is paused "to perform additional investigations into the compound's complex pharmacokinetics." [52]

1.2.1.2. *Leishmania donovani* and *L. major*

L. donovani is the causative agent of visceral leishmaniasis. The life cycle of *L. donovani* is similar to *T. cruzi* in that it replicates in host cells to eventually rupture from them and escape. As discussed above, potent and specific azabenzoxazoles, such as GNF5343, and triazolopyrimidines, like GNF6702, have been reported.

GNF6702 was further modified by Novartis by the addition of a methyl group to yield LXE408 (Fig. 1.4A) which further improved solubility and oral exposure.[51] Like its predecessors, LXE408 binds at the interface of the β4 and β5 subunits of Ld20S to allosterically inhibit β5 chymotrypsin-like activity. Mice infected with *L. major*, the causative agent of cutaneous leishmaniasis, were dosed orally with 1, 3, 10 and 20 mg/kg of LXE408 twice daily, and lesion size at the base of the tail was tracked. Administration of LXE408 for 10 days at a highest dose decreased lesion size to near zero and was comparable to that of liposomal amphotericin B, the most potent CL therapy on the market currently.[51]

1.2.2. Metamonada

The phylum Metamonada consists of a diverse group of flagellate protozoa. Rather than possessing typical mitochondria, these organisms contain mitochondrial-like organelles [53] that are more suitable to operating in low-oxygen conditions.[54]

1.2.2.1. *Trichomonas vaginalis*

The sexually transmitted disease, trichomoniasis, is caused by *T. vaginalis* with millions of cases worldwide. Several recent studies have shown that the proteasome is a viable target. Pereira-Neves *et al.,* in 2015, reported the presence of 20S genes in the genome of the related, trichomonad-model organism, *Tritrichomonas foetus*, and provided biochemical evidence for its activity.[55] They found that Tf20S was homogenously distributed in the cytosol and around the nucleus as punctate structures using an anti-*T. cruzi* proteasome antibody. A purification scheme involving ultracentrifugation was developed and the catalytic subunits of the enriched 20S were assayed with fluorogenic substrates. The PI, lactacystin (a *Streptomyces* product), at 10 and 20 μM for 18 h inhibited *T. foetus* growth and blocked transformation from the "pear-shaped" form to the pseudocystic (endoflagellar) form.[55] Interestingly, parasites produced more proteasome in response to incubation with 20 μM lactacystin, a phenomenon also reported for mammalian cells.[56, 57]

Characterization of the *T. vaginalis* 20S proteasome (Tv20S) was first reported by O'Donoghue *et al.* wherein a series of anti-cancer boronic acid and epoxyketone PIs were screened against the parasite.[58] Most of the inhibitors generated EC_{50} values between 0.1 and 1.0 μM, however, selectivity indices with respect to HeLa cells were <1. Several analogs of the peptidyl epoxyketone, carmaphycin B (a *Symploca* cyanobacterium product), were then evaluated and one, CP-17 (Fig. 1.5), generated a selectivity index of 11, principally based on decreased toxicity to HeLa cells. Importantly, parasite resistance to the current standard of care, metronidazole, did not influence PI activity. Using purified Tv20S, CP-17 targeted the β5 subunit and, less so, the β1 subunit, whereas only β5 in the human c20S was engaged, suggesting that Tv20S is functionally different from the human anti-target. In a mouse model of *T. foetus* infection, five doses of CP-17

in PBS were administered intravaginally over three days and a 20-fold decrease in parasitemia was recorded in vaginal washes. Thus, this report highlights the possibility of PIs as a novel therapeutic approach for trichomoniasis.[58]

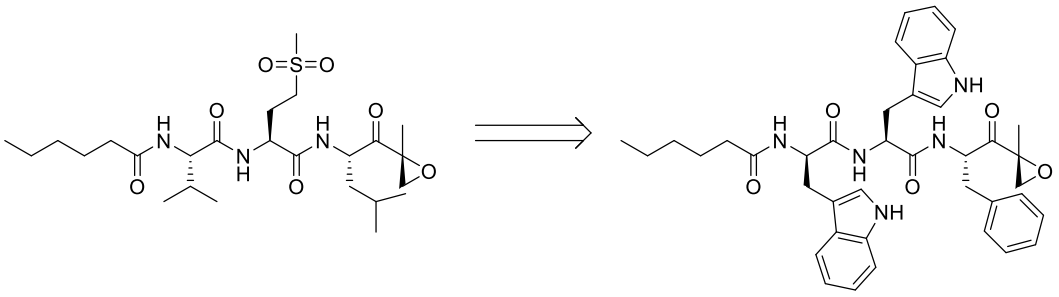


Figure 1.5. Carmaphycin B and its analog, CP-17, *vs*. *T. vaginalis in vitro*

In a follow up report, Fajtová *et al*. employed multiplex substrate profiling by mass spectrometry (MSP-MS) to characterize the cleavage specificities of each of the three Tv20S catalytic β subunits, information that is important to deriving more selective PIs.[59] MSP-MS was performed in the presence of various PIs that differentially inhibit one or other β subunit. The resulting cleavage profiles then informed the design and synthesis of β subunit-specific, tetrapeptidyl, fluorogenic substrates. These substrates were cleaved with higher specific activities than those used to measure the activities of the corresponding c20S β subunits.[59]

In a first for parasite proteasome research, and based on the report of Toste Rêo and da Fonseca with c20S [60], a fully active Tv20S was recombinantly expressed in Sf9 cells by Silhan *et al.*[61] This involved preparing baculovirus containing three plasmids that would express (i) the seven α subunits, (ii) the seven β subunits and (iii) Ump-1, which is required for the correct assembly and enzymatic activation of the proteasome.[62] In addition, a C-terminal twin-strep purification tag was encoded into the β7 subunit sequence. The β7 subunit is the last subunit

incorporated into the α/β half proteasome, and therefore, the C-terminal tag was predicted to have little effect on 20S assembly.[63, 64] After co-infection of Sf9 cells with baculovirus, the recombinant Tv20S was expressed and purified from cell extracts using a Strep-Tactin XT column and size-exclusion chromatography. Using fluorogenic substrates and the fluorescent ABP, Me4BodipyFL-Ahx3Leu3VS, the recombinant enzyme was determined to be biochemically indistinguishable from the native enzyme. As found for the native Tv20S [58], the CPB analog, CP-17, inhibited the recombinant Tv20S β5, as well as β2 (which had not been previously assayed), and MZB inhibited all three recombinant catalytic subunits. Produced in high yield (1 mg/L) and >95% pure, cryo-EM structural studies elucidated the binding modes of CP-17 and MZB with the recombinant Tv20S, and demonstrated that the S1 and S3 subsites of the β2 and β5 subunits are sufficiently different from those in the human c20S anti-target to support structure-guided inhibitor design.[61]

1.3. Tools to characterize the proteasome

Understanding the optimal amino acid sequence in a peptidyl PI for a particular parasite proteasome drives potency and specificity, while decreasing toxicity. In this context, techniques such as MSP-MS [65] and positional scanning synthetic combinatorial libraries [66] have been important in characterizing the cleavage specificities of individual proteasome β subunits.[67, 68] Both techniques employ peptidyl substrate libraries and the cleaved products can be quantified by either mass spectrometry or fluorimetry.

Such approaches have been successful for Tv20S [59], as described above, and the *Schistosoma mansoni* 20S proteasome (Sm20S).[68] Once catalytic β subunit-specific substrates have been identified and validated, they then become tools to interrogate the binding specificity of

PIs, or, are themselves converted into PIs by the incorporation of, for example, a vinyl sulfone [69] or epoxyketone warhead.[70]

Fluorescent ABPs such as Bodipy FL-Ahx(3)Leu(3)VS allow the formal identification of the catalytic β subunit(s) in a given parasite proteasome. This has been demonstrated for purified Tv20s [59] and Pf20S [71] whereby the individual fluorescent β subunit bands resolved by SDS-PAGE were excised and the component proteins identified by proteomics.

Importantly, as research with ABPs has progressed, it has become clear that not all ABPs react the same. For example, MV151 only bound to two of the three catalytic β subunits of Pf20S [72] whereas BMV037 (an epoxyketone PI based on carfilzomib) reacted with all three.[71] In addition, labelling by BMV037 revealed that the order in which the catalytic β subunits of Pf20S migrate by SDS-PAGE is different from that of c20S; specifically, highest to lowest, it was β1, β2 and β5 for Pf20S [71], but β2, β1 and β5 for c20S.[35] Thus, ABPs have helped identify differences between the parasite and host proteasome that should facilitate the development of parasite-specific PIs.

Finally, Cryo-EM has aided our understanding of the structural organization of the catalytic β subunits, as well their particular binding contacts with PIs, which, together, have improved the design of PIs, as reported for the Pf20S[73-75] and Tv20S.[61] With our recent ability to recombinantly express the 20S proteasome, based on the seminal work of Toste Rêo and da Fonseca with c20S [60] and, as recently described for Tv20S by Silhan *et al.* [61], cryo-EM will become an increasingly important tool in the design and synthesis cycle of PIs with improved potency and selectivity to the parasite 20S of interest.

1.4. Acknowledgements

Chapter 1 is an abridged version of the accepted manuscript in *Advance in Parasitology* titled "The proteasome as a drug target for treatment of parasitic diseases." Figures 1, 2 and 3 were created using Biorender.com (2024); otherwise, ChemDraw 20.1.1. was used to draw chemical structures. The research of the authors on parasite proteasomes is supported in part by NIH awards R21AI133393 and R21AI171824 to AJO and CRC, and R01AI158612 and R21AI146387 to AJO.

1.5. References

(1) Bard, J. A. M.; Goodall, E. A.; Greene, E. R.; Jonsson, E.; Dong, K. C.; Martin, A. Structure and Function of the 26S Proteasome. *Annu Rev Biochem* **2018**, *87*, 697-724. DOI: 10.1146/annurev-biochem-062917-011931.

(2) Sahu, I.; Glickman, M. H. Proteasome in action: substrate degradation by the 26S proteasome. *Biochem Soc Trans* **2021**, *49* (2), 629-644. DOI: 10.1042/bst20200382.

(3) Jung, T.; Grune, T. Structure of the proteasome. *Prog Mol Biol Transl Sci* **2012**, *109*, 1-39. DOI: 10.1016/b978-0-12-397863-9.00001-8.

(4) Bibo-Verdugo, B.; Jiang, Z.; Caffrey, C. R.; O'Donoghue, A. J. Targeting proteasomes in infectious organisms to combat disease. *FEBS J* **2017**, *284* (10), 1503-1517. DOI: 10.1111/febs.14029.

(5) Rousseau, A.; Bertolotti, A. Regulation of proteasome assembly and activity in health and disease. *Nat Rev Mol Cell Biol* **2018**, *19* (11), 697-712. DOI: 10.1038/s41580-018-0040-z.

(6) Kopp, F.; Hendil, K. B.; Dahlmann, B.; Kristensen, P.; Sobek, A.; Uerkvitz, W. Subunit arrangement in the human 20S proteasome. *Proc Natl Acad Sci U S A* **1997**, *94* (7), 2939-2944. DOI: 10.1073/pnas.94.7.2939.

(7) Tanaka, K. The proteasome: overview of structure and functions. *Proc Jpn Acad Ser B Phys Biol Sci* **2009**, *85* (1), 12-36. DOI: 10.2183/pjab.85.12.

(8) Collins, G. A.; Goldberg, A. L. The Logic of the 26S Proteasome. *Cell* **2017**, *169* (5), 792-806. DOI: 10.1016/j.cell.2017.04.023.

(9) Xie, S. C.; Dick, L. R.; Gould, A.; Brand, S.; Tilley, L. The proteasome as a target for protozoan parasites. *Expert Opin Ther Targets* **2019**, *23* (11), 903-914. DOI: 10.1080/14728222.2019.1685981.

(10) Seemüller, E.; Lupas, A.; Stock, D.; Löwe, J.; Huber, R.; Baumeister, W. Proteasome from Thermoplasma acidophilum: a threonine protease. *Science* **1995**, *268* (5210), 579-582. DOI: 10.1126/science.7725107.

(11) Morrison, H. *Enzyme Active Sites and their Reaction Mechanisms*; Academic Press, 2021.

(12) Lecker, S. H.; Goldberg, A. L.; Mitch, W. E. Protein degradation by the ubiquitin-proteasome pathway in normal and disease states. *J Am Soc Nephrol* **2006**, *17* (7), 1807-1819. DOI: 10.1681/asn.2006010083.

(13) Osana, S.; Kitajima, Y.; Naoki, S.; Takada, H.; Murayama, K.; Kano, Y.; Nagatomi, R. Little involvement of recycled-amino acids from proteasomal proteolysis in de novo protein synthesis. *Biochem Biophys Res Commun* **2022**, *634*, 40-47. DOI: 10.1016/j.bbrc.2022.09.113.
(14) Peth, A.; Nathan, J. A.; Goldberg, A. L. The ATP costs and time required to degrade ubiquitinated proteins by the 26 S proteasome. *J Biol Chem* **2013**, *288* (40), 29215-29222. DOI: 10.1074/jbc.M113.482570.
(15) Read, A.; Schröder, M. The Unfolded Protein Response: An Overview. *Biology (Basel)* **2021**, *10* (5). DOI: 10.3390/biology10050384.
(16) Hetz, C. The unfolded protein response: controlling cell fate decisions under ER stress and beyond. *Nat Rev Mol Cell Biol* **2012**, *13* (2), 89-102. DOI: 10.1038/nrm3270.
(17) Hetz, C.; Zhang, K.; Kaufman, R. J. Mechanisms, regulation and functions of the unfolded protein response. *Nat Rev Mol Cell Biol* **2020**, *21* (8), 421-438. DOI: 10.1038/s41580-020-0250-z.
(18) Ciechanover, A.; Schwartz, A. L. The ubiquitin-proteasome pathway: the complexity and myriad functions of proteins death. *Proc Natl Acad Sci U S A* **1998**, *95* (6), 2727-2730. DOI: 10.1073/pnas.95.6.2727.
(19) Obeng, E. A.; Carlson, L. M.; Gutman, D. M.; Harrington, W. J.; Lee, K. P.; Boise, L. H. Proteasome inhibitors induce a terminal unfolded protein response in multiple myeloma cells. *Blood* **2006**, *107* (12), 4907-4916. DOI: 10.1182/blood-2005-08-3531.
(20) Concannon, C. G.; Koehler, B. F.; Reimertz, C.; Murphy, B. M.; Bonner, C.; Thurow, N.; Ward, M. W.; Villunger, A.; Strasser, A.; Kögel, D.; Prehn J. H. M. Apoptosis induced by proteasome inhibition in cancer cells: predominant role of the p53/PUMA pathway. *Oncogene* **2007**, *26* (12), 1681-1692. DOI: 10.1038/sj.onc.1209974.
(21) Kisselev, A. F.; van der Linden, W. A.; Overkleeft, H. S. Proteasome inhibitors: an expanding army attacking a unique target. *Chem Biol* **2012**, *19* (1), 99-115. DOI: 10.1016/j.chembiol.2012.01.003.
(22) Chen, D.; Frezza, M.; Schmitt, S.; Kanwar, J.; Dou, Q. P. Bortezomib as the first proteasome inhibitor anticancer drug: current status and future perspectives. *Curr Cancer Drug Targets* **2011**, *11* (3), 239-253. DOI: 10.2174/156800911794519752.
(23) Groen, K.; van de Donk, N.; Stege, C.; Zweegman, S.; Nijhof, I. S. Carfilzomib for relapsed and refractory multiple myeloma. *Cancer Manag Res* **2019**, *11*, 2663-2675. DOI: 10.2147/cmar.S150653.
(24) Kim, K. B.; Crews, C. M. From epoxomicin to carfilzomib: chemistry, biology, and medical outcomes. *Nat Prod Rep* **2013**, *30* (5), 600-604. DOI: 10.1039/c3np20126k.
(25) Kuhn, D. J.; Chen, Q.; Voorhees, P. M.; Strader, J. S.; Shenk, K. D.; Sun, C. M.; Demo, S. D.; Bennett, M. K.; van Leeuwen, F. W.; Chanan-Khan, A. A.; Orlowski, R. Z. Potent activity of carfilzomib, a novel, irreversible inhibitor of the ubiquitin-proteasome pathway, against preclinical models of multiple myeloma. *Blood* **2007**, *110* (9), 3281-3290. DOI: 10.1182/blood-2007-01-065888.
(26) Ramirez, K. Ixazomib: An Oral Proteasome Inhibitor for the Treatment of Multiple Myeloma. *Journal of the Advanced Practitioner in Oncology* **2017**, *8* (4), 4.
(27) Muz, B.; Ghazarian, R. N.; Ou, M.; Luderer, M. J.; Kusdono, H. D.; Azab, A. K. Spotlight on ixazomib: potential in the treatment of multiple myeloma. *Drug Des Devel Ther* **2016**, *10*, 217-226. DOI: 10.2147/dddt.S93602.

(28) Hari, P.; Matous, J. V.; Voorhees, P. M.; Shain, K. H.; Obreja, M.; Frye, J.; Fujii, H.; Jakubowiak, A. J.; Rossi, D.; Sonneveld, P. Oprozomib in patients with newly diagnosed multiple myeloma. *Blood Cancer J* **2019**, *9* (9), 66. DOI: 10.1038/s41408-019-0232-6.
(29) Seavey, M. M.; Lu, L. D.; Stump, K. L.; Wallace, N. H.; Ruggeri, B. A. Novel, orally active, proteasome inhibitor, delanzomib (CEP-18770), ameliorates disease symptoms and glomerulonephritis in two preclinical mouse models of SLE. *Int Immunopharmacol* **2012**, *12* (1), 257-270. DOI: 10.1016/j.intimp.2011.11.019.
(30) Gulder, T. A.; Moore, B. S. Salinosporamide natural products: Potent 20 S proteasome inhibitors as promising cancer chemotherapeutics. *Angew Chem Int Ed Engl* **2010**, *49* (49), 9346-9367. DOI: 10.1002/anie.201000728.
(31) Potts, B. C.; Albitar, M. X.; Anderson, K. C.; Baritaki, S.; Berkers, C.; Bonavida, B.; Chandra, J.; Chauhan, D.; Cusack, J. C.; Fenical, W.; Ghobrial, I. M.; Groll, M.; Jensen, P. R.; Lam, K. S.; Lloyd, G. K.; McBride, W.; McConkey, D. J.; Miller, C. P.; Neuteboom, S. T. C.; Oki, Y.; Ovaa, H.; Pajonk, F.; Richardson, P. G.; Roccaro, A. M.; Sloss, C. M.; Spear, M. A.; Valashi, E.; Younes, A.; Palladino, M. A. Marizomib, a proteasome inhibitor for all seasons: preclinical profile and a framework for clinical trials. *Curr Cancer Drug Targets* **2011**, *11* (3), 254-284. DOI: 10.2174/156800911794519716. Di, K.; Lloyd, G. K.; Abraham, V.; MacLaren, A.; Burrows, F. J.; Desjardins, A.; Trikha, M.; Bota, D. A. Marizomib activity as a single agent in malignant gliomas: ability to cross the blood-brain barrier. *Neuro Oncol* **2016**, *18* (6), 840-848. DOI: 10.1093/neuonc/nov299.
(32) Di, K.; Lloyd, G. K.; Abraham, V.; MacLaren, A.; Burrows, F. J.; Desjardins, A.; Trikha, M.; Bota, D. A. Marizomib activity as a single agent in malignant gliomas: ability to cross the blood-brain barrier. *Neuro Oncol* **2016**, *18* (6), 840-848. DOI: 10.1093/neuonc/nov299.
(33) Manasanch, E. E.; Orlowski, R. Z. Proteasome inhibitors in cancer therapy. *Nat Rev Clin Oncol* **2017**, *14* (7), 417-433. DOI: 10.1038/nrclinonc.2016.206.
(34) Caffrey, C. R.; Steverding, D.; Ferreira, R. S.; de Oliveira, R. B.; O'Donoghue, A. J.; Monti, L.; Ballatore, C.; Bachovchin, K. A.; Ferrins, L.; Pollastri, M. P.; Zorn, K. M.; Foil, D. H.; Clark, A. M.; Mottin, M.; Andrade, C. H.; de Siqueira-Neto, J. L.; Ekins, S. Drug Discovery and Development for Kinetoplastid Diseases. *Burger's Medicinal Chemistry and Drug Discovery* **2021**, 79.
(35) Verdoes, M.; Florea, B. I.; Menendez-Benito, V.; Maynard, C. J.; Witte, M. D.; van der Linden, W. A.; van den Nieuwendijk, A. M.; Hofmann, T.; Berkers, C. R.; van Leeuwen, F. W.; Groothuis, T. A.; Leeuwenburgh, M. A.; Ovaa H.; Neefjes, J. J.; Filippov, D. V.; van der Marel, G. A.; Dantuma, N. P. Overkleeft, H. S. A fluorescent broad-spectrum proteasome inhibitor for labeling proteasomes in vitro and in vivo. *Chem Biol* **2006**, *13* (11), 1217-1226. DOI: 10.1016/j.chembiol.2006.09.013.
(36) MMV. *Medicines for Malaria Venture*. 2024. (accessed.
(37) DNDi. *Drugs for Neglected Disease Initiative*. 2024. (accessed.
(38) Schechter, I.; Berger, A. On the size of the active site in proteases. I. Papain. *Biochemical and Biophysical Research Communications* **1967**, *27*, 5.
(39) Cavalcanti, D. P.; de Souza, W. The Kinetoplast of Trypanosomatids: From Early Studies of Electron Microscopy to Recent Advances in Atomic Force Microscopy. *Scanning* **2018**, *2018*, 9603051. DOI: 10.1155/2018/9603051.

(40) Stuart, K.; Brun, R.; Croft, S.; Fairlamb, A.; Gürtler, R. E.; McKerrow, J.; Reed, S.; Tarleton, R. Kinetoplastids: related protozoan pathogens, different diseases. *J Clin Invest* **2008**, *118* (4), 1301-1310. DOI: 10.1172/jci33945.
(41) Hua, S.-b.; To, W.-Y.; Nguyen, T. T.; Wong, M.-L.; Wang, C. C. Purification and characterization of proteasomes from Trypanosoma brucei. *Molecular and biochemical Parasitology* **1996**, *78* (1-2), 13.
(42) Li, Z.; Zou, C. B.; Yao, Y.; Hoyt, M. A.; McDonough, S.; Mackey, Z. B.; Coffino, P.; Wang, C. C. An easily dissociated 26 S proteasome catalyzes an essential ubiquitin-mediated protein degradation pathway in Trypanosoma brucei. *J Biol Chem* **2002**, *277* (18), 15486-15498. DOI: 10.1074/jbc.M109029200.
(43) Wang, C. C.; Bozdech, Z.; Liu, C. L.; Shipway, A.; Backes, B. J.; Harris, J. L.; Bogyo, M. Biochemical analysis of the 20 S proteasome of Trypanosoma brucei. *J Biol Chem* **2003**, *278* (18), 15800-15808. DOI: 10.1074/jbc.M300195200.
(44) Nkemngu, N. J.; Rosenkranz, V.; Wink, M.; Steverding, D. Antitrypanosomal activities of proteasome inhibitors. *Antimicrob Agents Chemother* **2002**, *46* (6), 2038-2040. DOI: 10.1128/aac.46.6.2038-2040.2002.
(45) Steverding, D.; Spackman, R. W.; Royle, H. J.; Glenn, R. J. Trypanocidal activities of trileucine methyl vinyl sulfone proteasome inhibitors. *Parasitol Res* **2005**, *95* (1), 73-76. DOI: 10.1007/s00436-004-1253-y.
(46) Glenn, R. J.; Pemberton, A. J.; Royle, H. J.; Spackman, R. W.; Smith, E.; Jennifer Rivett, A.; Steverding, D. Trypanocidal effect of alpha',beta'-epoxyketones indicates that trypanosomes are particularly sensitive to inhibitors of proteasome trypsin-like activity. *Int J Antimicrob Agents* **2004**, *24* (3), 286-289. DOI: 10.1016/j.ijantimicag.2004.02.023.
(47) Ferrins, L.; Rahmani, R.; Sykes, M. L.; Jones, A. J.; Avery, V. M.; Teston, E.; Almohaywi, B.; Yin, J.; Smith, J.; Hyland, C.; White, K. L.; Ryan, E.; Campbell, M.; Charman, S. A.; Kaiser, M.; Baell, J. B. 3-(Oxazolo[4,5-b]pyridin-2-yl)anilides as a novel class of potent inhibitors for the kinetoplastid *Trypanosoma brucei*, the causative agent for human African trypanosomiasis. *Eur J Med Chem* **2013**, *66*, 450-465. DOI: 10.1016/j.ejmech.2013.05.007.
(48) Tatipaka, H. B.; Gillespie, J. R.; Chatterjee, A. K.; Norcross, N. R.; Hulverson, M. A.; Ranade, R. M.; Nagendar, P.; Creason, S. A.; McQueen, J.; Duster, N. A.; Nagle, A.; Supek, F.; Molteni, V.; Wenzler, T.; Brun, R.; Glynne, R.; Buckner, F. S.; Gelb, M. H. Substituted 2-phenylimidazopyridines: a new class of drug leads for human African trypanosomiasis. *J Med Chem* **2014**, *57* (3), 828-835. DOI: 10.1021/jm401178t.
(49) Khare, S.; Nagle, A. S.; Biggart, A.; Lai, Y. H.; Liang, F.; Davis, L. C.; Barnes, S. W.; Mathison, C. J.; Myburgh, E.; Gao, M. Y.; Gillespie, J. R.; Liu, X.; Tan, J. L.; Stinson, M.; Rivera, I. C.; Ballard, J.; Yeh, V.; Groessl, T.; Federe, G.; Koh, H. X. Y.; Venable, J. D.; Bursulaya, B.; Shaprio, M.; Kishra, P. K.; Spraggon, G.; Brock, A.; Mottram, J. C.; Buckner, F. S.; Rao, S. P. S.; Wen, B. G.; Walker, J. R.; Tuntland, T.; Molteni, V.; Glynne, R.; Supek, F. Proteasome inhibition for treatment of leishmaniasis, Chagas disease and sleeping sickness. *Nature* **2016**, *537* (7619), 229-233. DOI: 10.1038/nature19339.
(50) Wyllie, S.; Brand, S.; Thomas, M.; De Rycker, M.; Chung, C. W.; Pena, I.; Bingham, R. P.; Bueren-Calabuig, J. A.; Cantizani, J.; Cebrian, D.; Craggs, P. D.; Ferguson, L.; Goswami, P.; Hobrath, J.; Howe, J.; Jeacock, L.; Ko, E.; Korczynska, J.; Maclean, L.; Manthri, S.; Martinez, M. S.; Mata-Cantero, L.; Moniz, S.; Nühs, A.; Osuna-Cabello, M.; Pinto, E.;

Riley, J.; Robinson, S.; Rowland, P.; Simeons, F. R. C.; Shishikura, Y.; Spinks, D.; Stojanovski, L.; Thomas, J.; Thompson, S.; Gaza, E. V.; Wall, R. J.; Zuccotto, F.; Horn, D.; Ferguson, M. A. J.; Fairlamb, A. H.; Fiandor, J. M.; Martin, J.; Gray, D. W.; Miles, T. J.; Gilbert, I. H.; Read, K. D.; Marco, M.; Wyatt, P. G. Preclinical candidate for the treatment of visceral leishmaniasis that acts through proteasome inhibition. *Proc Natl Acad Sci U S A* **2019**, *116* (19), 9318-9323. DOI: 10.1073/pnas.1820175116.

(51) Nagle, A.; Biggart, A.; Be, C.; Srinivas, H.; Hein, A.; Caridha, D.; Sciotti, R. J.; Pybus, B.; Kreishman-Deitrick, M.; Bursulaya, B.; Lai, Y. H.; Gao, M.; Liang, F.; Mathison, J. N.; Liu, X.; Yeh, V.; Smith, J.; Lerario, I.; Xie, Y.; Chianelli, D.; Gibney, M.; Berman, A.; Chen, Y.; Jiricek, J.; Davis, L. C.; Liu, X.; Ballard, J.; Khare, S.; Eggimann, F. K.;Leneau, A.; Groessl, T.; Shaprio, M.; Richmond, W.; Johnson, K.; Rudewicz, P. J.; Rao, S. P. S.; Thompson, C.; Tuntland, T.; Spraggon G.; Glynne, R. J.; Supek, F.; Wiesmann, C.; Molteni, V. Discovery and Characterization of Clinical Candidate LXE408 as a Kinetoplastid-Selective Proteasome Inhibitor for the Treatment of Leishmaniases. *J Med Chem* **2020**, *63* (19), 10773-10781. DOI: 10.1021/acs.jmedchem.0c00499.

(53) Stairs, C. W.; Táborský, P.; Salomaki, E. D.; Kolisko, M.; Pánek, T.; Eme, L.; Hradilová, M.; Vlček, Č.; Jerlström-Hultqvist, J.; Roger, A. J.; Čepička, I. Anaeramoebae are a divergent lineage of eukaryotes that shed light on the transition from anaerobic mitochondria to hydrogenosomes. *Curr Biol* **2021**, *31* (24), 5605-5612.e5605. DOI: 10.1016/j.cub.2021.10.010.

(54) Leger, M. M.; Kolisko, M.; Kamikawa, R.; Stairs, C. W.; Kume, K.; Čepička, I.; Silberman, J. D.; Andersson, J. O.; Xu, F.; Yabuki, A.; Eme, L.; Zhang, Q.; Takishita, K.; Inagaki, Y.; Simpson, A. G. B.; Hashimoto, T.; Roger, A. J. Organelles that illuminate the origins of *Trichomonas* hydrogenosomes and *Giardia* mitosomes. *Nat Ecol Evol* **2017**, *1* (4), 0092. DOI: 10.1038/s41559-017-0092.

(55) Pereira-Neves, A.; Gonzaga, L.; Menna-Barreto, R. F.; Benchimol, M. Characterisation of 20S Proteasome in Tritrichomonas foetus and Its Role during the Cell Cycle and Transformation into Endoflagellar Form. *PLoS One* **2015**, *10* (6), e0129165. DOI: 10.1371/journal.pone.0129165.

(56) Balasubramanian, S.; Kanade, S.; Han, B.; Eckert, R. L. A proteasome inhibitor-stimulated Nrf1 protein-dependent compensatory increase in proteasome subunit gene expression reduces polycomb group protein level. *J Biol Chem* **2012**, *287* (43), 36179-36189. DOI: 10.1074/jbc.M112.359281.

(57) Steffen, J.; Seeger, M.; Koch, A.; Krüger, E. Proteasomal degradation is transcriptionally controlled by TCF11 via an ERAD-dependent feedback loop. *Mol Cell* **2010**, *40* (1), 147-158. DOI: 10.1016/j.molcel.2010.09.012.

(58) O'Donoghue, A. J.; Bibo-Verdugo, B.; Miyamoto, Y.; Wang, S. C.; Yang, J. Z.; Zuill, D. E.; Matsuka, S.; Jiang, Z.; Almaliti, J.; Caffrey, C. R.; Gerwick, W. H.; Eckmann, L. 20S Proteasome as a Drug Target in *Trichomonas vaginalis*. *Antimicrob Agents Chemother* **2019**, *63* (11). DOI: 10.1128/aac.00448-19.

(59) Fajtova, P.; Hurysz, B. M.; Miyamoto, Y.; Serafim, M.; Jiang, Z.; Trujillo, D. F.; Liu, L.; Somani, U.; Almaliti, J.; Myers, S. A.; Caffrey, C. R.; Gerwick, W. H.; Kirk, C. J.; Boura, E.; Eckmann, L.; O'Donoghue, A. J. Development of subunit selective substrates for *Trichomonas vaginalis* proteasome. *bioRxiv* **2023**. DOI: 10.1101/2023.04.05.535794.

(60) Toste Rêgo, A.; da Fonseca, P. C. A. Characterization of Fully Recombinant Human 20S and 20S-PA200 Proteasome Complexes. *Mol Cell* **2019**, *76* (1), 138-147.e135. DOI: 10.1016/j.molcel.2019.07.014.
(61) Silhan, J.; Fajtova, P.; Bartosova, J.; Hurysz, B. M.; Almaliti, J.; Miyamoto, Y.; Eckmann, L.; Gerwick, W. H.; O'Donoghue, A. J.; Boura, E. Structural elucidation of recombinant *Trichomonas vaginalis* 20S proteasome bound to covalent inhibitors. *bioRxiv* **2023**. DOI: 10.1101/2023.08.17.553660.
(62) Satoh, T.; Yagi-Utsumi, M.; Okamoto, K.; Kurimoto, E.; Tanaka, K.; Kato, K. Molecular and Structural Basis of the Proteasome α Subunit Assembly Mechanism Mediated by the Proteasome-Assembling Chaperone PAC3-PAC4 Heterodimer. *Int J Mol Sci* **2019**, *20* (9). DOI: 10.3390/ijms20092231.
(63) Hirano, Y.; Kaneko, T.; Okamoto, K.; Bai, M.; Yashiroda, H.; Furuyama, K.; Kato, K.; Tanaka, K.; Murata, S. Dissecting beta-ring assembly pathway of the mammalian 20S proteasome. *EMBO J* **2008**, *27* (16), 2204-2213. DOI: 10.1038/emboj.2008.148.
(64) Murata, S.; Yashiroda, H.; Tanaka, K. Molecular mechanisms of proteasome assembly. *Nat Rev Mol Cell Biol* **2009**, *10* (2), 104-115. DOI: 10.1038/nrm2630.
(65) O'Donoghue, A. J.; Eroy-Reveles, A. A.; Knudsen, G. M.; Ingram, J.; Zhou, M.; Statnekov, J. B.; Greninger, A. L.; Hostetter, D. R.; Qu, G.; Maltby, D. A.; Anderson, M. O.; DeRisi, J. L.; McKerrow, J. H.; Burlingame, A. L.; Craik, C. S. Global identification of peptidase specificity by multiplex substrate profiling. *Nat Methods* **2012**, *9* (11), 1095-1100. DOI: 10.1038/nmeth.2182.
(66) Schneider, E. L.; Craik, C. S. Positional scanning synthetic combinatorial libraries for substrate profiling. *Methods Mol Biol* **2009**, *539*, 59-78. DOI: 10.1007/978-1-60327-003-8_4.
(67) Xie, S. C.; Gillett, D. L.; Spillman, N. J.; Tsu, C.; Luth, M. R.; Ottilie, S.; Duffy, S.; Gould, A. E.; Hales, P.; Seager, B. A.; Charron, C. L.; Bruzzese, F.; Yang, X.; Zhao, X.; Huang, S.; Hutton, C. A.; Burrows, J. N.; Winzeler, E. A.; Avery, V. M.; Dick, L. R.; Tilley, L. Target Validation and Identification of Novel Boronate Inhibitors of the Plasmodium falciparum Proteasome. *J Med Chem* **2018**, *61* (22), 10053-10066. DOI: 10.1021/acs.jmedchem.8b01161.
(68) Jiang, Z.; Silva, E. B.; Liu, C.; Fajtová, P.; Liu, L. J.; El-Sakkary, N.; Skinner, D. E.; Syed, A.; Wang, S. C.; Caffrey, C. R.; O'Donoghue, A. J. Development of subunit selective proteasome substrates for S*chistosoma species*. *biorxiv* **2024**.
(69) Li, H.; O'Donoghue, A. J.; van der Linden, W. A.; Xie, S. C.; Yoo, E.; Foe, I. T.; Tilley, L.; Craik, C. S.; da Fonseca, P. C.; Bogyo, M. Structure- and function-based design of Plasmodium-selective proteasome inhibitors. *Nature* **2016**, *530* (7589), 233-236. DOI: 10.1038/nature16936.
(70) Almaliti, J.; Fajtová, P.; Calla, J.; LaMonte, G. M.; Feng, M.; Rocamora, F.; Ottilie, S.; Glukhov, E.; Boura, E.; Suhandynata, R. T.; Momper, J. D.; Gilson, M. K.; Winzeler, E. A.; Gerwick, W. H.; O'Donoghue, A. J. Development of Potent and Highly Selective Epoxyketone-Based Plasmodium Proteasome Inhibitors. *Chemistry* **2023**, *29* (20), e202203958. DOI: 10.1002/chem.202203958.
(71) Li, H.; van der Linden, W. A.; Verdoes, M.; Florea, B. I.; McAllister, F. E.; Govindaswamy, K.; Elias, J. E.; Bhanot, P.; Overkleeft, H. S.; Bogyo, M. Assessing subunit dependency of the Plasmodium proteasome using small molecule inhibitors and active site probes. *ACS Chem Biol* **2014**, *9* (8), 1869-1876. DOI: 10.1021/cb5001263.

(72) Li, H.; Ponder, E. L.; Verdoes, M.; Asbjornsdottir, K. H.; Deu, E.; Edgington, L. E.; Lee, J. T.; Kirk, C. J.; Demo, S. D.; Williamson, K. C.; Bogyo, M. Validation of the proteasome as a therapeutic target in Plasmodium using an epoxyketone inhibitor with parasite-specific toxicity. *Chem Biol* **2012**, *19* (12), 1535-1545. DOI: 10.1016/j.chembiol.2012.09.019.

(73) Xie, S. C.; Metcalfe, R. D.; Mizutani, H.; Puhalovich, T.; Hanssen, E.; Morton, C. J.; Du, Y.; Dogovski, C.; Huang, S. C.; Ciavarri, J.; Hales, P.; Griffin, R. J.; Cohen, L. H.; Chuang, B.; Wittlin, S.; Deni, I.; Yeo, T.; Ward, K. E.; Barry, D. C.; Liu, B.; Gillett, D. L.; Crespo-Fernandez, B. F.; Ottilie, S.; Mittal, N.; Churchyard, A.; Ferguson, D.; Aguiar, A. C.; Guido, R. V. C.; Baum, J.; Hanson, K. K.; Winzeler, E. A.; Gamo, F.; Fidock, D. A.; Baud, D.; Parker, M. W.; Brand, S.; Dick, L. R.; Grifin, M. D. W.; Gould, A. E.; Tilley, L. Design of proteasome inhibitors with oral efficacy *in vivo* against *Plasmodium falciparum* and selectivity over the human proteasome. *Proc Natl Acad Sci U S A* **2021**, *118* (39). DOI: 10.1073/pnas.2107213118.

(74) Li, H.; Bogyo, M.; da Fonseca, P. C. The cryo-EM structure of the Plasmodium falciparum 20S proteasome and its use in the fight against malaria. *FEBS J* **2016**, *283* (23), 4238-4243. DOI: 10.1111/febs.13780.

(75) Hsu, H. C.; Li, D.; Zhan, W.; Ye, J.; Liu, Y. J.; Leung, A.; Qin, J.; Crespo, B.; Gamo, F. J.; Zhang, H.; Cui, L.; Roth, A.; Kirkman, L. A.; Li, H.; Lin, G. Structures revealing mechanisms of resistance and collateral sensitivity of *Plasmodium falciparum* to proteasome inhibitors. *Nat Commun* **2023**, *14* (1), 8302. DOI: 10.1038/s41467-023-44077-2.

Chapter 2:

Clickable Probes for Pathogen Proteasomes: Synthesis and Applications

2.1. Introduction

The proteasome is a multi-subunit threonine protease that is essential for proteostasis in the cell.[1] The 20S catalytic core of the human constitutively expressed proteasome (c20S) is composed of four stacked heptameric rings wherein the outer two rings of α subunits sandwich two β subunit rings, of which, the β1, β2 and β5 subunits are catalytically active [2,3] Each of these active subunits has a preference for cleavage after specific amino acids in a peptide chain, and are categorized as possessing caspase-like (β1), trypsin-like (β2) or chymotrypsin-like activity (β5).[4]

Inhibition of the proteasome's catalytic activity is an established therapeutic strategy for various blood cancers, with three inhibitors so far approved.[5, 6] In addition, the proteasome is a validated drug target for a number of parasitic diseases, [7-9] and small molecule inhibitors are under development for treatment of malaria [10-12] and in clinical trials for trypanosomatid infections.[13]

Over the last decade, the research tools available to characterize the proteasome have advanced on various fronts, and include the use of optimized peptidyl fluorogenic substrates to measure the activity of each of the three catalytic β subunits,[14, 15] methodologies to purify the proteasome,[7, 16] and the availability of cryoEM structures to understand how small molecules engage the target.[11, 17] Also, active site-directed probes have been developed to define cellular localization, facilitate imaging in small animal models and understand the specificities of small molecule proteasome inhibitors.[18, 19]

In terms of active site-directed probes with which to visualize c20S (*e.g.*, after native or denaturing gel electrophoresis), the most commonly used is the irreversible, fluorescent, peptidyl vinyl sulfone, Me_4BodipyFL-Ahx$_3$L$_3$VS (Figure 2A), a derivative of the originally described MV151 (Bodipy TMR-Ahx$_3$L$_3$VS).[19, 20] During our efforts to characterize parasite 20S molecules as potential drug targets, we identified limitations to this probe. Specifically, it binds irreversibly

to cysteine proteases (SI 2.8.1), which are often highly expressed in parasites, [21, 22] and sometimes labels just two of the three catalytic β subunits [14, 15] even though the genomic/proteomic evidence indicates the presence of all three. Lastly, Me_4BodipyFL-Ahx$_3$L$_3$VS lacks the functionality to enable isolation of the catalytic subunits from protein extracts which would then facilitate their identification via proteomics. Combined, these limitations complicate the biochemical analysis of parasite proteasomes, information that is necessary for a campaign to develop specific anti-parasitic proteasome inhibitors.

Given the above limitations, we synthesized two activity-based probes that are based on the peptidyl scaffolds of the proteasome inhibitor drugs, carfilzomib (CFZ) and bortezomib (BTZ). These probes were designed with an N-terminal alkyne group to allow the attachment of an azide-containing reagent via click chemistry, in this case, a bifunctional group consisting of TAMRA and biotin. For two parasite species, we describe the utility of each probe to engage and visualize the 20S proteasome in cell extracts and enrich the target for identification of the constituent catalytic β subunits.

2.2. Results

We used the peptidyl backbones of the proteasome inhibitors, CFZ and BTZ, to synthesize two epoxyketone-based 20S probes. After binding of the probes to the target proteasome, they were then conjugated to a bifunctional group comprising TAMRA and biotin via bioorthogonal copper (I)-catalyzed azide-alkyne cycloaddition (CuAAC).[23] These probes facilitated the visualization and identification of the catalytic β subunits of the target proteasome in parasite extracts.

2.2.1. Synthesis of LJL-1 and -2, and their differential engagement of c20S subunits

Alkyne-homoPhe-Leu-Phe-Leu-epoxyketone (**8,** LJL-1; Figure 2.1A) is an analog of CFZ, an FDA-approved proteasome inhibitor. The alkyne group on LJL-1 allows coupling to TAMRA-Biotin azide via standard click chemistry.

The synthesis of LJL-1 was accomplished by first coupling the amino acids at P2-P4, Phe-Leu-homoPhe, using TBTU-based peptide synthesis to generate **3**. This was followed by a conversion of the methyl ester into a hydrazide (**4**) and then oxidation to an acyl azide that allowed peptide coupling to the leucine epoxyketone fragment (**5**) which then yielded the tetrapeptide-epoxyketone, **6**. Finally, deprotection of the N-Boc-protected homo-phenylalanine (**7**) allowed the alkyne to be attached using TBTU chemistry to yield **8**, which was named LJL-1 (Figure 2.1A).

The peptidyl sequence for the second probe, alkyne-Phe-Leu-epoxyketone (**12**, LJL-2; Figure 2.1B) was based on the FDA-approved proteasome inhibitor, BTZ. We replaced the reversible, covalent, boronate warhead of BTZ [6] with an irreversibly binding epoxyketone.[24] The synthesis of LJL-2 was accomplished via TBTU-based peptide coupling between the leucine epoxyketone fragment, **5**, and an N-Boc-protected phenylalanine, followed by Boc-deprotection and a subsequent *N*-acylation reaction with the acyl imidazole, **11** (Figure 2.1B).

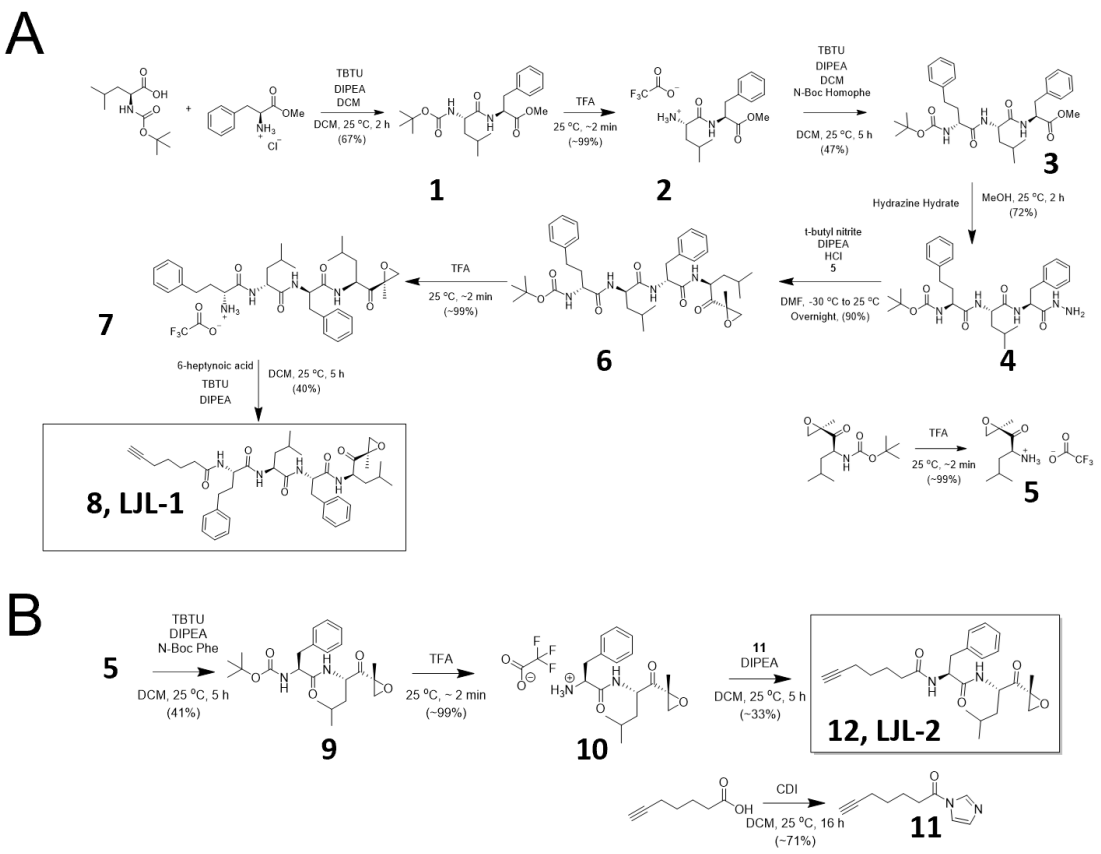


Figure 2.1. Synthetic schemes for LJL-1 and LJL-2.

The evaluation of Me_4BodipyFL-Ahx$_3$L$_3$VS (Figure 2.2A) alongside LJL-1 and LJL-2 using pure c20S revealed distinct binding patterns after SDS-PAGE and fluorescent imaging. The slight misalignment of the c20S β subunit banding patterns can be attributed to the different molecular masses of each probe: Me_4BodipyFL-Ahx$_3$L$_3$VS (1059.2 amu), LJL-1 (1875.3 amu) and LJL-2 (1600.9 amu). As anticipated, Me_4BodipyFL-Ahx$_3$L$_3$VS binds to all three catalytic β subunits (Figure 2.2B).[19, 25] Similarly, LJL-1 binds all three subunits with a stronger preference for β5 and β1 relative to β2. In contrast, LJL-2 binds strongly to the lower band, which seems to be composed of β1 and β5. Titrating LJL-1 with pure c20S shows preferential binding to the β5 subunit, with both β1 and β2 being labeled only at higher concentrations (Figure 2.2C). Titrating LJL-2 demonstrates labeling of β1 and β5 (Figure 2.2D), but with a weaker limit of detection of

c20S compared to LJL-1, *i.e.*, 50 ng *vs*. 5 ng. Lastly, the time needed for the click reaction between the azide and alkyne to proceed to completion was ~10 min for both probes (Figures 2.2E, 2.2F).

To verify probe selectivity for c20S in cell extracts, we preincubated HepG2 cell lysates with three class-specific protease inhibitors, namely, E64 (cysteine proteases), phenylmethylsulfonyl fluoride (PMSF; serine proteases) and marizomib (MZB; the proteasome) prior to addition of probe (Figure 2.2G). The binding patterns resolved for the DMSO controls were essentially identical to those noted for pure c20S (Figure 2.2B), *i.e*., three subunits using Me_4BodipyFL-Ahx$_3$L$_3$VS and LJL-1, and two subunits (appearing as one fused band) with LJL-2. Of the inhibitors tested, only MZB abolished binding by all three probes, confirming the identities of the bands as c20S catalytic β subunits. When evaluated for inhibition of growth of HEK293 cells *in vitro*, LJL-1 and LJL-2 generated similar EC_{50} values to those of CFZ and BTZ with values in the range of 5-20 nM (SI 2.8.2). Thus, the substitution of the N-terminal morpholine cap in CFZ for the alkyne group in LJL-1, and the substitution of the N-terminal pyrazine and the C-terminal boronate warhead in BTZ for the alkyne and epoxyketone, respectively, in LJL-2, did not dramatically alter compound potency.

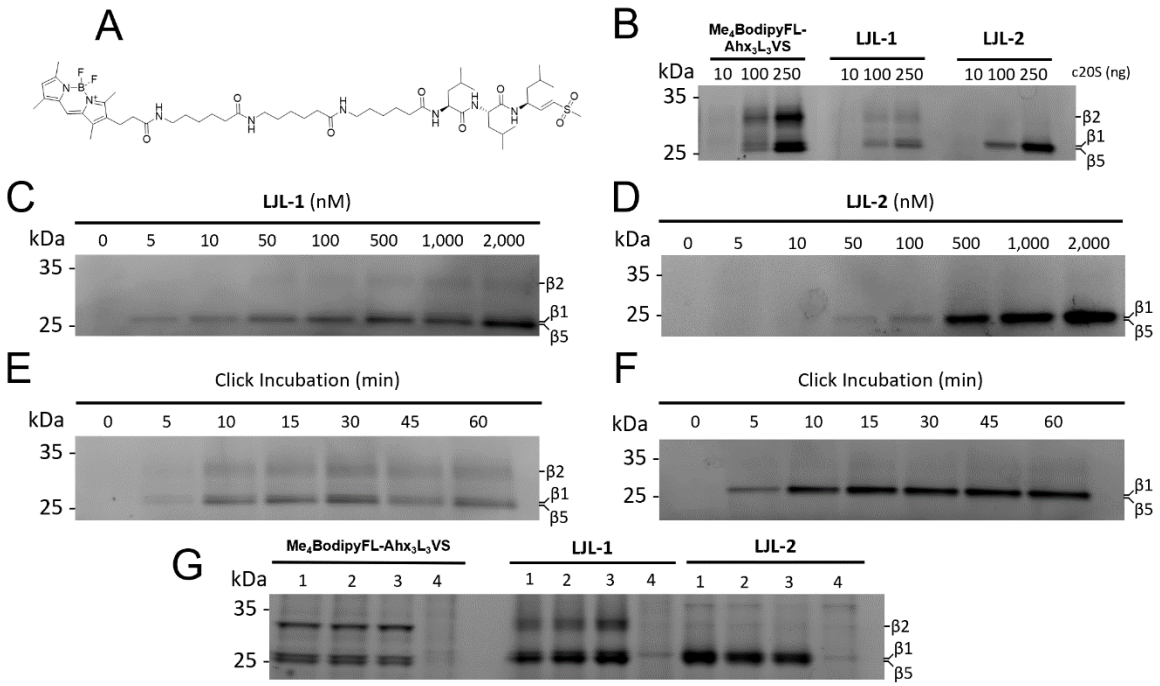
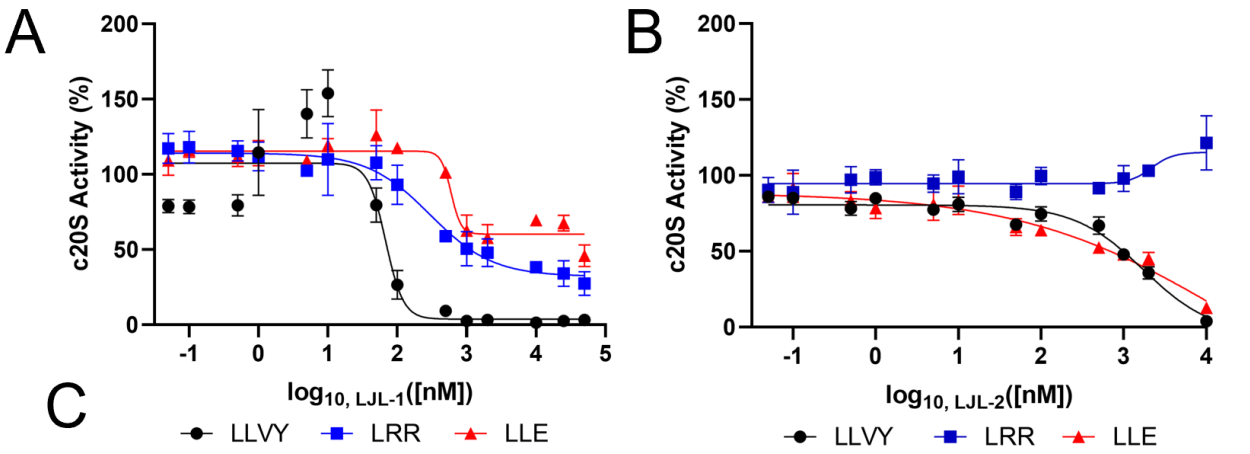


Figure 2.2. Probe engagement with purified c20S and HepG2 cell lysate under various conditions. A. Structure of Me_4BodipyFL-Ahx_3L_3VS. **B.** Florescence imaging of c20S β subunit banding patterns labeled by Me_4BodipyFL-Ahx_3L_3VS, LJL-1 and LJL-2. **C**, **D.** Concentration-dependent binding of LJL-1 and LJL-2, respectively, to c20S. **E**, **F.** Time-dependence of the click reaction for LJL-1 and LJL-2, respectively, with c20S. **G.** Subunit banding patterns generated by Me_4BodipyFL-Ahx_3L_3VS, LJL-1 and LJL-2 with HepG2 cell lysate. Lysate was preincubated with (1) DMSO, (2) 20 μM E64, (3) 2 mM PMSF or (4) 10 μM MZB, prior to addition of probe.

We next tested the ability of LJL-1 and LJL-2 to inhibit the individual β subunits of c20S in a microplate assay using β subunit-specific substrates as reporters of enzyme activity (Figure 2.3; SI 2.8.3).[26] LJL-1 was 2- and 73-fold more potent than CFZ at targeting the β5 and β2 subunits, respectively. Against β1, LJL-1 was partially effective at high concentrations (> 1 μM; Figure 2.3A) yet never generated an EC_{50} value (Figure 2.3C), whereas CFZ was ineffective (SI 2.8.3). LJL-2 inhibited only β1 and β5 (Figure 2.3B) and, for each respective subunit, was 33- and 18-fold weaker than BTZ (Figure 2.3C; SI 2.8.3). Neither LJL-2 nor BTZ engaged the β2 subunit, even at the highest concentration of 50 μM tested (Figure 2.3C). The decreased binding capacity of LJL-2 compared to BTZ suggests that the boronate warhead in BTZ confers stronger

proteasome engagement. Although this enhanced interaction might be favorable for therapeutic applications, boronates cross react with serine proteases, thus compromising probe selectivity.[27]

Overall, we show that both LJL probes can directly and indirectly characterize the catalytic β subunits of a target proteasome. Directly, the probes can be labeled with a fluorogenic reporter molecule after they have bound to the target subunit and the banding pattern then visualized via SDS-PAGE (Figures 2.2B, 2.2G). Indirectly, the probes can be employed as inhibitors that compete with the fluorogenic reporter substrates for binding to the catalytic β subunits (Figure 2.3).



Inhibitor	β1 IC_{50} (nM)	β2 IC_{50} (nM)	β5 IC_{50} (nM)
LJL-1	> 50,000	596 ± 27	68 ± 32
Carfilzomib	> 50,000	43,359 ± 5184	153 ± 52
LJL-2	2157 ± 27	> 50,000	1725 ± 42
Bortezomib	65 ± 55	> 50,000	97 ± 41

Figure 2.3. Inhibition of c20S catalytic β subunits by LJL-1 and LJL-2. Concentration-dependent inhibition by (**A**) LJL-1 and (**B**) LJL-2 of each the c20S β subunits using subunit-specific peptidyl AMC substrates, i.e., LLVY (β5), LRR (β2) and LLE (β1). **C.** EC_{50} values for the various proteasome inhibitors. Assays with LJL-1 and LJL-2 were performed twice each in triplicate (n=6). Assays with CFZ and BTZ were performed once in triplicate (n=3).

2.2.2. Parasite proteasome engagement and β subunit identification using LJL-1- and -2

Understanding the connection between inhibition of one or more 20S β subunit and anti-parasitic activity is fundamental to designing parasite-specific proteasome inhibitors. Employing a similar experimental design to that shown in Figure 2G with extracts of *Leishmania donovani* promastigotes and class-specific protease inhibitors (Figure 2.4A), we found that the commercial probe, Me_4BodipyFL-Ahx$_3$L$_3$VS, labeled just two of the three 20S β subunits, in addition to cysteine proteases which are abundant in this parasite.[21, 28] Engagement of cysteine proteases by Me_4BodipyFL-Ahx$_3$L$_3$VS is not surprising given that vinyl sulfone warheads react with the cysteine nucleophile in such proteases.[29, 30] By contrast, LJL-1 labeled three protein species, and this binding could be blocked by prior incubation with the broad-spectrum proteasome inhibitor, MZB. LJL-2 labeled a single band that was also inhibited by MZB (Figure 2.4A). Thus, and as seen with the HepG2 lysate, each probe resolves a different catalytic β subunit pattern.

Because LJL-1 labeled all three catalytic β subunits in the *L. donovani* lysate, we employed the biotin functionality to enrich the proteasome from lysate using neutravidin-bead chromatography. After binding, the beads were extensively washed, then boiled to release the biotin-bound proteins, and the supernatant was resolved by SDS-PAGE (Figure 2.4B). With the aid of the TAMRA functionality, each of the three bands was visualized, excised and identified by proteomics as β1 (Uniprot ID: A0A504X6A3), β2 (A0A3S7XA80) and β5 (A0A3Q8IIY4), from highest to lowest molecular weight (Figure 2.4C). Thus, the combined functionalities of the biotin and TAMRA components bound to LJL-1 were critical to identifying the three catalytic β subunits in *L. donovani* promastigotes and, further, demonstrated that their order of electrophoretic migration (β1, β2 and β5; highest to lowest;) differs from that for HepG2 cells (β2, β1 and β5).

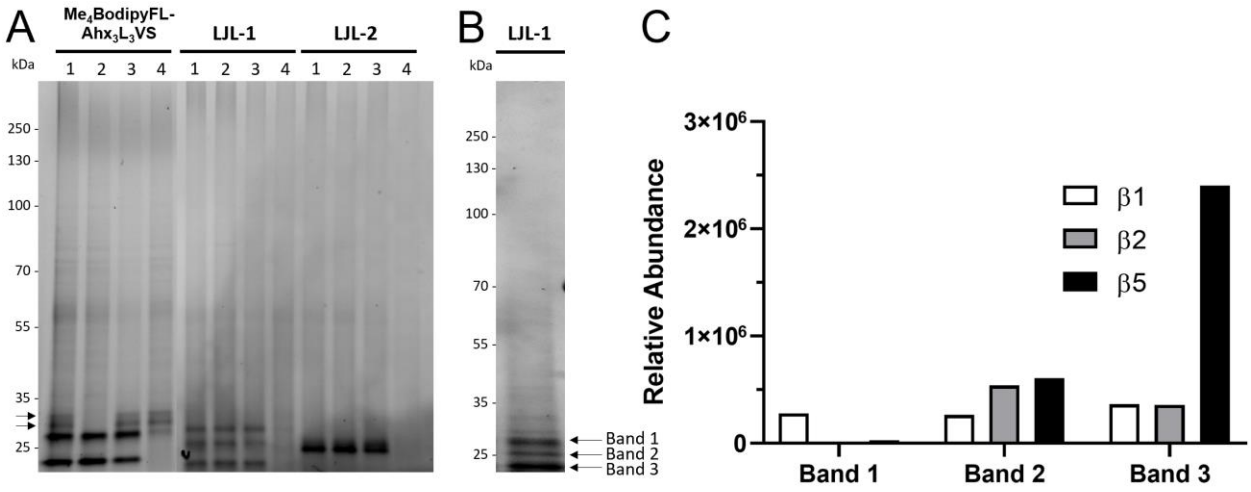


Figure 2.4. Probe engagement with, and enrichment and identification of, *L. donovani* promastigote 20S catalytic β subunits. A. Fluorescence imaging of banding patterns generated by Me_4BodipyFL-Ahx_3L_3VS, LJL-1 and LJL-2 in cell lysate. Lysate was preincubated with (1) DMSO, (2) 20 μM E64, (3) 2 mM PMSF or (4) 10 μM MZB prior to addition of probe. Engagement of cysteine proteases (bands sensitive to E64) by Me_4BodipyFL-Ahx_3L_3VS is marked with black arrows. **B.** Fluorescence imaging of 20S β subunits (three bands) after enrichment from parasite lysate using the biotin functionality of LJL-1. **C.** Label free peptide quantification of each of the excised bands.

With a second parasite, *Trichomonas vaginalis*, each of the three probes again showed differential binding to either two or three protein species in cell lysate that could be inhibited by prior incubation with MZB (Figure 2.5A). Notably, the background was less pronounced with LJL-1 and LJL-2 compared to that with Me_4BodipyFL-Ahx_3L_3VS. Previous research using purified Tv20S identified the electrophoretic migration order of the β subunits as β2, β1 and β5, from highest to lowest molecular weight.[15] Accordingly, we wished to employ inhibitors that selectively inactivate one or other β subunit such that the uninhibited subunit(s) would be available to bind to the probe. These subunits could then be isolated and visualized. In this case, LJL-2 was chosen as it bound to all three β subunits.

A number of 20S inhibitors and inhibitor combinations have been shown to preferentially inhibit one or more Tv20S catalytic β subunits.[15] The CPB analog, CP-17 [31] selectively inhibits β5 at 1 μM. CP-17 and CFZ at 10 μM inhibit both β5 and β2, and MZB at 10 μM inhibits all three subunits (Figure 2.5B). These inhibitors were incubated with *T. vaginalis* lysate prior to addition of LJL-2, which then bound to the uninhibited β subunits for their eventual visualization by SDS-PAGE after biotin-neutravidin chromatography (Figure 2.5C). For proteomic analysis, a large gel slice was excised from each lane, which corresponded to the region in which the three catalytic subunits had migrated (Figure 2.5C, red boxes). The excision step was much easier to perform than the precision required with the *L. donovani* samples above. Subsequent proteomic analysis demonstrated the utility of the strategy whereby the DMSO control lane had the highest relative abundance of each of the three β subunits (Figure 2.5D). Following pre-treatment with CP17, β5 subunit abundance was decreased by 6.7-fold whereas those for β1 and β2 subunits were only reduced by 1.5- and 3-fold, respectively. This indicates that CP-17 preferentially targets the β5 subunit (the lowest subunit on the gel; Figure 2.5C). Treatment with a combination of CP-17 and CFZ did not change the abundance of the β1 protein whereas those for the other two subunits were decreased. Accordingly, the remaining band visible in the CP-17/CFZ lane on the gel is the β1 subunit. MZB inhibited all three subunits (Figure 2.5C) with the consequence of little to no binding signal being returned by the probe (Figure 2.5D). Overall, the approach outlined here offers an alternative method to identifying individual catalytic β subunits in parasite lysates that circumvents the need to carefully excise individual and closely-juxtaposed bands from a gel.

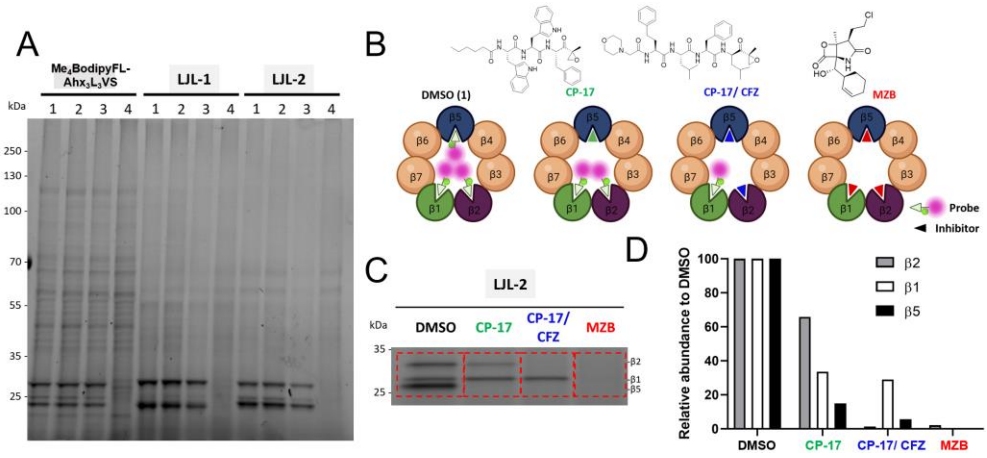


Figure 2.5. Probe engagement with, and enrichment and identification of, *T. vaginalis* 20S catalytic β subunits. A. Fluorescence imaging of banding patterns generated by Me_4BodipyFL-Ahx_3L_3VS, LJL-1 and LJL-2 in parasite cell lysate. Lysate was preincubated with (1) DMSO, (2) 20 μM E64, (3) 2 mM PMSF or (4) 10 μM MZB, prior to addition of probe. **B.** Schematic of inhibitors or inhibitor combinations known to inhibit one or more Tv20S β subunits.[15] **C.** Fluorescence imaging of Tv20S β subunits after incubation with β subunit-specific inhibitors or combinations of inhibitors, and enrichment from parasite lysate using the biotin functionality of LJL-2. **D.** Label free peptide quantification in each of the excised gel pieces (red boxes in **C**) that identifies each of the β subunits as a function of the inhibitor or combinations of inhibitors employed.

2.3. Discussion

The proteasome is an attractive anti-parasitic drug target,[9, 32] and small molecule inhibitors are preclinically progressing for treatment of malaria [10-12] or in the clinic for trypanosomatid diseases.[13] As described above, the tools to visualize and characterize the proteasome have advanced, however, just one activity-based probe, Me_4BodipyFL-Ahx_3L_3VS,[19] is commercially available. As shown here for parasitic organisms, this probe is not selective for the 20S proteasome as it reacts with cysteine proteases [30] which are abundant in many parasites,[21, 22] including *L. donovani*.[28] Further, unlike the situation for human c20S in HepG2 cell extracts, the commercial probe does not consistently label all three catalytic β subunits in parasite extracts, with two bands being labeled in *L. donovani* promastigotes and three in *T. vaginalis*. Last, the commercial probe was not designed to allow the identification of the individually resolved subunits.

Accordingly, to advance research into parasite 20S proteasomes as drug targets, we employed bioorthogonal copper (I)-catalyzed azide-alkyne cycloaddition (CuAAC),[23] or "click chemistry" to synthesize *bifunctional* probes to enable the isolation of the 20S from cell extracts and the identification of the component catalytic β subunits. LJL-1 and LJL-2 were based on the peptidyl backbones of the anti-cancer drugs, CFZ and BTZ, respectively, which have well understood c20S β subunit binding preferences,[33] and so far, seem to be universally anti-parasitic via engagement of the 20S proteasome.[7-9] Using two example parasites, *L. donovani* and *T. vaginalis*, the bifunctional probe strategy to isolate and identify 20S catalytic β subunits directly from cell extracts without interference by cysteine proteases worked well and should be more straightforward to implement than alternative time-consuming multi-step 20S purification methods,[14, 15] and the requisite for large quantities of often limiting and expensive parasite material. The probes also demonstrated that the order of electrophoretic migration of the β subunits is parasite-dependent and may not align with the profile established for human cells, similar to a previous finding for *P. falciparum* 20S using a fluorescent epoxyketone probe, BMV037.[10, 11] Lastly, the single, dual functionality probe containing both a fluorophore and biotin tag, is efficient compared to the time and costs associated with the need to synthesize separate probes for each functionality, *e.g.*, the serine hydrolase probes, biotin-fluorophosphonate and TAMRA-fluorophosphonate.[34]

The downstream utility of probes containing reactive alkynes is broad and a variety of azide-containing reagents can be coupled after labeling of the catalytic 20S β subunit(s).[35] In addition, rather than alkyne-containing APBs, the next generation probes could substitute the alkyne for difluorinated cyclooctyne[36] or bicyclo[6.1.0]nonyne,[37] which would allow for real-time, *in vivo* fluorescence imaging of proteasome activity, and its inhibition, using copper-free click chemistry.

Also, biotin, as a purification handle, may be substituted by desthiobiotin, which has lower binding affinity, [38] or by cleavable biotin linkers,[39] which would aid in the release of bound proteins after affinity purification. Finally, click chemistry could be used to conjugate a parasite-specific antibody to a proteasome inhibitor,[40] potentially improving on-target potency while minimizing host toxicity.

The importance of developing two probes based on tetrapeptidyl and dipeptidyl backbones is highlighted by the different SDS-PAGE profiles resolved for the 20S catalytic β subunits in HepG2 cells, *L. donovani* and *T. vaginalis*. Had we relied on just one or other probe, we would likely have been unable to enrich for and identify all three β subunits depending on the parasite. This realization comes after the fact and is fortuitous as we originally had intended to synthesize just LJL-1, and it may yet be the case that additional functional probes will be needed to functionally investigate other pathogen 20S proteasomes.

2.4. Conclusion

Two activity-based, epoxyketone probes, LJL-1 and LJL-2, were synthesized and each conjugated, via click chemistry, to a bifunctional TAMRA and biotin handle. Depending on the parasite, each probe generated a different labeling profile, and enriched the 20S from lysates of *L. donovani* promastigotes and *T. vaginalis* to facilitate the identification of the respective catalytic β subunits. Compared to a commercially available vinyl sulfone probe, the new probes did not cross-react with cysteine proteases and revealed that the order in which the β subunits migrate via SDS-PAGE differs depending on the originating species. As interest in the 20S proteasome as a drug target for treatment of parasitic infections expands, both probes will aid the characterization

of the 20S in complex cell extracts and support efforts to improve the potency and specificity of anti-parasitic 20S β subunit inhibitors.

2.5. Methods

All solvents were of reagent grade. All reagents were purchased from Alfa Aesar or Fisher and used as received. Thin-layer chromatography (TLC) was performed with 0.25 mm E. Merck precoated silica gel plates. Silica gel column chromatography was performed with silica gel 60 (pore volume 0.74−0.84 ml/g) supplied by Millipore Sigma (#105554). TLC spots were detected by viewing under a UV light. Proton (^{1}H) was recorded on a 500 MHz Bruker AMX-500 spectrometer and on a 600 MHz Bruker AVANCE III spectrometer. Chemical shifts were reported relative to solvents. Data for ^{1}H NMR spectra are reported as follows: chemical shift [ppm, referenced to protium; s = singlet, d = doublet, t = triplet, q = quartet, quint = quintet, dd = doublet of doublets, td = triplet of doublets, ddd = doublet of doublet of doublets, bs = broad singlet, m = multiplet, coupling constant (Hz), and integration]. High-resolution mass spectra (HRMS) were measured using an Agilent 6230 Accurate-Mass time-of-flight mass spectrometer with a Jet stream electrospray ionization source. Analytical reverse-phase (Sunfire C_{18}; 4.6 mm × 50 mm, 5 mL) HPLC was performed with a Gilson HPLC equipped with UV and a mass detector. All final compounds were found to be >95% pure by HPLC analysis.

2.5.1. Synthesis of LJL-1

***Boc-Leu-Phe-OMe* (1)**. To a stirred solution of acid Boc-Leu-OH (1 g, 4.3 mmol, 1 equiv.) in dry DCM at r.t. under N_2, methyl ester MeO-Phe-NH_3Cl (1 g, 4.3 mmol, 1 equiv.) and TBTU (1.5 g, 4.8 mmol, 1.1 equiv.) were added and the resulting solution was stirred for 2 h. 3.14 ml of

DIPEA (2.35 g**,** 18.1 mmol, 4.2 equiv.) was then added dropwise, and the resulting mixture was stirred for 15 min. The organic extract was washed with H_2O, brine, then dried over Na_2SO_4, filtered and concentrated *in vacuo*. Purification by silica gel column chromatography (30-35% EtOAc in Hexane) provided the title compound (1.141 g, 2.91 mmol, 67%) as a white solid powder. ^{1}H NMR (600 MHz, $CDCl_3$) δ 7.29 – 7.19 (m, 3H), 7.10 (d, *J* = 7.4 Hz, 2H), 6.56 (d, *J* = 7.8 Hz, 1H), 4.85 (dt, *J* = 19.9, 7.2 Hz, 2H), 4.10 (d, *J* = 14.4 Hz, 1H), 3.69 (s, 3H), 3.10 (ddd, *J* = 41.3, 14.0, 6.0 Hz, 2H), 1.67 – 1.55 (m, 2H), 1.42 (s, 10H), 0.89 (q, *J* = 6.0 Hz, 6H) ppm. HRMS (ES+): calcd for $C_{21}H_{32}N_2O_5$ $[M + Na]^+$, 415.2203; found, 415.2203.

***H_3N-Leu-Phe-OMe* (2).** A solution of **2** (0.580 g, 1.5 mmol, 1.00 equiv.) in TFA (2.5 mL) was stirred at r.t. for several minutes until generation of CO_2 in the reaction mixture was no longer visible. A steady stream of N_2 was used to remove all volatiles and the resulting material was used directly for the next step without further purification.

***Boc-Homophe-Leu-Phe-OMe* (3).** To a solution of **2** (0.995 g, 2.9 mmol, 1.00 equiv.) in dry DCM (29 mL) at r.t. under N_2, DIPEA (1.6 g, 12.2 mmol, 4.2 equiv.) was added dropwise, and the reaction mixture was stirred for 15 min. Boc-Homophe-OH (0.811 g, 2.9 mmol, 1 equiv.) and TBTU (1.0 g, 3.2 mmol, 1.1 equiv.) was added and the solution was stirred for 5 h at r.t. The reaction was quenched with H_2O and washed with brine. The organic layer was then dried over Na_2SO_4, filtered and concentrated *in vacuo*. Purification by silica gel column chromatography (40-50% EtOAc in Hexane) provided the title compound (0.760 g, 1.37 mmol, 47%) as a white solid powder. ^{1}H NMR (600 MHz, $CDCl_3$) δ 7.29 – 7.24 (m, 2H), 7.24 – 7.14 (m, 6H), 7.10 – 7.05 (m, 2H), 6.68 (d, *J* = 7.9 Hz, 1H), 6.59 (d, *J* = 8.0 Hz, 1H), 5.16 – 5.09 (m, 1H), 4.81 (dt, *J* = 7.9, 6.1

Hz, 1H), 4.43 (td, *J* = 8.5, 4.9 Hz, 1H), 4.11 – 4.03 (m, 1H), 3.67 (s, 3H), 3.14 – 3.01 (m, 2H), 2.64 (t, *J* = 8.0 Hz, 2H), 2.13 – 2.01 (m, 1H), 1.89 (dq, *J* = 13.8, 7.9 Hz, 1H), 1.66 – 1.56 (m, 2H), 1.54 – 1.47 (m, 1H), 1.44 (s, 10H), 0.88 (dd, *J* = 12.4, 6.0 Hz, 6H) ppm. HRMS (ES+): calcd for $C_{31}H_{44}N_3O_6$ $[M+H]^+$, 554.3225; found, 554.3232.

Boc-Homophe-Leu-Phe-Hydrazide **(4).** To a solution of **3** (0.357 g, 0.65 mmol, 1 equiv.) in MeOH (14.2 mL) at r.t. under N_2, a solution of hydrazine monohydrate (1.957 g, 39 mmol, 61 equiv.) was added dropwise and heated at reflux for 2 h. The reaction mixture was then diluted with 40 mL toluene and the remaining solvent was removed by rotary evaporation obtaining the title product, which was used directly without further purification. (0.260 g, 0.460 mmol, 72%) ^{1}H NMR (600 MHz, $CDCl_3$) δ 9.19 (s, 1H), 8.11 (d, *J* = 8.4 Hz, 1H), 7.82 (d, *J* = 8.5 Hz, 1H), 7.36 (t, *J* = 7.5 Hz, 2H), 7.27 – 7.23 (m, 8H), 7.19 – 7.14 (m, 2H), 4.51 (td, *J* = 8.4, 5.6 Hz, 1H), 4.40 (td, *J* = 9.1, 5.0 Hz, 1H), 4.26 (s, 1H), 3.99 (td, *J* = 8.5, 5.2 Hz, 1H), 2.98 (dd, *J* = 13.8, 5.7 Hz, 1H), 2.86 (dd, *J* = 13.8, 8.6 Hz, 1H), 2.67 (ddd, *J* = 15.4, 10.6, 5.2 Hz, 1H), 2.62 – 2.54 (m, 3H), 1.95 – 1.87 (m, 1H), 1.83 (q, *J* = 4.8 Hz, 1H), 1.64 (p, *J* = 6.6 Hz, 1H), 1.47 (s, 9H), 0.91 (dd, *J* = 21.6, 6.6 Hz, 6H) ppm. HRMS (ES+): calcd for $C_{30}H_{44}N_5O_5$ $[M+H]^+$, 554.3337; found, 554.3340.

H_3N-Leu-epoxyketone **(5).** A solution of Boc-L-Leucine epoxyketone (0.580 g, 2.14 mmol, 1.00 equiv.) in TFA (3.3 mL) was stirred at r.t. for several minutes until generation of CO_2 in the reaction mixture was no longer visible. A steady stream of N_2 was used to remove all volatiles, and the resulting material was used directly for the next step without further purification.

***Boc-Homophe-Leu-Phe-Leu-Ep* (6).** To a solution of **5** (0.100 g, 0.181 mmol, 1 equiv.) in dry DMF under N_2 and at -30 ^oC, a solution of 43 μL 4 M HCl in dioxane (0.017 g, 0.470 mmol, 2.6 equiv.) and tert-butyl nitrite (0.022 g, 0.217 mmol, 1.2 equiv.) was added and the solution was stirred for 5 h. A solution of **6** (0.057 g, 0.199 mmol, 1.1 equiv.) in 200 μL of dry DMF was then added dropwise to the reaction mixture followed by a dropwise addition of DIPEA (0.117 g, 0.903 mmol, 5 equiv.) and the resulting mixture was stirred overnight allowing the mixture to rise to r.t. The reaction mixture was first quenched by the addition of water, followed by organic extraction by DCM, and the remaining organic solvent was concentrated in vacuo providing the title compound (0.090 g, 0.331 mmol, 90%). ^{1}H NMR (600 MHz, $CDCl_3$) δ 7.35 (s, 1H), 7.21 (t, *J* = 7.4 Hz, 2H), 7.17 – 6.99 (m, 9H), 6.93 (s, 1H), 5.46 (d, *J* = 7.6 Hz, 1H), 4.83 (q, *J* = 7.6 Hz, 1H), 4.57 (td, *J* = 9.1, 3.8 Hz, 2H), 4.24 – 4.13 (m, 1H), 3.24 (d, *J* = 5.1 Hz, 1H), 3.06 – 2.97 (m, 1H), 2.93 (dd, *J* = 14.0, 7.6 Hz, 1H), 2.82 (d, *J* = 4.9 Hz, 1H), 2.69 – 2.53 (m, 2H), 2.02 – 1.84 (m, 2H), 1.54 (ddt, *J* = 15.4, 7.9, 3.9 Hz, 3H), 1.48 (s, 4H), 1.45 (s, 11H), 0.89 – 0.79 (m, 12H) ppm. HRMS (ES+): calcd for $C_{39}H_{57}N_4O_7$ $[M+H]^+$, 693.4222; found, 693.4228.

***H_3N-Homophe-Leu-Phe-Leu-Ep* (7).** A solution of **6** (0.050 g, 0.072 mmol, 1.00 equiv.) in TFA (0.11 mL) was stirred at r.t. for several minutes until generation of CO_2 in the reaction mixture was no longer visible. A steady stream of N_2 was used to remove all volatiles and the resulting material was used directly for the next step without further purification.

***Alkyne-Homophe-Leu-Phe-Leu-Ep*, LJL-1 (8).** To a solution of HBTU (0.025 g, 0.065 mmol, 1.2 equiv.) in dry DCM (0.337 mL) at r.t. under N_2, 38 μL DIPEA (0.028 g, 0.220 mmol, 4 equiv.) and 6-heptynoic acid (0.008 g, 0.065 mmol, 1.2 equiv.) were added and the resulting

mixture was stirred for 15 min. Afterwards, a solution of **7** (0.038 g, 0.054 mmol, 1 equiv.) in 1 mL of dry DCM was added dropwise, and, after the addition, the reaction mixture was stirred for 5 h. The reaction was quenched with H_2O, and washed with brine. The organic layer was then dried over Na_2SO_4, filtered and concentrated *in vacuo*. Purification by reverse phase HPLC afforded the title compound as a white solid (0.015 g, 0.021 mmol, 40%). ^{1}H NMR (600 MHz, $CDCl_3$) δ 8.37 (d, *J* = 111.5 Hz, 1H), 7.85 (s, 1H), 7.51 (s, 1H), 7.06 (d, *J* = 7.1 Hz, 4H), 7.00 – 6.90 (m, 6H), 6.85 (d, *J* = 7.5 Hz, 1H), 5.08 (d, *J* = 52.5 Hz, 3H), 4.66 (td, *J* = 9.3, 3.7 Hz, 1H), 3.22 – 3.15 (m, 1H), 3.03 – 2.86 (m, 2H), 2.82 (d, *J* = 4.7 Hz, 1H), 2.55 (td, *J* = 21.9, 6.7 Hz, 2H), 2.34 (ddt, *J* = 42.9, 14.5, 7.6 Hz, 2H), 2.26 – 2.20 (m, 2H), 1.99 – 1.85 (m, 3H), 1.85 – 1.72 (m, 3H), 1.72 – 1.64 (m, 1H), 1.64 – 1.52 (m, 4H), 1.48 (s, 3H), 1.47 – 1.42 (m, 1H), 0.84 (ddd, *J* = 17.7, 6.6, 3.9 Hz, 12H) ppm. HRMS (ES+): calcd for $C_{41}H_{57}N_4O_6$ $[M+H]^+$, 701.4273; found, 701.4272.

2.5.2. Synthesis of LJL-2

***Boc-Phe-Leu-Ep* (9).** To a solution of Boc-Phe-OH (0.254 g, 0.956 mmol, 1 equiv.) in dry DCM (1.90 ml) at r.t. under N_2, DIPEA (0.097 g, 0.75 mmol, 4 equiv.) was added dropwise, and the reaction mixture was stirred for 15 min. **5** (0.300 g, 1.1 mmol, 1.1 equiv.) and TBTU (0.368 g, 1.2 mmol, 1.2 equiv.) was added and the solution was stirred for 5 h at r.t.. The reaction was quenched with H_2O, and washed with brine. The organic layer was then dried over Na_2SO_4, filtered and concentrated *in vacuo*. Purification by silica gel column chromatography (20-40% EtOAc in Hexane) provided the title compound (0.032 g, 0.076 mmol, 41%) as a white solid powder. ^{1}H NMR (600 MHz, $CDCl_3$) δ 7.31 – 7.16 (m, 5H), 6.20 (d, *J* = 8.2 Hz, 1H), 4.96 (s, 1H), 4.57 (ddd, *J* = 11.0, 8.2, 3.2 Hz, 1H), 4.32 (s, 1H), 3.24 (s, 1H), 3.03 (qd, *J* = 14.0, 6.8 Hz, 2H), 2.88 (d, *J* =

5.0 Hz, 1H), 1.49 (s, 3H), 1.47 – 1.43 (m, 1H), 1.41 (s, 10H), 1.17 (ddd, *J* = 13.9, 10.3, 4.0 Hz, 1H), 0.92 (d, *J* = 6.4 Hz, 3H), 0.87 (d, *J* = 6.5 Hz, 3H) ppm. HRMS (ES+): calcd for $C_{23}H_{35}N_2O_5$ $[M+H]^+$, 419.2540; found, 419.2540.

***H_3N-Phe-Leu-Ep* (10).** A solution of **9** (0.058 g, 0.15 mmol, 1.00 equiv.) in TFA (0.21 mL) was stirred at r.t. for several minutes until generation of CO_2 in the reaction mixture was no longer visible. A steady stream of N_2 was used to remove all volatiles and the resulting material was used directly for the next step without further purification.

1-(1H-imidazol-1-yl)hept-6-yn-1-one (11). To a solution of 6-heptynoioc acid (0.997 g, 7.9 mmol, 1 equiv.) in dry DCM (19 ml) at r.t. under N_2, carbonyldiimidazole (1.5 g, 9.5 mmol, 1.2 equiv.) was added in one portion and the reaction mixture was stirred at r.t. overnight. Purification by silica gel column chromatography (60-65% EtOAc in hexane) provided the title compound (0.993 g, 5.636 mmol, 71%) as a white solid powder. ^{1}H NMR (600 MHz, $CDCl_3$) δ 8.17 (s, 1H), 7.46 (t, *J* = 1.5 Hz, 1H), 7.10 – 7.06 (m, 2H), 2.89 (t, *J* = 7.3 Hz, 2H), 2.25 (m, 2H), 1.96 (t, *J* = 2.7 Hz, 1H), 1.91 (q, *J* = 7.5 Hz, 2H), 1.68 – 1.61 (m, 2H) ppm. HRMS (ES+): calcd for $C_{10}H_{13}N_2O$ $[M+H]^+$, 177.1022; found, 177.1019.

***Alkyne-Phe-Leu-Ep,* LJL-2 (12).** To a solution of **9** (0.058 g, 0.130 mmol, 1 equiv.) in dry DCM at r.t. under N_2, **11** (0.026 g, 0.150 mmol, 1.1 equiv.) was added in one portion, and 28 μL DIPEA (0.021 g, 0.160 mmol, 1.2 equiv.) was added dropwise. The reaction mixture was stirred at r.t. for 5 h. The reaction was then quenched with H_2O, and washed with brine. The organic layer was then dried over Na_2SO_4, filtered and concentrated *in vacuo*. Purification by HPLC and

lyophilization afforded the title compound (0.019 g, 0.045 mmol, 33%) as an off-white solid. ^{1}H NMR (600 MHz, $CDCl_3$) δ 7.36 – 7.27 (m, 3H), 7.24 – 7.19 (m, 2H), 6.08 (dd, *J* = 13.3, 7.6 Hz, 2H), 4.66 (q, *J* = 7.3 Hz, 1H), 4.51 (ddd, *J* = 10.6, 7.7, 3.1 Hz, 1H), 3.21 (d, *J* = 5.0 Hz, 1H), 3.03 (qd, *J* = 14.0, 7.1 Hz, 2H), 2.89 (dd, *J* = 5.0, 2.6 Hz, 1H), 2.17 (dtd, *J* = 9.5, 7.2, 2.1 Hz, 5H), 1.94 (dt, *J* = 5.5, 2.7 Hz, 1H), 1.73 – 1.65 (m, 2H), 1.50 (s, 3H), 1.49 – 1.44 (m, 2H), 0.89 (dd, *J* = 16.4, 6.4 Hz, 6H) ppm. HRMS (ES+): calcd for $C_{25}H_{35}N_2O_4$ $[M+H]^+$, 427.2591; found, 427.2587.

2.5.3. Cell culture

HEK293 [41, 42] and HepG2 [43] cells were cultured in DMEM supplemented with 10% heat-inactivated FBS and 1% penicillin-streptomycin. Cells were grown in T75 cell culture flasks maintained at 37 °C in 5% CO_2, and passaged at 60-80% cell confluence.

L. donovani MHOM/ET/67/HU3 promastigotes were grown axenically at 28°C in M199 containing 40 mM HEPES, 0.1 mM adenine, 0.0001% biotin, 4.62 mM $NaHCO_3$, 10% heat-inactivated FBS and 1% streptomycin/penicillin in T25 cell culture flasks. The cultures were diluted every 3-4 days to maintain the parasite density between 10^6 and 4×10^7 parasites/mL, as determined microscopically with a hemocytometer.[44]

T. vaginalis F1623 trophozoites were grown in TYM (trypticase, yeast extract, maltose)-Diamond's medium supplemented with 180 mM ammonium iron (II) sulfate at 37 °C under anaerobic conditions. Trophozoites were seeded at approximately 1×10^5 cells/ml into 25 mL universal bottles, which were then completely filled and tightly capped for 24 h. Cells were passaged when at a density of ~1×10^6 cells/mL, as determined microscopically with a hemocytometer.[15]

2.5.4. Preparation of cell lysates

All cell types in their respective media were centrifuged for 10 min at 24,000 x *g* and 4 °C. The supernatant was discarded, and the cells resuspended in PBS before undergoing the same centrifugation again. This process was repeated once more. After the final centrifugation, the supernatant was removed and cell pellets were stored at -80 °C.

PBS was used as a lysis buffer and approximately twice the volume was added relative to the volume of the pellet so that a final concentration of 5-10 mg/mL was achieved. Cell lysis was performed on ice using a Qsonica CL-18 sonicator probe set to pulses of 2 s with 5 s rest periods over a total of 44 s. Sonicated samples were centrifuged for 10 min at 11,000 x *g* and 4 °C The supernatant was recovered, aliquoted, flash frozen in a dry ice/acetone bath and stored at -80 °C. Protein concentration was determined using the Pierce ™ BCA Protein Assay kit (Fisher #23227).

2.5.5. HEK293 cell viability assay

Resazurin was used to measure HEK293 cell viability as described previously.[42] All test compounds were dissolved and diluted in 100% DMSO. Compounds were diluted three-fold through an eight-point concentration down from 4 μM. Compound (1 μL) was spotted into each well of a clear, flat-bottomed 96-well plate (Fisher #FB012931) followed by addition of 49 μL DMEM medium. Cells were diluted to 4 x 10^5 cells/mL and a 50 μL solution dispensed into each well. Cells were incubated for 48 h at 37 °C in a 5% CO_2 atmosphere. After 48 h, 20 μL 0.5 mM resazurin in PBS was added into each well. Assay plates were incubated in the dark for 2 h at 37°C and 5% CO_2. Fluorescence was measured at 531/595 nm ex/em wavelengths in a 2104 EnVision® multilabel plate reader. EC_{50} values were calculated using GraphPad Prism 8 by normalizing

activity to DMSO controls and interpolating the data using the "Sigmoidal, 4PL, X is log(concentration)" algorithm.

2.5.6. Human c20S activity and inhibition assays

Inhibitors were first diluted in DMSO so that the final DMSO concentration in each assay well was 2.5%. All other dilutions were prepared in assay buffer containing 50 mM HEPES, 1 mM DTT, pH 7.5. To activate c20S, 4 nM c20S (R&D Systems; E-360) was mixed with 200 nM PA28α (R&D Systems; E-381) in equal volume proportions for one 1 h before addition of inhibitor. To normalize the DMSO concentration, all probes and inhibitors were diluted, 2- or 5-fold, in 100% DMSO before being transferred to wells containing c20S so that the final concentration was 2.5%. This mixture was incubated for 1 h at RT and 4 μL then transferred into 384-well small volume plates (Greiner #784900). Immediately afterwards, 4 μL of AMC substrate was added to a final concentration of 50 μM. The β1, β2 and β5 activities of c20S were measured using Z-LLE-AMC, Boc-LRR-AMC and Suc-LLVY-AMC, respectively. The rate of AMC cleavage was measured for 4 h and the potency of each inhibitor was compared to vehicle (DMSO) control. All reactions were performed at 37°C in triplicate in a final volume of 8 μL. Fluorescence was measured at ex/em 360 nm/460 nm in a Biotek Synergy™ HTX plate reader. IC_{50} values were calculated using GraphPad Prism 8 by normalizing activity to DMSO controls and interpolating the data using the "Sigmoidal, 4PL, X is log(concentration)" algorithm.

2.5.7. Probe incubation, click chemistry and SDS-PAGE

Each sample contained 1 μg/μL lysate using PBS to dilute as necessary. Inhibitors were first diluted with 100% DMSO to the appropriate concentration and 1 μL inhibitor or vehicle

(DMSO) was added into each sample and incubated for 1 h at 37 ºC. Afterwards, 1 μL probe was diluted in 100% DMSO so that the final concentration was 2 μM for Me_4BodipyFL-Ahx$_3$L$_3$VS with all three cell extracts, 10 μM for LJL-1 and LJL-2 with the *L. donovani* extracts, and 2 μM LJL-1 and LJL-2 with the *T. vaginalis* and HepG2 extracts. Probes were co-incubated with each sample for 3 h at 37 °C.

Samples requiring click chemistry, using a starting volume 16 μL, were denatured using 2.5 μL 1% SDS in PBS and briefly vortexed. To achieve a final concentration 1.5-fold greater than the alkyne, TAMRA biotin azide (Vector Laboratories #CCT-1048) was diluted in 100% DMSO and 0.5 μL was added to the sample. Next, 2.5 μL of the copper catalyst mixture was freshly prepared; specifically, a 3:1:1 ratio of 1.7 mM TBTA (in 20% DMSO in *t*-butanol), 50 mM $CuSO_4$ (in water) and 50 mM TCEP (in water and adjusted to pH 7.0 using 1 M NaOH). This sample mixture, now 21.5 μL, was left for 30 min at 37 °C.

Next, 8 μL 4X Bolt™ LDS sample buffer (Fisher #B0007) containing 250 mM DTT was added to each sample and boiled for 5 min at 95 °C. Samples were quickly centrifuged and placed into precast 10, 15- or 17- well Bolt™ 1 mm 4-12% Bis-Tris Plus mini protein gels (Fisher #NW04120BOX, NW04125BOX, NW04127BOX). Gels were placed in an Invitrogen™ mini gel tank (Fisher #A25977) containing 1X MOPS running buffer (Fisher #NP000102) at the designated volume. The last lane at either side of the gel was loaded with 1.5 μL PageRuler™ prestained protein ladder (Fisher #26616). Gels were first electrophoresed at 60 V until the dye front was approximately 15% below the comb, at which point, the voltage was increased to 120 V for the duration of electrophoresis. Gels were washed with water after electrophoresis and fixed for 5 min in 6:3:1 water:ethanol:acetic acid. Fluorescent imaging was performed using a Bio-Rad ChemiDoc

MP Imaging System with the settings optimized to visualize Qdots 525 (Bodipy) or Alexa 546 (TAMRA).

2.5.8. Affinity purification

To 500 µL 2 mg/mL lysate, 10 µL inhibitor(s) or vehicle (DMSO) was added and the lysate incubated for 1 h at 37 °C. Next, 10 µM (10 µL) LJL-1 for *L. donovani* and 2 µM LJL-2 for *T. vaginalis*, was added to the lysate and incubated for 1 h at 37°C. Proteins were denatured by adding 62.5 µL 1% SDS in PBS followed by brief vortexing. Click chemistry was initiated by adding 62.5 µL of the copper catalyst mixture to 12.5 µL TAMRA biotin azide (final concentrations of 15 and 3 µM for *L. donovani* and *T. vaginalis*, respectively) followed by a 30 min incubation at 37 °C.

After incubation, the lysate was precipitated using three volumes of cold acetone and standing in a -20 °C freezer for 30 min. The precipitated protein sample was centrifuged at 11,000 x *g* and 4 °C for 5 min to generate a pellet and the supernatant was aspirated. The protein pellet was washed three times with cold acetone. In each wash cycle, the supernatant was aspirated, the pellet resuspended in cold acetone and centrifuged. After the final wash step, the supernatant was aspirated, and the protein pellet was left to air dry. Once dried, the pellet was resuspended in 250 µL 1% SDS in PBS and vortexed. The resuspended sample was centrifuged at 11,000 x *g* and 4 °C for 5 min and the supernatant was retained, while any insoluble proteins formed a pellet and were discarded. This supernatant was added to 75 µL NeutrAvidin™ Agarose resin (Fisher #PI29200) and rotated overnight at r.t. on an end-over-end Labquake® Shaker/Rotisserie. The following day, this suspension was transferred onto a Bio-Rad Micro Bio-Spin™ column (Bio-Rad #7326204) and centrifuged at 11,000 x *g* for 30 sec. The beads were washed five times with each of the following solutions: 1) 4 M Urea, 250 mM NaCl and 2% SDS; 2) 8 M urea; and 3) 50

mM ammonium bicarbonate. After the final wash, the beads were transferred into a separate microfuge tube and 40 µL 4x Bolt™ LDS sample buffer containing 250 mM DTT were added. Each sample was boiled for 15 min at 95 °C to disrupt biotin-neutravidin binding. Samples were quickly centrifuged and the supernatant placed into precast 15 well Bolt™ 1 mm 4-12% Bis-Tris Plus mini protein gels. Electrophoresis, gel fixation and fluorescence visualization were as described above.

2.5.9. In-gel trypsin digest

The protocol published by Shevchenko et al. (2006) [45] was used for in-gel trypsin digestion of all protein bands of interest.

2.5.10. Proteomic sample preparation and analysis

Tryptic samples were desalted using custom made C18 spin tips by packing Empore™ C18 extraction disks (Fisher #13-110-019) into P1000 pipette tips. C18 tips were placed into centrifuge adapters (GL sciences #5010-21514) and then into 2 mL microfuge tubes. P1000 pipette tips were trimmed at the largest end so that they would fit inside a benchtop centrifuge.

C18 was equilibrated with 150 µL LC-MS grade ACN and centrifuged at 400 x *g* for 1 min at RT. Next, 150 µL 0.1% TFA in LC-MS grade water was centrifuged through the tips at 400 x *g* for 2 min at r.t. twice. During centrifugation, the proteomic sample(s) were acidified with TFA to achieve a final pH <3.0. Afterwards, the acidified sample was transferred to the C18 tip and centrifuged at 400 x *g* for 4 min or until all the liquid eluted through the tip. The C18 was centrifuged using 150 µL 0.1% TFA in LC-MS grade water at 400 x *g* for 4 min. This was repeated four times. After the last wash, the microfuge vials were replaced with max recovery tubes and the

peptides were eluted using 150 µL 0.1% TFA in 50% ACN in water and centrifuged at 400 x *g* for 4 min and two cycles. The final elution involved 150 µL 0.1% TFA in 80% ACN in water followed by centrifugation at 400 x *g* for 4 min. Approximately 450 µL sample was then placed in a rotary evaporator until dryness and stored at -80 °C.

Proteome analysis was performed using an Easy- nLC coupled to an Orbitrap Eclipse mass spectrometer (Thermo Fisher Scientific). The 71-min method, 60 min effective gradient of solvent A (2% ACN, 0.1% FA) to solvent B (80% ACN, 0.1% FA) started at 3% to 23% B over 45 min; from 23% to 40% B over 15 min; from 40% to 95% B over one min and holding for 10 min. The flow rate was 200 nL/min. The Orbitap Eclipse mass spectrometer was performed in positive mode. MS1 spectra were scanned in a range of 375- 1500 m/z, at a resolution of 60000, with a maximum injection time (max IT) in automatic mode, and an AGC target in standard mode. The data acquisition mode was set with a time between master scans of 3 s. The MS2 quadrupole isolation mode had an isolation width of 0.7 m/z. The MS2 spectra scanned range was set in auto mode with a resolution of 15,000. The AGC target was set at 400 % with a maximum injection time of 22 ms. The normalized collision energy was set to 30 % and the dynamic exclusion was set at 60 s.

RAW data were processed using Peaks 8.5 (Bioinformatics Solutions Inc.). MS2 data were searched against either the *L. donovani* (Proteome ID: UP000008980) or the *T. vaginalis* (Proteome ID: UP000001542) proteome. A precursor tolerance of 20 ppm and 0.01 Da for MS2 fragments was defined. Trypsin was used for protease digestion. Data were filtered to a 1% peptide false discovery rate with the target-decoy strategy. Peptides were quantified with label free quantification.

2.6. Acknowledgements

Chapter 2, in full, is a reprint of a manuscript that is currently under review at *ACS Omega* as of May 2024. The research described was supported by the NIH grants R21AI171824 to AJO and CRC, and R01AI158612 to AJO. HR-MS data were collected at the UC San Diego Chemistry and Biochemistry Molecular Mass Spectrometry Facility (MMSF). NMR spectra were collected at the UC San Diego Skaggs School of Pharmacy and Pharmaceutical Sciences NMR Facility. We thank Jair Lage De Siqueira-Neto and Miriam Giardini for providing *L. donovani* pellets, Lars Eckmann and Yukiko Miyamoto for the *T. vaginalis* lysate, and Elizabeth Winzeler for the live HepG2 cells.

2.7. References

(1) Thibaudeau, T. A.; Smith, D. M. A Practical Review of Proteasome Pharmacology. *Pharmacol Rev* **2019**, *71* (2), 170-197. DOI: 10.1124/pr.117.015370. Ciechanover, A.; Schwartz, A. L. The ubiquitin-proteasome pathway: the complexity and myriad functions of proteins death. *Proc Natl Acad Sci U S A* **1998**, *95* (6), 2727-2730. DOI: 10.1073/pnas.95.6.2727. Saha, A.; Oanca, G.; Mondal, D.; Warshel, A. Exploring the Proteolysis Mechanism of the Proteasomes. *J Phys Chem B* **2020**, *124* (27), 5626-5635. DOI: 10.1021/acs.jpcb.0c04435.

(2) Adams, J. The development of proteasome inhibitors as anticancer drugs. *Cancer Cell* **2004**, *5* (5), 4.

(3) Kopp, F.; Hendil, K. B.; Dahlmann, B.; Kristensen, P.; Sobek, A.; Uerkvitz, W. Subunit arrangement in the human 20S proteasome. *Proc Natl Acad Sci U S A* **1997**, *94* (7), 2939-2944. DOI: 10.1073/pnas.94.7.2939.

(4) Moore, B. S.; Eustáquio, A. S.; McGlinchey, R. P. Advances in and applications of proteasome inhibitors. *Curr Opin Chem Biol* **2008**, *12* (4), 434-440. DOI: 10.1016/j.cbpa.2008.06.033. Collins, G. A.; Goldberg, A. L. The Logic of the 26S Proteasome. *Cell* **2017**, *169* (5), 792-806. DOI: 10.1016/j.cell.2017.04.023.

(5) Groen, K.; van de Donk, N.; Stege, C.; Zweegman, S.; Nijhof, I. S. Carfilzomib for relapsed and refractory multiple myeloma. *Cancer Manag Res* **2019**, *11*, 2663-2675. DOI: 10.2147/cmar.S150653. Shirley, M. Ixazomib: First Global Approval. *Drugs* **2016**, *76* (3), 405-411. DOI: 10.1007/s40265-016-0548-5.

(6) Chen, D.; Frezza, M.; Schmitt, S.; Kanwar, J.; Dou, Q. P. Bortezomib as the first proteasome inhibitor anticancer drug: current status and future perspectives. *Curr Cancer Drug Targets* **2011**, *11* (3), 239-253. DOI: 10.2174/156800911794519752.

(7) Bibo-Verdugo, B.; Wang, S. C.; Almaliti, J.; Ta, A. P.; Jiang, Z.; Wong, D. A.; Lietz, C. B.; Suzuki, B. M.; El-Sakkary, N.; Hook, V.; Galvesen, G. S.; Gerwick, W. H.; Caffrey, C. R.; O'Donoghue, A. J. The Proteasome as a Drug Target in the Metazoan Pathogen, *Schistosoma mansoni*. *ACS Infect Dis* **2019**, *5* (10), 1802-1812. DOI: 10.1021/acsinfecdis.9b00237.

(8) O'Donoghue, A. J.; Bibo-Verdugo, B.; Miyamoto, Y.; Wang, S. C.; Yang, J. Z.; Zuill, D. E.; Matsuka, S.; Jiang, Z.; Almaliti, J.; Caffrey, C. R.; Gerwick, W. H.; Eckmann, L. 20S Proteasome as a Drug Target in *Trichomonas vaginalis*. *Antimicrob Agents Chemother* **2019**, *63* (11). DOI: 10.1128/AAC.00448-19. Jalovecka, M.; Hartmann, D.; Miyamoto, Y.; Eckmann, L.; Hajdusek, O.; O'Donoghue, A. J.; Sojka, D. Validation of Babesia proteasome as a drug target. *Int J Parasitol Drugs Drug Resist* **2018**, *8* (3), 394-402. DOI: 10.1016/j.ijpddr.2018.08.001.

(9) Caffrey, C. R.; Steverding, D.; Ferreira, R. S.; de Oliveira, R. B.; O'Donoghue, A. J.; Monti, L.; Ballatore, C.; Bachovchin, K. A.; Ferrins, L.; Pollastri, M. P.; Zorn, K. M.; Foil, D. H.; Clark, A. M.; Mottin, M.; Andrade, C. H.; de Siqueira-Neto, J. L.; Ekins, S. Drug Discovery and Development for Kinetoplastid Diseases. *Burger's Medicinal Chemistry and Drug Discovery* **2021**, 79.

(10) Xie, S. C.; Gillett, D. L.; Spillman, N. J.; Tsu, C.; Luth, M. R.; Ottilie, S.; Duffy, S.; Gould, A. E.; Hales, P.; Seager, B. A.; Charron, C. L.; Bruzzese, F.; Yang, X.; Zhao, X.; Huang, S.; Hutton, C. A.; Burrows, J. N.; Winzeler, E. A.; Avery, V. M.; Dick, L. R.; Tilley, L. Target Validation and Identification of Novel Boronate Inhibitors of the Plasmodium falciparum Proteasome. *J Med Chem* **2018**, *61* (22), 10053-10066. DOI: 10.1021/acs.jmedchem.8b01161.

(11) Li, H.; O'Donoghue, A. J.; van der Linden, W. A.; Xie, S. C.; Yoo, E.; Foe, I. T.; Tilley, L.; Craik, C. S.; da Fonseca, P. C.; Bogyo, M. Structure- and function-based design of Plasmodium-selective proteasome inhibitors. *Nature* **2016**, *530* (7589), 233-236. DOI: 10.1038/nature16936.

(12) Zhang, H.; Ginn, J.; Zhan, W.; Liu, Y. J.; Leung, A.; Toita, A.; Okamoto, R.; Wong, T. T.; Imaeda, T.; Hara, R.; Yukawa, T.; Michino, M.; Vendome, J.; Beuming, T.; Sato, K.; Aso, K.; Meinke, P. T.; Nathan, C. F.; Krikman, L. A.; Lin, G. Design, Synthesis, and Optimization of Macrocyclic Peptides as Species-Selective Antimalaria Proteasome Inhibitors. *J Med Chem* **2022**, *65*

(13) LaMonte, G. M.; Almaliti, J.; Bibo-Verdugo, B.; Keller, L.; Zou, B. Y.; Yang, J.; Antonova-Koch, Y.; Orjuela-Sanchez, P.; Boyle, C. A.; Vigil, E.; Wang, L.; Goldgof, G. M.; Gerwick, L.; O'Donoghue, A. J.; Winzeler, E. A.; Gerwick, W. H.; Ottilie, S. Development of a Potent Inhibitor of the Plasmodium Proteasome with Reduced Mammalian Toxicity. *J Med Chem* **2017**, *60* (15), 6721-6732. DOI: 10.1021/acs.jmedchem.7b00671.

(13) Wyllie, S.; Brand, S.; Thomas, M.; De Rycker, M.; Chung, C. W.; Pena, I.; Bingham, R. P.; Bueren-Calabuig, J. A.; Cantizani, J.; Cebrian, D.; Craggs, P. D.; Ferguson, L.; Goswami, P.; Hobrath, J.; Howe, J.; Jeacock, L.; Ko, E.; Korczynska, J.; Maclean, L.; Manthri, S.; Martinez, M. S.; Mata-Cantero, L.; Moniz, S.; Nühs, A.; Osuna-Cabello, M.; Pinto, E.; Riley, J.; Robinson, S.; Rowland, P.; Simeons, F. R. C.; Shishikura, Y.; Spinks, D.; Stojanovski, L.; Thomas, J.; Thompson, S.; Gaza, E. V.; Wall, R. J.; Zuccotto, F.; Horn, D.; Ferguson, M. A. J.; Fairlamb, A. H.; Fiandor, J. M.; Martin, J.; Gray, D. W.; Miles, T. J.; Gilbert, I. H.; Read, K. D.; Marco, M.; Wyatt, P. G. Preclinical candidate for the

treatment of visceral leishmaniasis that acts through proteasome inhibition. *Proc Natl Acad Sci U S A* **2019**, *116* (19), 9318-9323. DOI: 10.1073/pnas.1820175116.
(14) Jiang, Z.; Silva, E. B.; Liu, C.; Fajtová, P.; Liu, L. J.; El-Sakkary, N.; Skinner, D. E.; Syed, A.; Wang, S. C.; Caffrey, C. R.; O'Donoghue, A. J. Development of subunit selective proteasome substrates for S*chistosoma species*. *biorxiv* **2024**.
(15) Fajtova, P.; Hurysz, B. M.; Miyamoto, Y.; Serafim, M.; Jiang, Z.; Trujillo, D. F.; Liu, L.; Somani, U.; Almaliti, J.; Myers, S. A.; Caffrey, C. R.; Gerwick, W. H.; Kirk, C. J.; Boura, E.; Eckmann, L.; O'Donoghue, A. J. Development of subunit selective substrates for *Trichomonas vaginalis* proteasome. *bioRxiv* **2023**. DOI: 10.1101/2023.04.05.535794.
(16) Hua, S.-b.; To, W.-Y.; Nguyen, T. T.; Wong, M.-L.; Wang, C. C. Purification and characterization of proteasomes from Trypanosoma brucei. *Molecular and biochemical Parasitology* **1996**, *78* (1-2), 13. Beyette, J. R.; Hubbell, T.; Monaco, J. J. Purification of 20S proteasomes. *Methods Mol Biol* **2001**, *156*, 1-16. DOI: 10.1385/1-59259-062-4:1.
(17) Dong, Y.; Zhang, S.; Wu, Z.; Li, X.; Wang, W. L.; Zhu, Y.; Stoilova-McPhie, S.; Lu, Y.; Finley, D.; Mao, Y. Cryo-EM structures and dynamics of substrate-engaged human 26S proteasome. *Nature* **2019**, *565* (7737), 49-55. DOI: 10.1038/s41586-018-0736-4. Morris, E. P.; da Fonseca, P. C. A. High-resolution cryo-EM proteasome structures in drug development. *Acta Crystallogr D Struct Biol* **2017**, *73* (Pt 6), 522-533. DOI: 10.1107/s2059798317007021.
(18) Hewings, D. S.; Flygare, J. A.; Wertz, I. E.; Bogyo, M. Activity-based probes for the multicatalytic proteasome. *FEBS J* **2017**, *284* (10), 1540-1554. DOI: 10.1111/febs.14016. Li, H.; van der Linden, W. A.; Verdoes, M.; Florea, B. I.; McAllister, F. E.; Govindaswamy, K.; Elias, J. E.; Bhanot, P.; Overkleeft, H. S.; Bogyo, M. Assessing subunit dependency of the Plasmodium proteasome using small molecule inhibitors and active site probes. *ACS Chem Biol* **2014**, *9* (8), 1869-1876. DOI: 10.1021/cb5001263.
(19) Verdoes, M.; Florea, B. I.; Menendez-Benito, V.; Maynard, C. J.; Witte, M. D.; van der Linden, W. A.; van den Nieuwendijk, A. M.; Hofmann, T.; Berkers, C. R.; van Leeuwen, F. W.; Groothuis, T. A.; Leeuwenburgh, M. A.; Ovaa H.; Neefjes, J. J.; Filippov, D. V.; van der Marel, G. A.; Dantuma, N. P. Overkleeft, H. S. A fluorescent broad-spectrum proteasome inhibitor for labeling proteasomes in vitro and in vivo. *Chem Biol* **2006**, *13* (11), 1217-1226. DOI: 10.1016/j.chembiol.2006.09.013.
(21) Siqueira-Neto, J. L.; Debnath, A.; McCall, L. I.; Bernatchez, J. A.; Ndao, M.; Reed, S. L.; Rosenthal, P. J. Cysteine proteases in protozoan parasites. *PLoS Negl Trop Dis* **2018**, *12* (8), e0006512. DOI: 10.1371/journal.pntd.0006512.
(22) Caffrey, C. R.; Goupil, L.; Rebello, K. M.; Dalton, J. P.; Smith, D. Cysteine proteases as digestive enzymes in parasitic helminths. *PLoS Negl Trop Dis* **2018**, 20.
(23) Kolb, H.; Finn, M.; Sharpless, K. Click Chemistry: Diverse Chemical Function from a Few Good Reactions. **2001**, *40*, 1983-2181.
(24) Huber, E. M.; de Bruin, G.; Heinemeyer, W.; Paniagua Soriano, G.; Overkleeft, H. S.; Groll, M. Systematic Analyses of Substrate Preferences of 20S Proteasomes Using Peptidic Epoxyketone Inhibitors. *J Am Chem Soc* **2015**, *137* (24), 7835-7842. DOI: 10.1021/jacs.5b03688.
(25) Berkers, C. R.; van Leeuwen, F. W.; Groothuis, T. A.; Peperzak, V.; van Tilburg, E. W.; Borst, J.; Neefjes, J. J.; Ovaa, H. Profiling proteasome activity in tissue with fluorescent probes. *Mol Pharm* **2007**, *4* (5), 739-748. DOI: 10.1021/mp0700256.

(26) Kisselev, A. F.; Garcia-Calvo, M.; Overkleeft, H. S.; Peterson, E.; Pennington, M. W.; Ploegh, H. L.; Thornberry, N. A.; Goldberg, A. L. The caspase-like sites of proteasomes, their substrate specificity, new inhibitors and substrates, and allosteric interactions with the trypsin-like sites. *J Biol Chem* **2003**, *278* (38), 35869-35877. DOI: 10.1074/jbc.M303725200. Geurink, P. P.; van der Linden, W. A.; Mirabella, A. C.; Gallastegui, N.; de Bruin, G.; Blom, A. E.; Voges, M. J.; Mock, E. D.; Florea, B. I.; van der Marel, G. A.; Driessen, C.; van der Stelt, M.; Groll, M.; Overkleeft, H. S.; Kisselev, A. F. Incorporation of non-natural amino acids improves cell permeability and potency of specific inhibitors of proteasome trypsin-like sites. *J Med Chem* **2013**, *56* (3), 1262-1275. DOI: 10.1021/jm3016987. Muli, C. S.; Trader, D. J. 20S proteasome hydrolysis of LLVY substrates to determine preferences for moieties in its primed substrate channel. *Bioorg Med Chem Lett* **2023**, *85*, 129233. DOI: 10.1016/j.bmcl.2023.129233.

(27) Lidumniece, E.; Withers-Martinez, C.; Hackett, F.; Collins, C. R.; Perrin, A. J.; Koussis, K.; Bisson, C.; Blackman, M. J.; Jirgensons, A. Peptidic boronic acids are potent cell-permeable inhibitors of the malaria parasite egress serine protease SUB1. *Proc Natl Acad Sci U S A* **2021**, *118* (20). DOI: 10.1073/pnas.2022696118.

(28) Grewal, J. S.; Catta-Preta, C. M. C.; Brown, E.; Anand, J.; Mottram, J. C. Evaluation of clan CD C11 peptidase PNT1 and other Leishmania mexicana cysteine peptidases as potential drug targets. *Biochimie* **2019**, *166*, 150-160. DOI: 10.1016/j.biochi.2019.08.015.

(29) Wang, G.; Mahesh, U.; Chen, G. Y.; Yao, S. Q. Solid-phase synthesis of peptide vinyl sulfones as potential inhibitors and activity-based probes of cysteine proteases. *Org Lett* **2003**, *5* (5), 737-740. DOI: 10.1021/ol0275567. McKerrow, J. H. Update on drug development targeting parasite cysteine proteases. *PLoS Negl Trop Dis* **2018**, *12* (8), e0005850. DOI: 10.1371/journal.pntd.0005850.

(30) Palmer, J. T.; Rasnick, D.; Klaus, J. L.; Brömme, D. Vinyl sulfones as mechanism-based cysteine protease inhibitors. *J Med Chem* **1995**, *38* (17), 3193-3196. DOI: 10.1021/jm00017a002.

(31) Pereira, A. R.; Kale, A. J.; Fenley, A. T.; Byrum, T.; Debonsi, H. M.; Gilson, M. K.; Valeriote, F. A.; Moore, B. S.; Gerwick, W. H. The carmaphycins: new proteasome inhibitors exhibiting an α,β-epoxyketone warhead from a marine cyanobacterium. *Chembiochem* **2012**, *13* (6), 810-817. DOI: 10.1002/cbic.201200007.

(32) Cromm, P. M.; Crews, C. M. The Proteasome in Modern Drug Discovery: Second Life of a Highly Valuable Drug Target. *ACS Cent Sci* **2017**, *3* (8), 830-838. DOI: 10.1021/acscentsci.7b00252. Bibo-Verdugo, B.; Jiang, Z.; Caffrey, C. R.; O'Donoghue, A. J. Targeting proteasomes in infectious organisms to combat disease. *FEBS J* **2017**, *284* (10), 1503-1517. DOI: 10.1111/febs.14029.

(33) Besse, A.; Besse, L.; Kraus, M.; Mendez-Lopez, M.; Bader, J.; Xin, B. T.; de Bruin, G.; Maurits, E.; Overkleeft, H. S.; Driessen, C. Proteasome Inhibition in Multiple Myeloma: Head-to-Head Comparison of Currently Available Proteasome Inhibitors. *Cell Chem Biol* **2019**, *26* (3), 340-351.e343. DOI: 10.1016/j.chembiol.2018.11.007.

(34) Liu, Y.; Patricelli, M. P.; Cravatt, B. F. Activity-based protein profiling: the serine hydrolases. *Proc Natl Acad Sci U S A* **1999**, *96* (26), 14694-14699. DOI: 10.1073/pnas.96.26.14694. Porta, E. O. J.; Isern, J. A.; Kalesh, K.; Steel, P. G. Discovery of Leishmania Druggable Serine Proteases by Activity-Based Probe Profiling. *Front Pharmacol* **2022**, *13*, 929493. DOI: 10.3389/fphar.2022.929493.

(35) Manoharan, A.; Jayan, J.; Rangarajan, T. M.; Bose, K.; Benny, F.; Ipe, R. S.; Kumar, S.; Kukreti, N.; Abdelgawad, M. A.; Ghoneim, M. M.; Kim, H.; Wathew, B. "Click Chemistry": An Emerging Tool for Developing a New Class of Structural Motifs against Various Neurodegenerative Disorders. *ACS Omega* **2023**, *8* (47), 44437-44457. DOI: 10.1021/acsomega.3c04960. Li, X.; Xiong, Y. Application of "Click" Chemistry in Biomedical Hydrogels. *ACS Omega* **2022**, *7* (42), 36918-36928. DOI: 10.1021/acsomega.2c03931.
(36) Baskin, J. M.; Prescher, J. A.; Laughlin, S. T.; Agard, N. J.; Chang, P. V.; Miller, I. A.; Lo, A.; Codelli, J. A.; Bertozzi, C. R. Copper-free click chemistry for dynamic in vivo imaging. *Proc Natl Acad Sci U S A* **2007**, *104* (43), 16793-16797. DOI: 10.1073/pnas.0707090104.
(37) Leunissen, E. H.; Meuleners, M. H.; Verkade, J. M.; Dommerholt, J.; Hoenderop, J. G.; van Delft, F. L. Copper-free click reactions with polar bicyclononyne derivatives for modulation of cellular imaging. *Chembiochem* **2014**, *15* (10), 1446-1451. DOI: 10.1002/cbic.201402030.
(38) Zanon, P. R. A.; Lewald, L.; Hacker, S. M. Isotopically Labeled Desthiobiotin Azide (isoDTB) Tags Enable Global Profiling of the Bacterial Cysteinome. *Angew Chem Int Ed Engl* **2020**, *59* (7), 2829-2836. DOI: 10.1002/anie.201912075.
(39) Leriche, G.; Chisholm, L.; Wagner, A. Cleavable linkers in chemical biology. *Bioorg Med Chem* **2012**, *20* (2), 571-582. DOI: 10.1016/j.bmc.2011.07.048.
(40) MacGregor, P.; Gonzalez-Munoz, A. L.; Jobe, F.; Taylor, M. C.; Rust, S.; Sandercock, A. M.; Macleod, O. J. S.; Van Bocxlaer, K.; Francisco, A. F.; D'Hooge, F.; Tiberghien, A.; Barry, C. S.; Howard, P.; Higgins, M. K.; Vaugham T. J.; Minter, R.; Carrington, M. A single dose of antibody-drug conjugate cures a stage 1 model of African trypanosomiasis. *PLoS Negl Trop Dis* **2019**, *13* (5), e0007373. DOI: 10.1371/journal.pntd.0007373.
(41) Monti, L.; Liu, L. J.; Varricchio, C.; Lucero, B.; Alle, T.; Yang, W.; Bem-Shalom, I.; Gilson, M.; Brunden, K. R.; Brancale, A.; Caffrey, C. R.; Ballatore, C. Structure-Activity Relationships, Tolerability and Efficacy of Microtubule-Active 1,2,4-Triazolo[1,5-a]pyrimidines as Potential Candidates to Treat Human African Trypanosomiasis. *ChemMedChem* **2023**, *18* (20), e202300193. DOI: 10.1002/cmdc.202300193.
(42) Francisco, K. R.; Monti, L.; Yang, W.; Park, H.; Liu, L. J.; Watkins, K.; Amarasinghe, D. K.; Nalli, M.; Roberto Polaquini, C.; Regasini, L. O.; Magalhães, L. G.; Caffrey, C. R. Structure-activity relationship of dibenzylideneacetone analogs against the neglected disease pathogen, Trypanosoma brucei. *Bioorg Med Chem Lett* **2023**, *81*, 129123. DOI: 10.1016/j.bmcl.2023.129123.
(43) Mittal, N.; Davis, C.; McLean, P.; Calla, J.; Godinez-Macias, K. P.; Gardner, A.; Healey, D.; Orjuela-Sanchez, P.; Ottilie, S.; Chong, Y.; Gibson, C.; Winzeler, E. A. Human nuclear hormone receptor activity contributes to malaria parasite liver stage development. *Cell Chem Biol* **2023**, *30* (5), 486-498.e487. DOI: 10.1016/j.chembiol.2023.04.011.
(44) Siqueira-Neto, J. L.; Moon, S.; Jang, J.; Yang, G.; Lee, C.; Moon, H. K.; Chatelain, E.; Genovesio, A.; Cechetto, J.; Freitas-Junior, L. H. An image-based high-content screening assay for compounds targeting intracellular Leishmania donovani amastigotes in human macrophages. *PLoS Negl Trop Dis* **2012**, *6* (6), e1671. DOI: 10.1371/journal.pntd.0001671.

(45) Shevchenko, A.; Tomas, H.; Havlis, J.; Olsen, J. V.; Mann, M. In-gel digestion for mass spectrometric characterization of proteins and proteomes. *Nat Protoc* **2006**, *1* (6), 2856-2860. DOI: 10.1038/nprot.2006.468.
(46) Caffrey, C. R.; Hansell, E.; Lucas, K. D.; Brinen, L. S.; Hernandez, A. A.; Cheng, J.; Gwaltney II, S. L.; Roush, W. R.; Stierhof, Y.-D.; Bogyo, M.; Steverding, D.; McKerrow, J. H. Active site mapping, biochemical properties and subcellular localization of rhodesain, the major cysteine protease of *Trypanosoma brucei rhodesiense*. *Molecular and Biochemical Parasitology* **2001**, *118* (1), 12.

2.8. Supporting information

Supporting information: RAW files for all proteomic analysis can be found on: ftp://massive.ucsd.edu/v07/MSV000094658/.

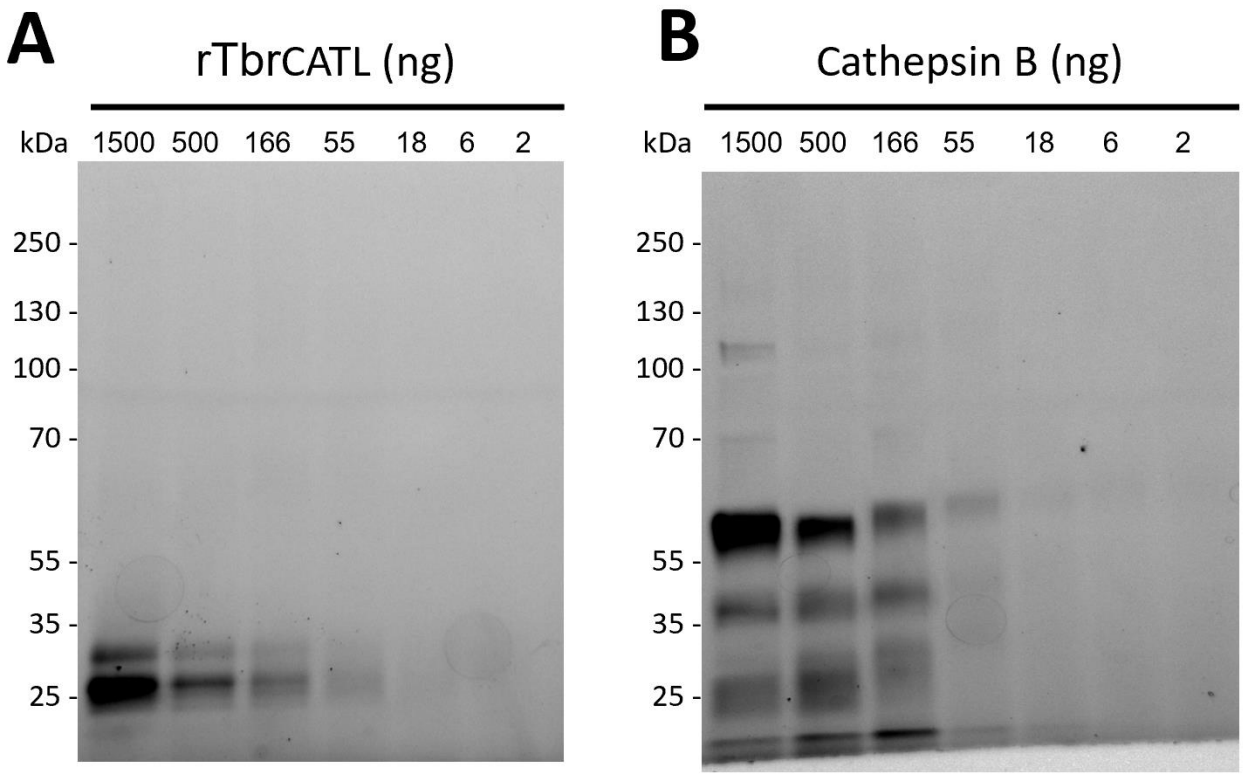


Figure 2.8.1. Me_4BodipyFL-Ahx$_3$L$_3$VS reacts with cysteine proteases. SDS-PAGE visualizing the reaction of Me_4BodipyFL-Ahx$_3$L$_3$VS with various concentrations of recombinant *T. brucei* cathepsin L [46] (**A**) and human cathepsin B (R&D Systems #953-CY-010) (**B**).

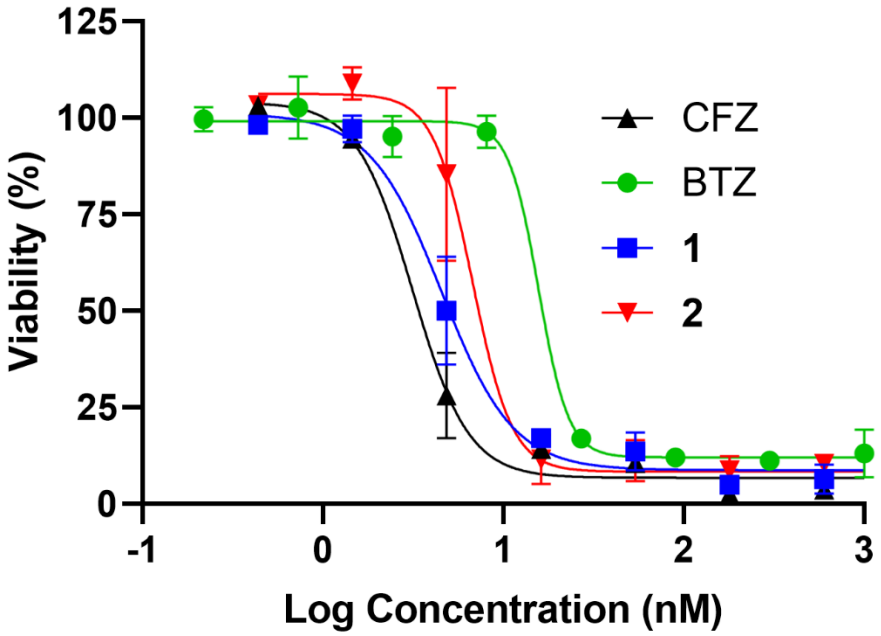


Figure 2.8.2. HEK293 cell viability in the presence of proteasome inhibitors. Concentration-dependent inhibition of growth of HEK29 cells in the presence of LJL-1 and -2, and the anti-cancer proteasome inhibitors, CFZ and BTZ. One biological assay performed in triplicate (n=3).

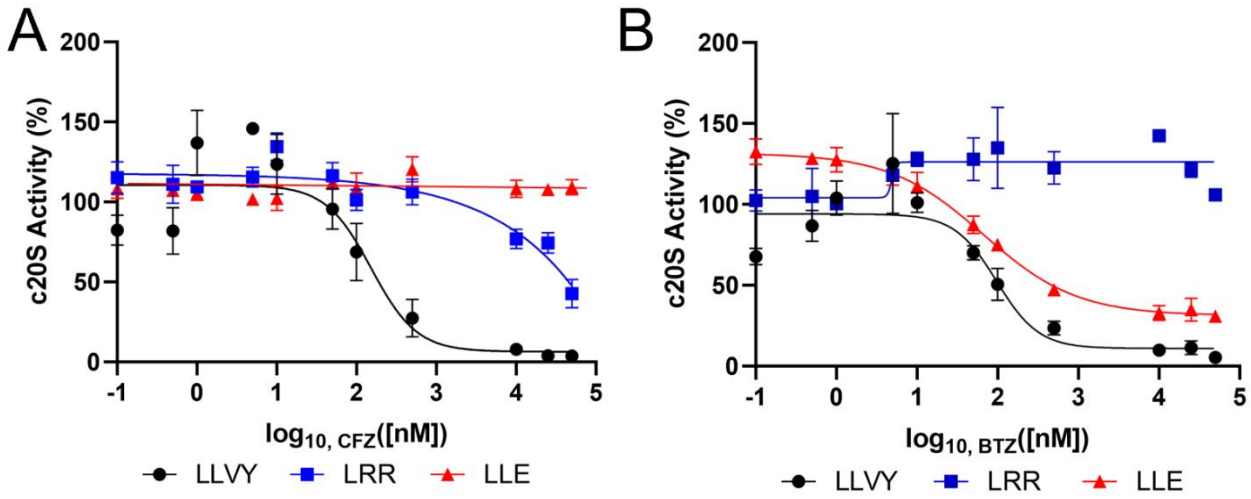


Figure 2.8.3. Inhibition of human c20S activity by CFZ and BTZ. Concentration-dependent inhibition of c20S catalytic β subunits by CFZ (**A**) and BTZ (**B**) as measured with subunit-specific AMC substrates for β5 (LLVY), β2 (LRR) and β1 (LLE). One biological assay performed in triplicate (n=3).

Chapter 3:

Carmaphycin B-based proteasome inhibitors to treat human African trypanosomiasis; structure-activity relationship and *in vivo* efficacy

3.1. Introduction

The *Trypanosoma* protozoan parasite causes the vector-borne disease, African Trypanosomiasis (AT) that affects both humans (HAT; Sleeping Sickness)[1, 2] and animals (AAT; Nagana).[3] Approximately 70 million people throughout sub-Saharan Africa are at risk of infection,[4] and two subspecies, *Trypanosoma brucei rhodesiense* and *Trypanosoma brucei gambiense,* are responsible for East and West African HAT, respectively.[5] AAT is caused by a broader range of *Trypanosoma* spp. affecting hundreds of millions of sheep, cattle and goats, with annual cattle production losses being estimated at USD $1 billion.[3] Transmission to humans occurs via the painful bite of an infected tsetse fly, and the disease progresses through two stages with different clinical manifestations: Stage 1 (hemolymphatic) may be asymptomatic or present flu-like symptoms, and the much more serious Stage 2 (meningo-encephalitic), which is associated with mood and behavioral changes, *e.g.*, hallucinations and disruption of sleep cycles, that ultimately deteriorate to coma and death if the infection is not adequately treated.[4, 6]

There is no vaccine[7] and drug treatment depends on the infecting subspecies and stage of disease.[8] Most of the traditional treatment options involve high frequency and/or long-duration parenteral administration of drugs that are associated with side effects,[9] some potentially life-threatening,[9, 10] and which require significant health care resources that are challenging for what is a rural disease of poverty.[11] The recent registration of the oral drug, fexinidazole,[12] and the continued clinical progression of the oral drug candidate, acoziborole,[13] will greatly simplify treatment. Yet, in spite of this encouraging progress, the ability of the *Trypanosoma* parasite to generate resistance,[14, 15] including cross resistance to some of the current drugs,[16, 17] underscores the need for pharmaco-readiness.

An exciting molecular target to have emerged over the last 20 years for the trypanosomatid parasites, *i.e.*, African and South American trypanosomes, and *Leishmania* spp., is the proteasome.[18-21] In humans, the 26S proteasome is a cytosolic, multi-subunit, protein degradative complex that is required for proteostasis in the cell.[22] The 26S complex comprises a barrel-shaped 20S proteasome core that is capped at either end by a 19S regulatory particle.[23, 24] The 20S core is composed of two rings of seven β subunits that are sandwiched between two rings of seven α subunits.[25] The β1, β2 and β5 subunits are proteolytically active and have caspase-, trypsin- and chymotrypsin-like activities, respectively.[26, 27] Reversible allosteric inhibitors that bind to a unique interface between the β4 and β5 subunits of the trypanosomatid 20S proteasome to sterically block the latter's hydrolytic activity, are in clinical development for treatment of visceral leishmaniasis.[28]

For the 20S proteasome of a number of protozoan[29, 30] and helminth[31] parasites, our approach has been to directly inhibit the activities of the catalytic β subunits using synthetic analogs of CPB, a peptidyl, marine natural product derived from the cyanobacterium *Symploca* spp.[32] CPB contains a C-terminal epoxyketone reactive group that covalently and irreversibly reacts with the active site threonine of the 20S catalytic β subunits.[32] For the malaria parasite, *Plasmodium falciparum*, preclinical studies with CPB analogs have advanced as essentially non-toxic compounds with nanomolar *in vitro* potencies against the parasite and proof-of-principle efficacy in animal models of infection.[29, 33]

Here, CPB and 27 analogs from the above-stated *P. falciparum* program were tested *in vitro* against *T. brucei*. We describe the structure-activity relationship (SAR) that involves engagement of the Tb20S catalytic β5 subunit and the finding that a D-configuration at the P3 position of the peptidyl backbone generates large selectivity indices *vs*. mammalian cells. For one such compound, we demonstrate a therapeutic benefit in a mouse model of *T. brucei* infection,

suggesting that mechanism-based, irreversible inhibitors of Tb20S might provide a new therapeutic strategy for treatment of AT and, possibly, other kinetoplastid diseases.

3.2. Results

3.2.1. SAR for antitrypanosomal activity *in vitro* by CPB and its analogs

CPB was tested for activity against *T. brucei brucei* Lister 427 *in vitro* using an established cell viability assay.[34, 35] After a 72-h incubation, an EC_{50} value of 31 nM was achieved, indicating that this compound has potent antitrypanosomal activity. However, CPB is also highly cytotoxic to HepG2[29, 33] cells with a CC_{50} value of 13 nM. Thus, with its selectivity index (SI; HepG2 CC_{50} / *T. brucei* EC_{50}) of <1, CPB was too cytotoxic to test in a mouse infection model. Therefore, we evaluated a set of 27 analogs of CPB, many of which had reduced HepG2 cytotoxicity.

CPB can be divided into four structural subunits: the leucine epoxyketone (EK) (P1), methionine sulfone (P2), valine (P3) and hexanoic acid (P4). The analogs tested here, for which a nomenclature has already been established[29, 33], consist of a C-terminal EK warhead, various amino acid sidechains at P1 through P3, and different N-terminal capping groups (Table 3.1). Many of the compounds in this series have a norleucine (Nle) in the P2 position and **J-1** differs from CPB only by the replacement of the P2 methionine sulfone with Nle. This replacement resulted in a compound with at least a 130-fold lower antitrypanosomal activity, but also a 10-fold lower HepG2 cytotoxicity.

Examining first the P3 position, we compared L-Val in **J-1** to L-Phe (**J-2**), 4-NH_2-L-Phe (**J-3**), 4-Boc-NH-L-Phe (**J-5**) and L-Trp (**J-6**) and found that none improved the SI. However, **J-6** was the most potent compound from this group with an EC_{50} value of 195 nM. We next tested four related analogs, **J-7**, **J-9**, **J-10** and **J-11**, that had the same P2 L-Nle as **J-2** through **J-6** but where

the P1 L-Leu had been replaced with L-Phe, and varied substituents at P3. The most selective analog (SI = 6) contained 4-NH_2-L-Phe at P3 (**J-9**), with EC_{50} and CC_{50} values of 567 and 3,410 nM, respectively.

Next, P2 was examined, and three compounds with 4-NH_2-L-Phe, 4-Boc-NH-L-Phe or L-Trp in the P2 position were coupled to derivatives with 4-NH_2-L-Phe (**J-12**), 4-Boc-NH-L-Phe (**J-14**) or L-Trp (**J-16**) at the P3, respectively. Although these compounds were more potent (EC_{50} values < 500 nM) than **J-9**, they were also more cytotoxic. **J-5** (EC_{50} > 4000 nM) and **J-14** (465 nM) both contain a P1 L-Leu and a P3 4-Boc-NH-L-Phe but differ at the P2 position (L-Nle *vs*. L-4-Boc-NH-L-Phe, respectively). The 10-fold increase in potency with **J-14** indicates, therefore, a preference for bulky, aromatic groups at P2.

The next analog tested, **J-19**, had D-Trp at P3, L-Nle at P2 and L-Leu at P1. This inhibitor differed from **J-6** only by the configuration of the P3 residue and had a similar antitrypanosomal activity (EC_{50} = 298 *vs*. 195 nM). However, **J-19** had 286-fold lower HepG2 toxicity and, therefore, better selectivity. Substitution of the P1 L-Leu in **J-19** for L-Phe in **J-51** increased potency by 5-fold and toxicity by 3-fold, but with a slightly improved SI. Fixing L-Phe at P1 and L-Nle at P2, we evaluated four additional compounds with D-amino acids at P3, specifically, D-Val (**J-50**), D-(OtBu)-Glu (**J-71**), D-Glu (**J-74**) and D-Gln (**J-76**). Of these, **J-71** was the most potent and selective compound with an SI of 122. These data reveal that a D-amino acid in the P3 position is the single biggest driver of selectivity for this group of compounds.

Finally, examining the P4 N-terminal cap, and using **J-50** (EC_{50} = 319 nM) as a starting point, cyclic P4 substituents such as morpholine (**J-53**), cyclohexyl (**J-55**) and phenyl (**J-56**) exhibited robust antitrypanosomal activity with EC_{50} values ranging from 88 to 568 nM. By contrast, linear substituents such as octanoyl (**J-54**) and 2-(meth-oxymethoxy)acetyl (**J-75**) were

inactive (>4000 nM). The striking difference in activity between the presence of hexanoyl (**J-50**; 319 nM) and octanoyl (**J-54**; >4000 nM) suggests a degree of steric sensitivity at the P4 position. Notably, the cyclization of P4 to cyclohexyl in **J-55** (88 nM) led to improved potency against *T. brucei*. Overall, these data suggest some preference for hydrophobic cyclic over linear hydrocarbon groups at P4 that may also be limited by length.

Table 3.1. CPB and analogs. P4-P1 substituents, activity against *T. brucei*, cytotoxicity against HepG2 cells and selectivity indices.

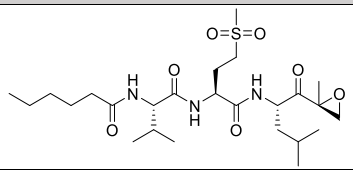
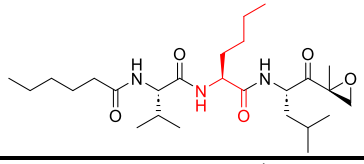
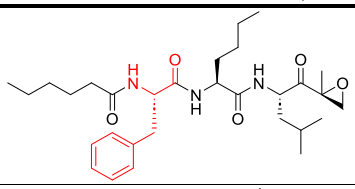
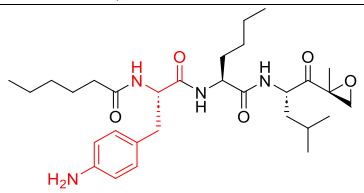
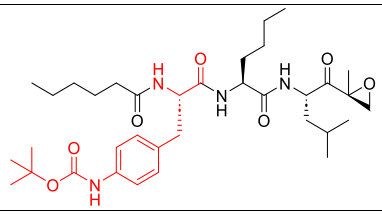
Compound	Structure	P4	P3	P2	P1	EC_{50} *T. brucei* (nM)[b]	CC_{50} HepG2 (nM)[c]	SI (CC_{50}/EC_{50})
CPB		Hexanoyl	L-Val	L-Met-Ox	L-Leu-EK	31 ± 4	13 ± 2	<1
J-1[a]		Hexanoyl	L -Val	L-Nle[a]	L-Leu-EK	>4000	134 ± 87	<1
J-2		Hexanoyl	L-Phe	L-Nle	L-Leu-EK	1036 ± 358	22 ± 8	<1
J-4		Hexanoyl	4-NH_2-L-Phe	L-Nle	L-Leu-EK	228 ± 49	6 ± 5	<1
J-5		Hexanoyl	4-Boc-NH-L-Phe	L-Nle	L-Leu-EK	>4000	80 ± 27	<1

Table 3.1. CPB and analogs. (Continued)

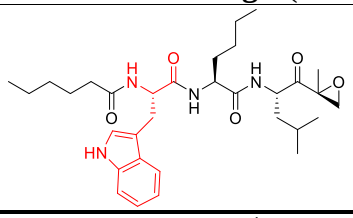
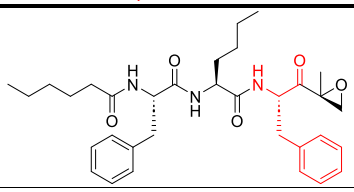
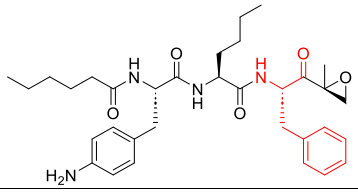
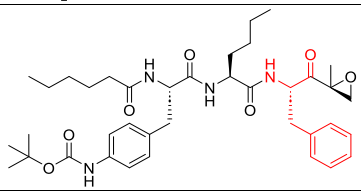
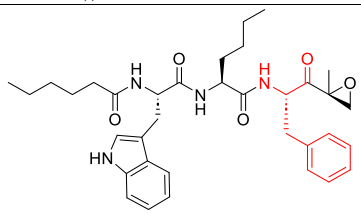
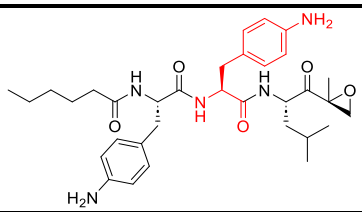
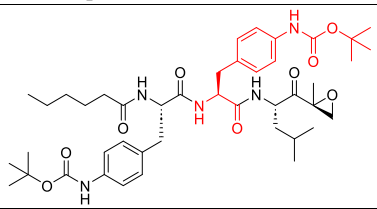
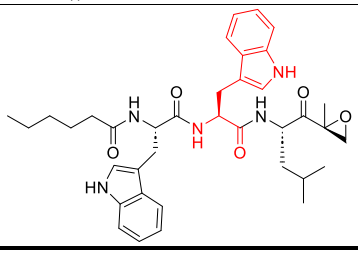
J-6		Hexanoyl	L-Trp	L-Nle	L-Leu-EK	195 ± 62	3.2 ± 1.3	<1
J-7		Hexanoyl	L-Phe	L-Nle	L-Phe-EK	>4000	31 ± 14	<1
J-9		Hexanoyl	4-NH_2-L-Phe	L-Nle	L-Phe-EK	567 ± 349	3410 ± 2310	6
J-10		Hexanoyl	4-Boc-NH-L- Phe	L-Nle	L-Phe-EK	2715 ± 1487	478 ± 126	<1
J-11		Hexanoyl	L-Trp	L-Nle	L-Phe-EK	52 ± 34	6 ± 2	<1
J-12		Hexanoyl	4-NH_2-L-Phe	4-NH_2-L-Phe	L-Leu-EK	222 ± 77	0.9 ± 0.3	<1
J-14		Hexanoyl	4-Boc-NH-L- Phe	4-Boc-NH-L-Phe	L-Leu-EK	465 ± 299	118 ± 22	<1
J-16		Hexanoyl	L-Trp	L-Trp	L-Leu-EK	93 ± 36	12 ± 3	<1

Table 3.1. CPB and analogs. (Continued)

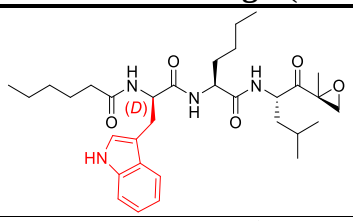
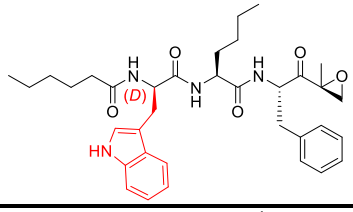
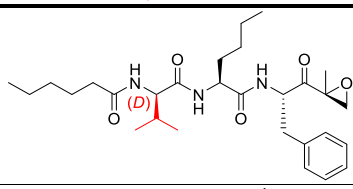
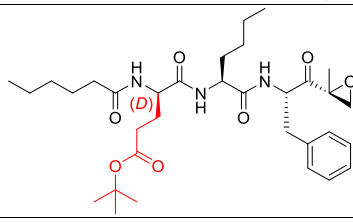
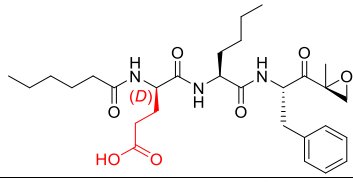
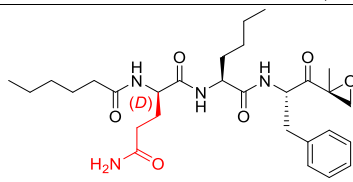
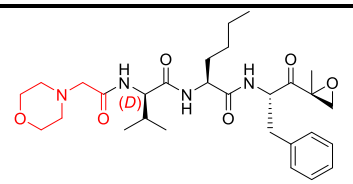
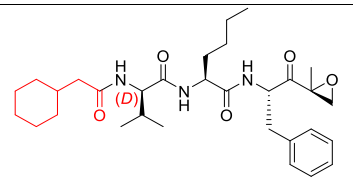
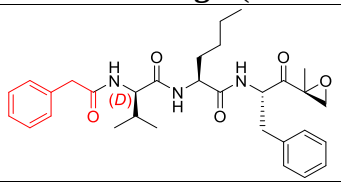
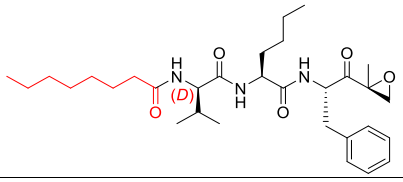
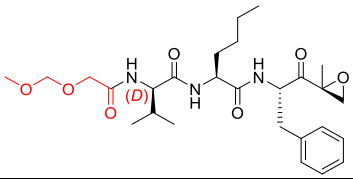
J-19		Hexanoyl	D-Trp	L-Nle	L-Leu-EK	298 ± 137	915 ± 289	3
J-51		Hexanoyl	D-Trp	L-Nle	L-Phe-EK	64 ± 35	308 ± 77	4
J-50		Hexanoyl	D-Val	L-Nle	L-Phe-EK	319 ± 86	4608 ± 721	14
J-71		Hexanoyl	D-(OtBu)-Glu	L-Nle	L-Phe-EK	128 ± 41	15680 ± 1680	122
J-74		Hexanoyl	D-Glu	L-Nle	L-Phe-EK	1591 ± 305	>50,000	31
J-76		Hexanoyl	D-Gln	L-Nle	L-Phe-EK	>4000	12600 ± 3870	<3
J-53		4-morpholine-acetyl	D-Val	L-Nle	L-Phe-EK	568 ± 96	1068 ± 330	2
J-55		Cyclohexyl acetyl	D-Val	L-Nle	L-Phe-EK	88 ± 32	1529 ± 16	17

Table 3.1. CPB and analogs. (Continued)

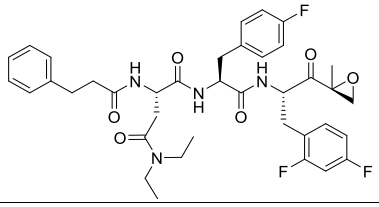
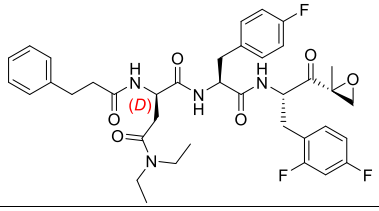
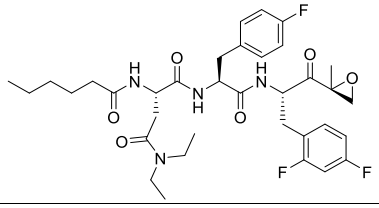
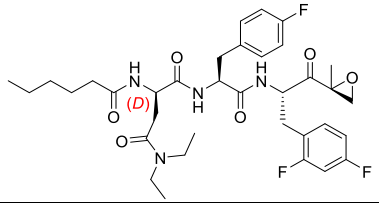
J-56		Phenyl acetyl	D-Val	L-Nle	L-Phe-EK	307 ± 126	1588 ± 213	5
J-54		Octanoyl	D-Val	L-Nle	L-Phe-EK	>4000	1546 ± 132	<1
J-75		Methoxy methoxy acetate	D-Val	L-Nle	L-Phe-EK	>4000	12535 ± 122	<3

[a]The substituent in the chemical structure that changes relative to the previous group of analogs is colored in red. [b]Antitrypanosomal activity was determined using the SYBR green cell viability assay. Data shown represent the means ± SD of three or more biological replicates each conducted in triplicate. [c]HepG2 cytotoxicity data were previously published. [29, 33]

The last set of four compounds (Table 3.2) was originally designed based on ML9, a reversible proteasome inhibitor of *Mycobacterium tuberculosis 20S*[36] that was subsequently modified with an epoxyketone group.[29] This set explored the P4 substitution of a 3-phenyl acetyl group for a hexanoyl as well as the P3 stereochemistry of an *N,N*-diethyl-L-Asn moiety. Whereas the P4 substitution had no major effect on antitrypanosomal activity, the L-configuration at P3 was slightly preferred, with 8.6- and 2.9-fold greater antitrypanosomal activity for **J-77** *vs*. **J-78**, and **J-79** *vs*. **J-80**, respectively. Although all four compounds were relatively nontoxic to HepG2 cells, the P3 D-analogs were at least one order of magnitude less so than the L-analogs, with **J-80** outstanding with its SI of 155. Interestingly, this ability to accommodate the D-configuration at P3 has been noted before for *P. falciparum.*[29, 33] In addition, it has been reported that P3 D-analogs preferentially engage the immunoproteasome (i20S) over the constitutive c20S proteasome.[37]

Overall, the ability to accept the D-configuration by *T. brucei* offers opportunities to identify inhibitors with increased selectivity.

Table 3.2. ML9 based epoxyketone inhibitors. P4-P1 substituents, activity against *T. brucei*, cytotoxicity against HepG2 Cells and selectivity indices.

Compound	Structure	P4	P3	P2	P1	EC_{50} *T. brucei* (nM)[a]	CC_{50} HepG2 (nM)[b]	SI (CC_{50}/EC_{50})
J-77		3-phenyl acetyl	(*N*,*N*-Diethyl)-L-Asn	4-Fluoro-L-Phe	2,4,-Difluoro-L-Phe-Ek	30 ± 14	2580 ± 362	86
J-78		3-phenyl acetyl	(*N*,*N*-Diethyl)-D-Asn	4-Fluoro-L-Phe	2,4,-Difluoro-L-Phe-Ek	474 ± 138	30,300 ± 11400	64
J-79		Hexanoyl	(*N*,*N*-Diethyl)-L-Asn	4-Fluoro-L-Phe	2,4,-Difluoro-L-Phe-Ek	39 ± 6	1417 ± 44	36
J-80		Hexanoyl	(*N*,*N*-Diethyl)-D-Asn	4-Fluoro-L-Phe	2,4,-Difluoro-L-Phe-Ek	157 ± 40	24,300 ± 2130	155

[a]Antitrypanosomal activity was determined with the SYBR green cell viability assay. Data shown represent the means ± SD of three or more biological replicates each conducted in triplicate. [b]HepG2 cytotoxicity data were previously published. [29, 33]

3.2.2. CPB analogs engage the Tb20S β5 subunit

We selected three compounds, **J-71**, **J-77** and **J-80** for follow-up studies as they shared similar potencies to that of pentamidine (Figure 3.1A), an approved drug for treatment of trypanosomiasis, and were the only compounds with selectivity values >80 (Figure 3.1B). To confirm their engagement of the Tb20S target, we used a commercially available activity-based probe, Me_4BodipyFL-Ahx$_3$Leu$_3$VS [38], that binds covalently to the catalytic threonine residues of proteasomes and can be used to visualize the target protein via SDS-PAGE. This probe labeled two of the three catalytic subunits in *T. brucei* (Figure 3.1C), which previous reports identified as β2 (upper band) and β5 (lower band).[39] When parasite lysates were pre-incubated with 0.1 to 10 μM of each compound for 1 h and then incubated with the probe we observed a concentration-dependent reduction in β5 labelling. Complete inhibition of β5 occurred in the presence of 1 μM of each compound. At 10 μM, **J-71** also inhibited Tb20S β2 by approximately 84% based on densitometric analysis. The data suggest, therefore, that engagement of the β5 subunit is associated with the inhibition of *T. brucei* growth *in vitro.* Whether there is added value in inhibiting β2 in addition to β5 is not yet clear. It has been reported for *Plasmodium falciparum* that dual inhibition of β2 and β5 facilitated killing of all blood stage parasites while inhibition of β5 alone was only associated with activity against the schizont stage.[40] However, even though **J-71** engaged Tb20S β2 at 10 μM (Figure 3.1C), the minimal concentration necessary to kill all of the parasites *in vitro* by this and the other inhibitors was < 1 μM (Figure 3.1A), suggesting that β5 is the critical target.

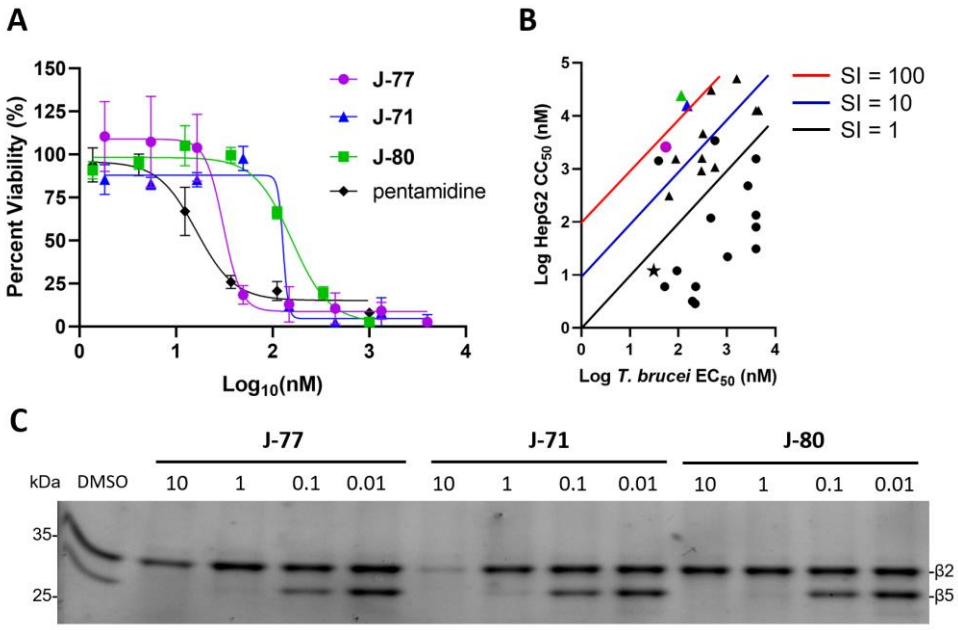


Figure 3.1. CPB analogs decrease *T. brucei* growth and engage the Tb20S β5 subunit. A. Concentration response curves for three top-performing CPB analogs against T. brucei: the assay was performed once in triplicate and means ± SD values are shown. **B.** Plot of log T. brucei EC_{50} vs. log HepG2 CC_{50}. Lines indicate SI cut-offs. The star represents the CPB progenitor compound, the triangles represent those compounds with a D-configuration at P3, and the blue, purple and green symbols represent **J-71**, **J-77 and J-80,** respectively. **C.** Binding-competition assay in T. brucei lysates with CPB analogs using the fluorescent activity-based probe, Me_4BodipyFL-Ahx_3Leu_3VS.

3.2.3. J-80 is predicted to have greater selectivity towards the Tb20S β5 binding pocket

J-80 was chosen for molecular docking studies with Tb20S β5, as it had the highest SI value and was confirmed to inhibit only the β5 subunit. A homology model of the Tb20S β5 subunit sequence (from Met103 to Ser309 using FASTA) was generated based on the crystal structure of c20S β5 (PDB ID: 8UD9), and both covalent[41] and non-covalent[42, 43] docking simulations were performed with **J-80**. For comparison, similar docking simulations were also performed with the β5 subunit of human c20S.

Covalent docking calculations using Glide XP revealed that **J-80** (Figure 3.2A) formed seven potential interactions with the Tb20S β5 subunit (Figure 3.2B). The P1 residue (2,4-difluoro-L-Phe) interacted specifically with Ser21, Lys33 and Ala49. Similarly, the P2 4-fluoro- L-Phe interacted with both Gly47 and Lys117, while both the P3 *N*,*N*-diethyl-D-Asn and the P4 hexanoyl interacted with Ser96. By contrast, **J-80** formed only three potential interactions with c20S β5, involving Thr21 and Gly47 at P2, and Ala49 at P3 (Figure 3.2C). Therefore, the potency and selectivity of **J-80** against *T. brucei* may be attributed to the change in configuration at the P3 position and the stabilization of interactions with the other positions on the inhibitor.

The non-covalent docking simulations for **J-80** using GOLD predicted higher scores (CHEMPLP fitness)[42] for Tb20S β5 compared to c20S β5 (Figure 3.2D). The scores were essentially the same for CPB with both targets, consistent with its equipotent activities against *T. brucei* and HepG2 cells. Also, using DockThor as a different scoring system to predict affinity (kcal/mol)[43], a decrease in binding affinity was predicted for **J-80** when docked with c20S β5 relative to Tb20S β5 (Figure 3.2D). Thus, the non-covalent docking results are consistent with the *in vitro* data indicating that the D-configuration at P3 can be accommodated by Tb20S and less so by c20S. Conversely, the binding scores for CPB were similar regardless of the target, again, in line with the *in vitro* data indicating that CPB is similarly active against both *T. brucei* and HepG2 cells.

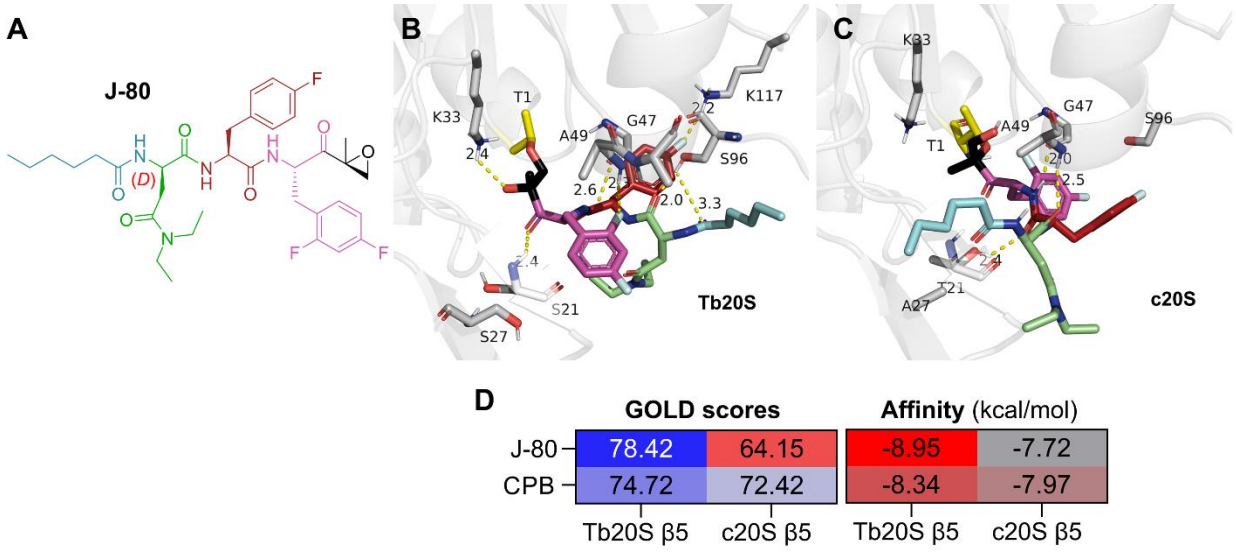


Figure 3.2. Covalent and non-covalent docking simulations predict a greater selectivity of J-80 for Tb20S β5. Predicted covalent docking pose of **J-80** (**A**) using Glide XP in the modeled β5 pockets (gray) of Tb20S (**B**) and c20S (**C**). The compound is predicted to engage the Tb20S β5 binding pocket (seven interactions) more robustly than the β5 pocket of c20S (three interactions). Hydrogen atoms were hidden for clarity. Potential ligand interactions with residues are dashed in yellow. Images were generated with PyMOL software (v2.5.7). **D**. Non-covalent docking simulations using two different scoring algorithms whereby the higher GOLD score and lower affinity each indicate preferential binding of **J-80** to Tb20S β5 compared to the human ortholog.

3.2.4. J-77 and J-80 decrease parasitemia in a mouse model of Stage 1 *T. brucei* infection

The ability of the top three CPB analogs, **J-71**, **J-77** and **J-80**, to interfere with the growth of *T. brucei* in a mouse model of Stage 1 infection was assessed. Briefly, six-week-old, female BALB/C female mice were infected (day 0) intraperitoneally (i.p.) with 100,000 *T. b. brucei* Lister 427 parasites. Parasitemia was established two days post infection (2 d.p.i.) as evidenced by the presence of 10^6 - 10^7 parasites/mL blood (Figure 3.3). Groups of three infected mice (n=3) were then dosed once i.p. with 40 mg/kg of compound. Drug (pentamidine at 4 mg/kg once i.p.) and vehicle controls were also set up (each n=3). After dosing, parasitemia was again measured 3 d.p.i.

In the vehicle control mice, parasitemia increased by almost two log orders to 10^8 parasites/mL from 2 to 3 d.p.i., whereas pentamidine decreased parasitemia to below the detectable limit of 2.5 x10^5 parasites/mL (log_{10} value 5.4; Figure 3.3). Vehicle-treated mice were euthanized 3 d.p.i. to prevent mice dying from uncontrolled parasitemia. **J-71** was seemingly ineffective as the increase in parasitemia after dosing was not statistically different from that of the vehicle control, whereas **J-77** significantly limited the increase to $10^{7.5}$ parasites/mL. By contrast, **J-80**, halted the proliferation of parasites whereby the level of parasitemia remained at ~$10^{6.5}$ parasites/mL between days 2 and 3 d.p.i. Based on these data, **J-80** was chosen for survival studies in mice infected with *T. brucei*.

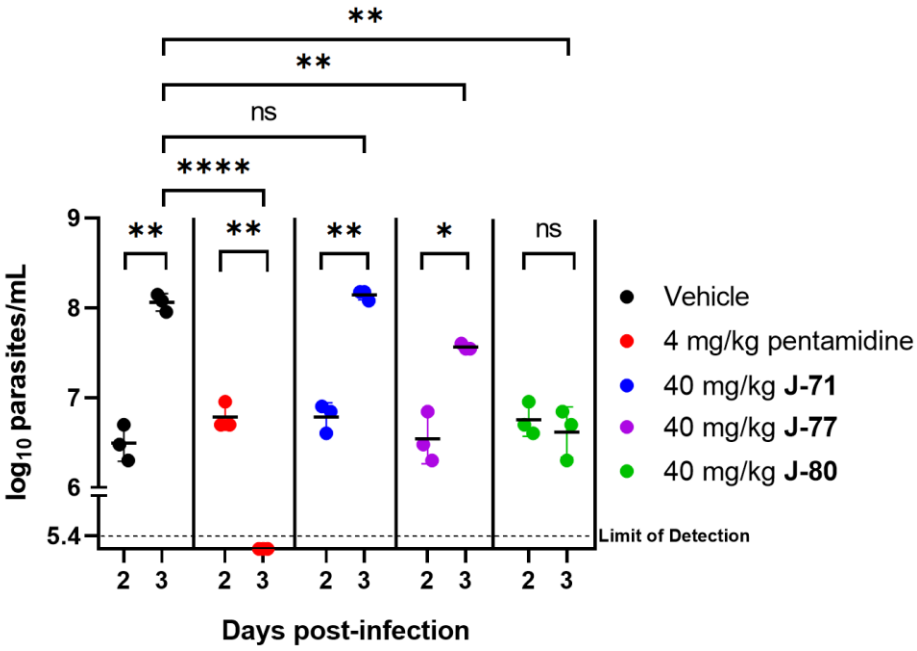


Figure 3.3. Effect of CPB analogs on blood parasitemia. Mice (n=3) were infected with 100,000 *T. brucei* on day 0 and treated i.p. with the named compounds, at the doses indicated, 2 d.p.i. Parasitemia was measured as described in the main text: the limit of detection was 2.5 x 10^5 parasites/mL blood, and data are represented as means ± SD. The Student's paired *t*-test was used for intra-group data, *i.e.*, between 2 and 3 d.p.i., whereas the Student's unpaired *t*-test was used for inter-group data (*vs*. vehicle control) 3 d.p.i. *p<0.05, ***p<0.01, ***p<0.001, ****p<0.0001, ns = not significant.

3.2.5. J-80 extends the survival of mice infected with *T. brucei*

For survival studies, groups of five and three mice were set up for drug/compound and vehicle treatments, respectively. Pentamidine was administered as described above and apparently cured the mice as parasitemia never returned (not shown); also, the mice survived to the end of the experiment at 9 d.p.i. when they were euthanized (Figure 3.4B). By contrast, vehicle treated mice developed parasitemia >10^8 parasites/mL on 3 d.p.i., and were euthanized. **J-80** was administered twice-daily (every 12 h) i.p. at 50 mg/kg for five days starting 2 d.p.i. With this dosing regimen, blood parasitemia levels remained below the limit of detection (2.5 x 10^5 parasites/mL), and up to 48 h after the cessation of dosing 6 d.p.i. (Figure 3.4A). Also, all of the treated mice appeared healthy and behaved normally during the dosing campaign. At 8 d.p.i., parasitemia became detectable in four of the five mice, and by day 9, parasitemia in all five mice ranged between $10^{6.5}$ and 10^9 parasites/mL, at which point, the mice were euthanized, and the experiment concluded. Clearly, therefore, **J-80** exerted a powerful anti-trypanosomal effect.

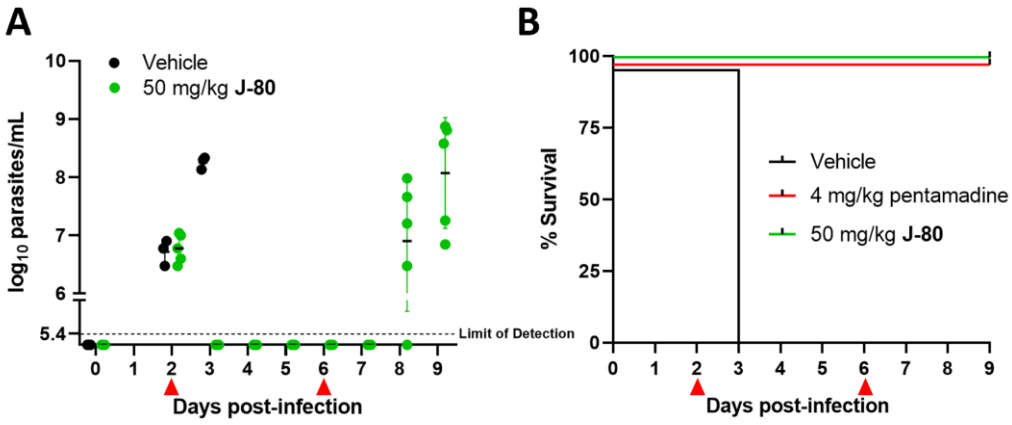


Figure 3.4. J-80 extends the survival of *T. brucei*-infected mice. (**A**) Parasitemia was measured after i.p. administration of 50 mg/kg **J-80** twice daily for five days (n=5), or vehicle control once on day 2 d.p.i. (n=3). Not shown for clarity is the parasitemia subsequent to the i.p. administration of 4 mg/kg pentamidine once on day 2 d.p.i (n=5). Red triangles represent the first and last dosing days for **J-80**. (**B**) Kaplan-Meier survival curves for infected mice treated as indicated.

3.2.6. J-80 is equipotent against three sub-species of *T. brucei*

Finally, we tested the activity of **J-80** against isolates of the two *T. brucei* subspecies responsible for infection in humans, namely *T. b. gambiense* and *T. b. rhodesiense,* in addition to the animal-infective parasite, *T. b. brucei* (Table 3.3). All three subspecies were equally susceptible to this compound.

Table 3.3. Susceptibility of three *T. brucei* subspecies to J-80.

Sub-species	**Pentamidine** (nM) [a]	**J-80** (nM) [a]
T. b. brucei Lister 427	16 ± 4	157 ± 47
T. b. gambiense 348BT	9 ± 7	220 ± 51
T. b. rhodesiense 1852	27 ± 11	156 ± 36

[a] The experiment was conducted once in triplicate.

3.3. Discussion

Two structurally similar triazolopyrimidine inhibitors of the trypanosomatid 20S proteasome are currently in clinical development for treatment of visceral leishmaniasis.[28, 44] Both drug candidates allosterically bind to an interface between the β4 and β5 subunits that is unique to kinetoplastids, blocking the catalytic activity of β5.[45, 46] Our focus with a number of parasites[29-31, 33] has been on the mechanism-based, covalent and irreversible inhibition of the 20S catalytic subunits using analogs of CPB, a peptidyl, epoxyketone natural product that was originally discovered in the marine cyanobacterium, *Symploca* sp.[32]

We screened *T. brucei* in culture with a selection of compounds from a library of CPB analogs that had been synthesized in a campaign to identify inhibitors of the *P. falciparum* 20S proteasome (Pf20S) [29, 33]. Many of these Pf20S inhibitors possessed D-stereochemistry at the P3 position which was accommodated well by the Pf20S β5 subunit and associated with impressive SI values relative to HepG2 cells [29, 33] Beyond factors like size limitations and preferred binding sites influencing *T. brucei* activity, a key finding here for the *T. brucei* SAR is that Tb20S also accommodates inhibitors with the D-configuration at P3, as exemplified by the two matched inhibitor pairs, **J-77** *vs.* **J-78**, and **J-79** *vs.* **J-80**. Whereas all four of these compounds generated low to mid-nanomolar EC_{50} values against the parasite, only those with the P3 D-configuration *i.e.*, **J-78** and **J-80**, were essentially non-toxic to HepG2 cells with CC_{50} values ≥ 25 μM.

Engagement of the intended Tb20S target by the top-performing CPB analogs, **J-71**, **J-77** and **J-80**, was confirmed by binding-competition experiments with the activity-based probe, Me_4BodipyFL-Ahx$_3$Leu$_3$VS, and visualization after SDS-PAGE. These experiments also indicated that inhibition of β5 is associated with parasite killing. In support of this notion, both the number of potential interactions between **J-80** and the β5 subunit identified by covalent docking and the scores generated by the non-covalent docking simulations were consistent with the biochemical data. Tb20S β2 was also engaged by one of the three top inhibitors (**J-71**) but only at 10 μM, a concentration greater than that necessary to kill the parasite in culture. We were not able to judge whether β1 was also targeted by any of the top three CPB analogs as it could not be visualized by the activity-based probe, however, this seems unlikely given that the set of CPB analogs tested primarily react with Pf20S β5.[29, 33]

That the inhibition of β5 is associated with trypanocidal activity is consistent with the known importance of this subunit for the survival of other parasites, including *P. falciparum*[29], *L.*

donovani[44, 45] and *Trypanosoma cruzi*[47]. For *P. falciparum*, inhibition of Pf20S β5 is sufficient to decrease the survival of synchronous trophozoites[48] and schizogony[40]. Added value is brought by co-inhibition of two or more subunits, whereby all the intraerythrocytic life stages are killed *in vitro*[40, 49]. This value extends to the demonstration that inhibition of β2 can overcome β5 resistance [40, 50] and also synergize with dihydroartemisinin to kill early ring stage parasites[51]. These studies highlight the importance of understanding the relative contribution of individual Tb20S β subunits to survival, especially if drug resistance were to emerge to one or more subunit.

The three top performing CPB analogs, **J-71**, **J-77** and **J-80**, were tested for their ability to decrease blood parasitemia in a mouse model of Stage 1 infection by *T. brucei*. After a single i.p. dose, **J-80** stood out as being the only compound to halt growth of the parasite over a 24 h period. Further, using a twice-daily i.p. dosing regimen over five days, **J-80** decreased parasitemia to below the detectable limit and prolonged the survival of infected mice, which appeared healthy, with parasite recrudescence only occurring 48 h after the last dose. This *in vivo* proof-of-principle by a mechanism-based proteasome inhibitor of Tb20S is encouraging. Nonetheless, the short plasma half-life of 2.4 h for **J-80** [29] necessitated its twice-daily delivery to demonstrate efficacy and, likely, contributed to the lack of cure. Further research with next-generation CPB analogs will aim to improve metabolic stability and demonstrate oral bioavailability while maintaining or improving potency and selectivity. In addition, the issue of blood-brain barrier penetrance to clear stage 2 *T. brucei* infection must be dealt with to eventually deliver a single-dose oral cure of HAT, as is currently the case for the drug candidate, acoziborole.[13, 52]

3.4. Conclusion

By whole-organism screening of *T. brucei in vitro* with a selection of CPB analogs designed to interact with the Pf20S proteasome, we discovered several compounds with nanomolar anti-trypanosomal potency that were essentially not toxic to HepG2 cells. We identified the Tb20S β5 subunit as the key target. Underlying the large selectivity values was the ability of Tb20S β5 to accommodate a D-amino acid at the P3 position of the peptidyl inhibitor backbone, in contrast to the c20S β5 anti-target. One compound, **J-80**, which was equipotent against all three *T. brucei* sub-species, halted parasite growth and prolonged host survival in a mouse model of Stage 1 *T. brucei* infection. Thus far, the SAR for Tb20S seems similar to that demonstrated in an ongoing program targeting Pf20S, suggesting that further 'piggybacking' opportunities may exist to accelerate the identification of potent and selective Tb20S inhibitors.

3.5. Methods

3.5.1. CPB analogs

CPB and analogs were synthesized as described previously.[29, 33] Compounds were stored at 10 mM in 100% DMSO in 96-well, u-bottomed polypropylene plates that were stored at -80 ^{o}C.

3.5.2. Maintenance of *T. brucei*

Bloodstream forms of *T. b. brucei* Lister 427, *T. b. gambiense* 348BT and *T. b. rhodesiense* 1852 were cultured as described.[34, 53]

3.5.3. *T. brucei* viability assay

SYBR green was used to measure *T. brucei* cell viability as previously described.[34, 35] Briefly, compounds were serially diluted in DMSO (Thermo Fisher Scientific™, Cat. No. 85190)

across eight concentrations ranging from 4 μM to 0.87 nM. Parasites in log-phase growth were suspended at 2×10^5 parasites/mL in HMI-9 medium under continuous agitation. Cells were dispensed as 100 μL aliquots into 96-well black or white plates with flat and clear bottoms (Corning®, Cat. No. 3903) containing 1 μL of compound in 0.5% DMSO. Additional medium (99 μL) was added, and the plates were incubated for 72 h at 37 °C and 5% CO_2. Parasites were lysed with 50 μL/well of lysis solution (30 mM Tris, pH 7.5, 7.5 mM EDTA, 0.012% saponin (Alfa Aesar, Cat. No. A18820) and 0.12% Triton X-100 (Sigma Aldrich, Cat. No. T8787) containing 0.3 μL/mL SYBR Green I (10,000× in DMSO; Lonza, Cat. No. 50513). Plates were incubated in the dark for at least 1 h at r.t. Fluorescence was measured in a 2104 EnVision® multilabel plate reader (PerkinElmer, Waltham, MA) at 485/535 excitation/emission wavelengths. The activity of test compounds was normalized to those of the DMSO controls in the same plate. Concentration response curves and EC_{50} values, *i.e.*, the concentration of compound required to generate a 50% inhibition of the parasite growth rate, were calculated using GraphPad Prism version 8.0.1 (GraphPad Software, San Diego, CA, www.graphpad.com). At least three biological replicates each in triplicate were performed for each CPB analog.

3.5.4. Docking studies

The Tb20S β5 sequence, truncated from Met103 to Ser309 (FASTA) was modelled after the human c20S anti-target β5 subunit (PDB ID: 8UD9). Modelling employed Maestro (Schrödinger Release 2024.1 Maestro, Schrödinger, LLC, New York, NY, 2024) and OPLS4 force-field[54] as templates utilizing the advanced homology modelling tool available in the Schrödinger suite (v2023.2). Missing amino acid's side chains were placed using Prime, followed by loop refinement using the same software. Proteins were prepared using Protein Preparation

Wizard (Schrödinger LLC, New York, NY, 2024). Missing hydrogen atoms were added, bond orders were assigned using the CCD database, and protonation states of amino acids were optimized with PROPKA[55] (Schrödinger, LLC, New York, NY, 2023) at pH 7.4. Given the truncated nature of the models, both the N- and C-termini were capped. Final structures were optimized for hydrogen positions using the H-bond assignment algorithm, PROPKA, in the Protein Preparation Wizard tool of Maestro, to select the most likely protonation states and tautomer for the histidine residues. Acceptance of the software suggestions was followed by optimization of the generated H-bonding species. Finally, all structures underwent global energy minimization using the steep descent method.

Prior to docking simulations, ligands were prepared using LigPrep (Schrödinger, LLC, New York, NY, 2024) to assign the protonation state (at pH 7.0 ± 1.0) and the partial charges. Simulations were performed using Glide v7.7 with extra precision (XP). Initially, non-covalent docking was calculated within a pocket of 13 Å around co-crystallized ligands of the original templates. These generated up to 10 poses per ligand that were used as a starting point for covalent docking. Next, using CovDocking, covalent docking poses were generated with similar parameters by selecting an epoxy opening reaction with Thr107, *i.e.*, Thr1, as the reactive residue. Representative poses were selected based on the docking score and by visual inspection of the warhead position covalently bound to the threonine.

Additional non-covalent docking was performed using GOLD 5.1[42] and DockThor[43] (https://dockthor.lncc.br/v2/) in a consensus approach with two different scoring systems (*i.e.*, algorithms), CHEMPLP fitness and affinity (kcal/mol), respectively. Simulations with GOLD were performed by building a default grid box of 10 Å around the co-crystallized inhibitor TDI-8304[56] bound to the c20S β5 subunit, which was inserted[57] into the modeled Tb20S β5 structure.

The parameters used in GOLD were: (i) all protein rotatable bonds were fixed; (ii) the binding site was defined with the co-crystallized ligand or the inserted position with all atoms within 10 Å; (iii) chemscore_kinase was used as the template; (iv) 200 genetic algorithm runs performed; (v) CHEMPLP used as the scoring function with no early termination allowed; and (vi) the genetic algorithm search option was set as slow. The representative pose with the highest fitness score was selected by visual inspection among the top three predicted poses. Simulations with DockThor considered the inserted grid box with a default size of 20 x 20 x 20 Å, and were conducted with standard run analysis and no soft docking. A maximum of 24 generated poses was simulated considering RMSD values ≤ 2.0 Å for the cluster conformers. The pose with the highest affinity score (kcal/mol) was selected from among the top three predicted poses.

3.5.5. CPB competition assay with the activity-based probe

Cultured *T. brucei* was aspirated from flasks and centrifuged for 10 min at 24,000 x *g* at 4 ^{o}C three times. After each centrifugation, the supernatant was discarded and the pellet was resuspended in PBS before centrifugation again. After the final centrifugation, the supernatant was removed, and the cell pellet were stored at -80 ^{o}C.

PBS containing 10 μM E64 was used as a lysis buffer and approximately twice the volume was added relative to the volume of the pellet so that a final concentration of 5-10 mg/mL was achieved. Cell lysis was performed on ice using a Qsonica CL-18 sonicator probe set to pulses of 2 s with 5 s rest periods over a total of 44 s. Sonicated samples were centrifuged for 10 min at 11,000 X *g* and 4 ^{o} C. The supernatant was recovered, aliquoted, flash frozen in a dry ice/acetone bath and stored at -80 ^{o}C. The protein concentration was measured using the Pierce ^{TM} BCA Protein Assay kit (Fisher #23227).

T. brucei lysate was diluted to a final concentration of 1 μg/μL and 14 μL was incubated with 1 μL of the specified CPB analog or DMSO concentration, diluted in 100% DMSO, for 1 h at 37 ºC. Afterwards, 1 μL Me_4BodipyFL-Ahx_3Leu_3VS (Ubiqbio #UbiQ-018), diluted in 100% DMSO, was added so that a final concentration of 2 μM was achieved and co-incubated for 1 h at 37 ºC. Next, 8 μL 4X Bolt™ LDS sample buffer (Fisher #B0007) containing 250 mM DTT was added to each sample and boiled for 5 min at 95 °C. Samples were then loaded on a 4-12% Bis-Tris gel (Fisher #NW04127BOX) with 1X MOPS running buffer (Fisher #NP000102). Gels were first electrophoresed at 60 V until the dye front was approximately 15% below the comb, at which point, the voltage was increased to 120 V for the duration of electrophoresis. Gels were washed with water after electrophoresis and fixed for 5 min in 6:3:1 water:ethanol:acetic acid. Fluorescent imaging was performed using a Bio-Rad ChemiDoc MP Imaging System with the settings optimized to visualize Qdots 525 (Bodipy). Densitometric analysis was accomplished using Bio-Rad Image Lab 6.1.

3.5.6. Mouse model efficacy study

Vertebrate animal use was supported under a protocol approved by UC San Diego´s Institutional Animal Care and Use Committee. Approval was granted under the Animal Welfare Act and Regulations (AWAR) Act and the United States Public Health Service Policy on Humane Care and Use of Laboratory Animals.

Infections and treatments were set up and executed essentially as described.[34] Briefly, six-week-old, wild-type, BALB/c, female mice were infected with 1×10^5 *T. b. brucei* Lister 427 cells by i.p. injection. Mice were divided into groups of three or five, and 48 h after infection, compound

or vehicle alone was administered i.p. in 9% DMSO and 91% corn oil at the doses indicated in the Results section. Pentamidine (Sigma-Aldrich, Cat No. P0547) was used as reference drug.

Blood parasitemia was measured by microscopic examination of tail blood every 24 h starting at 48 h post-infection. Specifically, 5 µL blood was withdrawn and diluted immediately with 5 µL heparin solution (0.5 mg/mL in sterile water) before administering drug. Samples were diluted a further 100-fold in PBS at 37 ˚C and the parasites counted using a Neubauer chamber. The lower limit for accurate counting of cells in a Neubauer chamber is 2.5×10^5 cells/mL. Mice were monitored every day for general appearance and behaviour.

3.6. Acknowledgements

Chapter 3, in full, is a reprint of a manuscript that is currently under review in ACS *Infectious Diseases* as of May 2024. The research described was supported by the NIH grant R21AI171824 to AJO and CRC. The CPB analogs used in this study were synthesized with support from the Bill and Melinda Gates Foundation INV-037899 to AJO and WHG. AJO and WHG also acknowledge the support of R01AI158612. KRF acknowledges support of the CARING T32 Training Grant (T32AI007036). WE was supported by a scholarship to the CDIPD from the US Agency for International Development (USAID) / The Egyptian Ministry of Higher Education, Central Department of Missions (CDM). JA acknowledges the deanship of scientific research at the University of Jordan for his scientific leave and the St. Baldrick's Foundation for the International Scholar award 2022—2025 (Award #940892). TK acknowledges funding by the Clusters of Excellence TüCAD2 and the Excellence Strategy of the German Federal and State Governments – Germany, by the means of the German Center for Infection Research (DZIF,

TTU06.716). MSMS acknowledges his PDE scholarship funded by the Conselho Nacional de Desenvolvimento Científico e Tecnológico (CNPq; grant # 442896/2023-9 and 200069/2024-1).

3.7. References

(1) Büscher, P.; Cecchi, G.; Jamonneau, V.; Priotto, G. Human African trypanosomiasis. *Lancet* **2017**, *390* (10110), 12.
(2) Steverding, D. The history of African trypanosomiasis. *Parasit Vectors* **2008**, *1* (1), 3. DOI: 10.1186/1756-3305-1-3.
(3) Venturelli, A.; Tagliazucchi, L.; Lima, C.; Venuti, F.; Malpezzi, G.; Magoulas, G. E.; Santarem, N.; Calogeropoulou, T.; Cordeiro-da-Silva, A.; Costi, M. P. Current treatments to control African trypanosomiasis and one health perspective. *Microorganisms* **2022**, *10* (7). DOI: 10.3390/microorganisms10071298.
(4) Papagni, R.; Novara, R.; Minardi, M. L.; Frallonardo, L.; Panico, G. G.; Pallara, E.; Cotugno, S.; Bartoli, T. A.; Guido, G.; Vita, E. D.; Ricciardi, A.; Totaro, V.; Camporeale, M.; Segala, F. V.; Bavaro, D. F.; Patti, G.; Brindicci, G.; Pellegrino, C.; Mariani, M. F.; Putoto, G.; Samrati, L.; Castellani, C.; Saracino, A.; Gennaro, F. D.; Nicastri, E. Human African trypanosomiasis (sleeping sickness): Current knowledge and future challenges. *Front. Trop. Dis* **2023**, *4*.
(5) Franco, J. R.; Simarro, P. P.; Diarra, A.; Jannin, J. G. Epidemiology of human African trypanosomiasis. *Clin Epidemiol* **2014**, *6*, 257-275. DOI: 10.2147/CLEP.S39728.
(6) Kennedy, P. G. Clinical features, diagnosis, and treatment of human African trypanosomiasis (sleeping sickness). *Lancet Neurology* **2013**, *12* (2), 8.
(7) Magez, S.; Li, Z.; Nguyen, H. T. T.; Pinto Torres, J. E.; Van Wielendaele, P.; Radwanska, M.; Began, J.; Zoll, S.; Sterckx, Y. G. The history of anti-trypanosome vaccine development shows that highly immunogenic and exposed pathogen-derived antigens are not necessarily good target candidates: Enolase and ISG75 as Examples. *Pathogens* **2021**, *10* (8). DOI: 10.3390/pathogens10081050.
(8) Jamabo, M.; Mahlalela, M.; Edkins, A. L.; Boshoff, A. Tackling sleeping sickness: Current and promising therapeutics and treatment strategies. *Int J Mol Sci* **2023**, *24* (15). DOI: 10.3390/ijms241512529.
(9) Kennedy, P. G. E.; Rodgers, J. Clinical and neuropathogenetic aspects of human African trypanosomiasis. *Front Immunol* **2019**, *10*, 39. DOI: 10.3389/fimmu.2019.00039.
(10) Kennedy, P. G. Human African trypanosomiasis of the CNS: current issues and challenges. *J Clin Invest* **2004**, *113* (4), 496-504. DOI: 10.1172/JCI21052.
(11) Lutumba, P.; Makieya, E.; Shaw, A.; Meheus, F.; Boelaert, M. Human African trypanosomiasis in a rural community, Democratic Republic of Congo. *Emerg Infect Dis* **2007**, *13* (2), 248-254. DOI: 10.3201/eid1302.060075.
(12) Bernhard, S.; Kaiser, M.; Burri, C.; Mäser, P. Fexinidazole for human African trypanosomiasis, the fruit of a successful public-private partnership. *Diseases* **2022**, *10* (4). DOI: 10.3390/diseases10040090.
(13) Tarral, A.; Hovsepian, L.; Duvauchelle, T.; Donazzolo, Y.; Latreille, M.; Felices, M.; Gualano, V.; Delhomme, S.; Valverde Mordt, O.; Blesson, S.; Voiriot, P.; Strub-

Wourgaft, N. Determination of the optimal single dose treatment for acoziborole, a novel drug for the treatment of human African trypanosomiasis: First-in-Human Study. *Clin Pharmacokinet* **2023**, *62* (3), 481-491. DOI: 10.1007/s40262-023-01216-8.
(14) Gehrig, S.; Efferth, T. Development of drug resistance in *Trypanosoma brucei rhodesiense* and *Trypanosoma brucei gambiense*. Treatment of human African trypanosomiasis with natural products. *International Journal of Molecular Medicine* **2008**, *22* (4), 8.
(15) Baker, N.; de Koning, H. P.; Mäser, P.; Horn, D. Drug resistance in African trypanosomiasis: the melarsoprol and pentamidine story. *Trends Parasitol* **2013**, *29* (3), 110-118. DOI: 10.1016/j.pt.2012.12.005.
(16) Legros, D.; Evans, S.; Maiso, F.; Enyaru, J. C. K.; Mbulamberi, D. Risk factors for treatment failure after melarsoprol for *Tryanosoma brucei gambiense* trypanosomiasis in Uganda. *Transactions of the Royal Society of Tropical Medicine and Hygiene* **1999**, *93*, 3.
(17) de Koning, H. P. Ever-increasing complexities of diamidine and arsenical crossresistance in African trypanosomes. *Trends Parasitol* **2008**, *24* (8), 345-349. DOI: 10.1016/j.pt.2008.04.006.
(18) Nkemngu, N. J.; Rosenkranz, V.; Wink, M.; Steverding, D. Antitrypanosomal activities of proteasome inhibitors. *Antimicrob Agents Chemother* **2002**, *46* (6), 2038-2040. DOI: 10.1128/AAC.46.6.2038-2040.2002.
(19) Glenn, R. J.; Pemberton, A. J.; Royle, H. J.; Spackman, R. W.; Smith, E.; Jennifer Rivett, A.; Steverding, D. Trypanocidal effect of alpha',beta'-epoxyketones indicates that trypanosomes are particularly sensitive to inhibitors of proteasome trypsin-like activity. *Int J Antimicrob Agents* **2004**, *24* (3), 286-289. DOI: 10.1016/j.ijantimicag.2004.02.023.
(20) Steverding, D.; Spackman, R. W.; Royle, H. J.; Glenn, R. J. Trypanocidal activities of trileucine methyl vinyl sulfone proteasome inhibitors. *Parasitol Res* **2005**, *95* (1), 73-76. DOI: 10.1007/s00436-004-1253-y.
(21) Caffrey, C. R.; Steverding, D.; Ferreira, R. S.; de Oliveira, R. B.; O'Donoghue, A. J.; Monti, L.; Ballatore, C.; Bachovchin, K. A.; Ferrins, L.; Pollastri, M. P.; Zorn, K. M.; Foil, D. H.; Clark, A. M.; Mottin, M.; Andrade, C. H.; Siqueira-Neto, J. L.; Ekins, S. Drug Discovery and Development for Kinetoplastid Diseases. *Burger's Medicinal Chemistry and Drug Discovery* **2021**, 79.
(22) Collins, G. A.; Goldberg, A. L. The logic of the 26S Proteasome. *Cell* **2017**, *169* (5), 792-806. DOI: 10.1016/j.cell.2017.04.023.
(23) Bard, J. A. M.; Goodall, E. A.; Greene, E. R.; Jonsson, E.; Dong, K. C.; Martin, A. Structure and function of the 26S Proteasome. *Annu Rev Biochem* **2018**, *87*, 697-724. DOI: 10.1146/annurev-biochem-062917-011931.
(24) Sahu, I.; Glickman, M. H. Proteasome in action: substrate degradation by the 26S proteasome. *Biochem Soc Trans* **2021**, *49* (2), 629-644. DOI: 10.1042/BST20200382.
(25) Kopp, F.; Hendil, K. B.; Dahlmann, B.; Kristensen, P.; Sobek, A.; Uerkvitz, W. Subunit arrangement in the human 20S proteasome. *Proc Natl Acad Sci U S A* **1997**, *94* (7), 2939-2944. DOI: 10.1073/pnas.94.7.2939.
(26) Rousseau, A.; Bertolotti, A. Regulation of proteasome assembly and activity in health and disease. *Nat Rev Mol Cell Biol* **2018**, *19* (11), 697-712. DOI: 10.1038/s41580-018-0040-z.

(27) Tanaka, K. The proteasome: overview of structure and functions. *Proc Jpn Acad Ser B Phys Biol Sci* **2009**, *85* (1), 12-36. DOI: 10.2183/pjab.85.12.
(28) DNDi. *Drugs for Neglected Disease Initiative*. https://dndi.org/diseases/visceral-leishmaniasis/ (Accessed May 1, 2024).
(29) Almaliti, J.; Fajtová, P.; Calla, J.; LaMonte, G. M.; Feng, M.; Rocamora, F.; Ottilie, S.; Glukhov, E.; Boura, E.; Suhandynata, R. T.; Momper, J. D.; Gilson, M. K.; Winzeler, E. A.; Gerwick, W. H.; O'Donoghue, A. J. Development of potent and highly selective epoxyketone-based *Plasmodium* proteasome inhibitors. *Chemistry* **2023**, *29* (20), e202203958. DOI: 10.1002/chem.202203958.
(30) O'Donoghue, A. J.; Bibo-Verdugo, B.; Miyamoto, Y.; Wang, S. C.; Yang, J. Z.; Zuill, D. E.; Matsuka, S.; Jiang, Z.; Almaliti, J.; Caffrey, C. R.; Gerwick, W. H.; Eckmann, L. 20S proteasome as a drug target in *Trichomonas vaginalis*. *Antimicrob Agents Chemother* **2019**, *63* (11). DOI: 10.1128/aac.00448-19.
(31) Bibo-Verdugo, B.; Wang, S. C.; Almaliti, J.; Ta, A. P.; Jiang, Z.; Wong, D. A.; Lietz, C. B.; Suzuki, B. M.; El-Sakkary, N.; Hook, V.; Galvesen, G. S.; Gerwick, W. H.; Caffrey, C. R.; O'Donoghue, A. J. The Proteasome as a Drug Target in the Metazoan Pathogen, *Schistosoma mansoni*. *ACS Infect Dis* **2019**, *5* (10), 1802-1812. DOI: 10.1021/acsinfecdis.9b00237.
(32) Pereira, A. R.; Kale, A. J.; Fenley, A. T.; Byrum, T.; Debonsi, H. M.; Gilson, M. K.; Valeriote, F. A.; Moore, B. S.; Gerwick, W. H. The carmaphycins: new proteasome inhibitors exhibiting an α,β-epoxyketone warhead from a marine cyanobacterium. *Chembiochem* **2012**, *13* (6), 810-817. DOI: 10.1002/cbic.201200007.
(33) LaMonte, G. M.; Almaliti, J.; Bibo-Verdugo, B.; Keller, L.; Zou, B. Y.; Yang, J.; Antonova-Koch, Y.; Orjuela-Sanchez, P.; Boyle, C. A.; Vigil, E.; Wang, L.; Goldgof, G. M.; Gerwick, L.; O'Donoghue, A. J.; Winzeler, E. A.; Gerwick, W. H.; Ottilie, S. Development of a potent inhibitor of the *Plasmodium* proteasome with reduced mammalian toxicity. *J Med Chem* **2017**, *60* (15), 6721-6732. DOI: 10.1021/acs.jmedchem.7b00671.
(34) Monti, L.; Liu, L. J.; Varricchio, C.; Lucero, B.; Alle, T.; Yang, W.; Bem-Shalom, I.; Gilson, M.; Brunden, K. R.; Brancale, A.; Caffrey, C. r.; Ballatore, C. Structure-activity relationships, tolerability and efficacy of microtubule-active 1,2,4-Triazolo[1,5-a]pyrimidines as potential candidates to treat human African trypanosomiasis. *ChemMedChem* **2023**, *18* (20), e202300193. DOI: 10.1002/cmdc.202300193.
(35) Francisco, K. R.; Monti, L.; Yang, W.; Park, H.; Liu, L. J.; Watkins, K.; Amarasinghe, D. K.; Nalli, M.; Roberto Polaquini, C.; Regasini, L. O.; Magalhães, L. G.; Caffrey, C. R. Structure-activity relationship of dibenzylideneacetone analogs against the neglected disease pathogen, *Trypanosoma brucei*. *Bioorg Med Chem Lett* **2023**, *81*, 129123. DOI: 10.1016/j.bmcl.2023.129123.
(36) Lin, G.; Chidawanyika, T.; Tsu, C.; Warrier, T.; Vaubourgeix, J.; Blackburn, C.; Gigstad, K.; Sintchak, M.; Dick, L.; Nathan, C. N,C-Capped dipeptides with selectivity for mycobacterial proteasome over human proteasomes: role of S3 and S1 binding pockets. *J Am Chem Soc* **2013**, *135* (27), 9968-9971. DOI: 10.1021/ja400021x.
(37) de Bruin, G.; Huber, E. M.; Xin, B.-T.; van Rooden, E. J.; Al-Ayed, K.; Kim, K.-B.; Kisselev, A. F.; Driessen, C.; van der Stelt, M.; van der Marel, G. A.; Groll, M.; Overkleeft, H. S. Structure-Based Design of β1i or β5i Specific Inhibitors of Human Immunoproteasomes. *Journal of Medicinal Chemistry* **2014**, *54* (14), 12.

(38) Verdoes, M.; Florea, B. I.; Menendez-Benito, V.; Maynard, C. J.; Witte, M. D.; van der Linden, W. A.; van den Nieuwendijk, A. M.; Hofmann, T.; Berkers, C. R.; van Leeuwen, F. W.; Groothuis, T. A.; Leeuwenburgh, M. A.; Ovaa H.; Neefjes, J. J.; Filippov, D. V.; van der Marel, G. A.; Dantuma, N. P. Overkleeft, H. S. A fluorescent broad-spectrum proteasome inhibitor for labeling proteasomes *in vitro* and *in vivo*. *Chem Biol* **2006**, *13* (11), 1217-1226. DOI: 10.1016/j.chembiol.2006.09.013.
(39) Wang, C. C.; Bozdech, Z.; Liu, C. L.; Shipway, A.; Backes, B. J.; Harris, J. L.; Bogyo, M. Biochemical analysis of the 20S proteasome of *Trypanosoma brucei*. *J Biol Chem* **2003**, *278* (18), 15800-15808. DOI: 10.1074/jbc.M300195200.
(40) Li, H.; van der Linden, W. A.; Verdoes, M.; Florea, B. I.; McAllister, F. E.; Govindaswamy, K.; Elias, J. E.; Bhanot, P.; Overkleeft, H. S.; Bogyo, M. Assessing subunit dependency of the *Plasmodium* proteasome using small molecule inhibitors and active site probes. *ACS Chem Biol* **2014**, *9* (8), 1869-1876. DOI: 10.1021/cb5001263.
(41) Friesner, R. A.; Banks, J. L.; Murphy, R. B.; Halgren, T. A.; Klicic, J. J.; Mainz, D. T.; Repasky, M. P.; Knoll, E. H.; Shelley, M.; Perry, J. K.; Shaw, D. E.; Francis, P.; Shenkin, P. S. Glide: a new approach for rapid, accurate docking and scoring. 1. Method and assessment of docking accuracy. *J Med Chem* **2004**, *47* (7), 1739-1749. DOI: 10.1021/jm0306430.
(42) Verdonk, M. L.; Cole, J. C.; Hartshorn, M. J.; Murray, C. W.; Taylor, R. D. Improved protein-ligand docking using GOLD. *Proteins* **2003**, *52* (4), 609-623. DOI: 10.1002/prot.10465.
(43) Magalhães, C. S. d.; Almeida, D. M.; Barbosa, H. J. C.; Dardenne, L. E. A dynamic niching genetic algorithm strategy for docking highly flexible ligands. *Information Sciences* **2014**, *289*, 18.
(44) Nagle, A.; Biggart, A.; Be, C.; Srinivas, H.; Hein, A.; Caridha, D.; Sciotti, R. J.; Pybus, B.; Kreishman-Deitrick, M.; Bursulaya, B.; Lai, Y. H.; Gao, M.; Liang, F.; Mathison, J. N.; Liu, X.; Yeh, V.; Smith, J.; Lerario, I.; Xie, Y.; Chianelli, D.; Gibney, M.; Berman, A.; Chen, Y.; Jiricek, J.; Davis, L. C.; Liu, X.; Ballard, J.; Khare, S.; Eggimann, F. K.;Leneau, A.; Groessl, T.; Shaprio, M.; Richmond, W.; Johnson, K.; Rudewicz, P. J.; Rao, S. P. S.; Thompson, C.; Tuntland, T.; Spraggon G.; Glynne, R. J.; Supek, F.; Wiesmann, C.; Molteni, V. Discovery and characterization of clinical candidate LXE408 as a kinetoplastid-selective proteasome inhibitor for the treatment of leishmaniases. *J Med Chem* **2020**, *63* (19), 10773-10781. DOI: 10.1021/acs.jmedchem.0c00499.
(45) Wyllie, S.; Brand, S.; Thomas, M.; De Rycker, M.; Chung, C. W.; Pena, I.; Bingham, R. P.; Bueren-Calabuig, J. A.; Cantizani, J.; Cebrian, D.; Craggs, P. D.; Ferguson, L.; Goswami, P.; Hobrath, J.; Howe, J.; Jeacock, L.; Ko, E.; Korczynska, J.; Maclean, L.; Manthri, S.; Martinez, M. S.; Mata-Cantero, L.; Moniz, S.; Nühs, A.; Osuna-Cabello, M.; Pinto, E.; Riley, J.; Robinson, S.; Rowland, P.; Simeons, F. R. C.; Shishikura, Y.; Spinks, D.; Stojanovski, L.; Thomas, J.; Thompson, S.; Gaza, E. V.; Wall, R. J.; Zuccotto, F.; Horn, D.; Ferguson, M. A. J.; Fairlamb, A. H.; Fiandor, J. M.; Martin, J.; Gray, D. W.; Miles, T. J.; Gilbert, I. H.; Read, K. D.; Marco, M.; Wyatt, P. G. Preclinical candidate for the treatment of visceral leishmaniasis that acts through proteasome inhibition. *Proc Natl Acad Sci U S A* **2019**, *116* (19), 9318-9323. DOI: 10.1073/pnas.1820175116.
(46) Khare, S.; Nagle, A. S.; Biggart, A.; Lai, Y. H.; Liang, F.; Davis, L. C.; Barnes, S. W.; Mathison, C. J.; Myburgh, E.; Gao, M. Y.; Gillespie, J. R.; Liu, X.; Tan, J. L.; Stinson, M.; Rivera, I. C.; Ballard, J.; Yeh, V.; Groessl, T.; Federe, G.; Koh, H. X. Y.; Venable, J.

D.; Bursulaya, B.; Shaprio, M.; Kishra, P. K.; Spraggon, G.; Brock, A.; Mottram, J. C.; Buckner, F. S.; Rao, S. P. S.; Wen, B. G.; Walker, J. R.; Tuntland, T.; Molteni, V.; Glynne, R.; Supek, F. Proteasome inhibition for treatment of leishmaniasis, Chagas disease and sleeping sickness. *Nature* **2016**, *537* (7619), 229-233. DOI: 10.1038/nature19339.

(47) Thomas, M. G.; McGonagle, K.; Rowland, P.; Robinson, D. A.; Dodd, P. G.; Camino-Díaz, I.; Campbell, L.; Cantizani, J.; Castañeda, P.; Conn, D.; Craggs, P. D.; Edwards, D.; Ferguson, L.; Fosberry, A.; Frame, L.; Goswami, P.; Hu, X.; Korczynska, J.; MacLean, L.; Martin, J.; Mutter, N.; Osuna-Cabello, M.; Paterson, C.; Peña, I.; Pinto, E. G.; Pont, C.; Riley, J.; Shishikura, Y.; Simeons, F. R. C.; Stojanovski, L.; Thomas, J.; Wrobel, K.; Young, R. J.; Zmuda, F.; Zuccotto, F.; Read, K. D.; Gilbert, I. H.; Marco, M.; Miles, T. J.; Manzano, P.; Rycker, M. D. Structure-guided design and synthesis of a pyridazinone series of *Trypanosoma cruzi* proteasome inhibitors. *J Med Chem* **2023**, *66* (15), 10413-10431. DOI: 10.1021/acs.jmedchem.3c00582.

(48) Li, H.; Ponder, E. L.; Verdoes, M.; Asbjornsdottir, K. H.; Deu, E.; Edgington, L. E.; Lee, J. T.; Kirk, C. J.; Demo, S. D.; Williamson, K. C.; Boygo, M. Validation of the proteasome as a therapeutic target in *Plasmodium* using an epoxyketone inhibitor with parasite-specific toxicity. *Chem Biol* **2012**, *19* (12), 1535-1545. DOI: 10.1016/j.chembiol.2012.09.019.

(49) Li, H.; Tsu, C.; Blackburn, C.; Li, G.; Hales, P.; Dick, L.; Bogyo, M. Identification of potent and selective non-covalent inhibitors of the *Plasmodium falciparum* proteasome. *J Am Chem Soc* **2014**, *136* (39), 13562-13565. DOI: 10.1021/ja507692y.

(50) Xie, S. C.; Gillett, D. L.; Spillman, N. J.; Tsu, C.; Luth, M. R.; Ottilie, S.; Duffy, S.; Gould, A. E.; Hales, P.; Seager, B. A.; Charron, C. L.; Bruzzese, F.; Yang, X.; Zhao, X.; Huang, S.; Hutton, C. A.; Burrows, J. N.; Winzeler, E. A.; Avery, V. M.; Dick, L. R.; Tilley, L. Target validation and identification of novel boronate inhibitors of the *Plasmodium falciparum* proteasome. *J Med Chem* **2018**, *61* (22), 10053-10066. DOI: 10.1021/acs.jmedchem.8b01161.

(51) Li, H.; O'Donoghue, A. J.; van der Linden, W. A.; Xie, S. C.; Yoo, E.; Foe, I. T.; Tilley, L.; Craik, C. S.; da Fonseca, P. C.; Bogyo, M. Structure- and function-based design of *Plasmodium*-selective proteasome inhibitors. *Nature* **2016**, *530* (7589), 233-236. DOI: 10.1038/nature16936.

(52) DNDi. *Acoziborole: Investigational single-dose oral treatment raises hope for elimination of sleeping sickness in Africa*. 2022. (accessed.

(53) Monti, L.; Wang, S. C.; Oukoloff, K.; Smith, A. B.; Brunden, K. R.; Caffrey, C. R.; Ballatore, C. Brain-penetrant triazolopyrimidine and phenylpyrimidine microtubule stabilizers as potential leads to treat human African trypanosomiasis. *ChemMedChem* **2018**, *13* (17), 1751-1754. DOI: 10.1002/cmdc.201800404.

(54) Lu, C.; Wu, C.; Ghoreishi, D.; Chen, W.; Wang, L.; Damm, W.; Ross, G. A.; Dahlgren, M. K.; Russell, E.; Von Bargen, C. D.; Abel, R.; Friesner, R. A.; Harder, E. D. OPLS4: Improving force field accuracy on challenging regimes of chemical space. *J Chem Theory Comput* **2021**, *17* (7), 4291-4300. DOI: 10.1021/acs.jctc.1c00302.

(55) Li, H.; Robertson, A. D.; Jensen, J. H. Very fast empirical prediction and rationalization of protein pKa values. *Proteins* **2005**, *61* (4), 704-721. DOI: 10.1002/prot.20660.

(56) Hsu, H. C.; Li, D.; Zhan, W.; Ye, J.; Liu, Y. J.; Leung, A.; Qin, J.; Crespo, B.; Gamo, F. J.; Zhang, H.; Cui, L.; Roth, A.; Kirkman, L. A.; Li, H.; Lin, G. Structures revealing

mechanisms of resistance and collateral sensitivity of *Plasmodium falciparum* to proteasome inhibitors. *Nat Commun* **2023**, *14* (1), 8302. DOI: 10.1038/s41467-023-44077-2.

(57) Serafim, M. S. M.; Kronenberger, T.; Oliveira, R. B. d.; Kroon, E. G.; Abrah ã o, J. S.; Mota, B. E. F.; Maltarollo, V. G. Synthetic curcumin analogues present antiflavivirus activity in vitro with potential multiflavivirus activity from a thiazolylhydrazone moiety. *Future Pharmacol.* **2023**, *3* (2).